Evaluation of phosphoric rock and steel slags as raw materials for the development of iron phosphate cements for applications in building materials

Carlos Andrés Cárdenas Balaguera

This thesis is presented as a partial requirement to apply for the title of Materials Engineering Doctor

Advisor
Dr. (PhD) Maryory Astrid Gómez Botero

Universidad de Antioquia
Facultad de Ingeniería
Doctorado en Ingeniería de Materiales
Medellín, Antioquia, Colombia
2021

The doctoral thesis is based on the experimental work carried out at the Center for Research, Innovation and Development of Materials - CIDEMAT, of the University of Antioquia, Medellín - Colombia, under the advisory of the Professor Maryory Gómez. The study was sponsored by invitation 733 from Colciencias, as part of the program for formation of high-level human talent for the regions, from the Government of Boyacá.

Some results come from the research internship in the Materials Analysis laboratory of the Institute of Theoretical and Applied Mechanics of the Czech Academy of Sciences, Telc, Czech Republic, under the supervision of the Professor Alberto Viani.

Acknowledgements / Agradecimientos

"Clama a mí, y yo te responderé, y te enseñare cosas grandes y ocultas que tú no conoces"… Jeremías 33:3 (Biblia RV-1960). Con profunda gratitud a Dios, mi creador. Su compañía y fortaleza hicieron la diferencia a través de los difíciles momentos de este proceso.

A mi esposa Lucely, a mis hijos Ammy y Samuel. Su amor, apoyo y paciencia fueron el aliciente necesario para abordar los retos de cada día.

A mi Padre Leonidas (q.e.p.d.), por soñar y creer que era posible la realización de todos los sueños.

A mis hermanos, suegros, cuñados y familia que siempre me apoyaron incondicionalmente, compartiendo las alegrías y tristezas.

A mi tutora, la profesora Maryory Gómez por sus conocimientos científicos, orientación, apoyo y por la maravillosa habilidad de creer y confiar en las personas.

A cada uno de mis compañeros del grupo CIDEMAT, por brindarme la amistad y compañerismo en muchas de los desafíos del aprendizaje.

A la Gobernación de Boyacá y el programa de formación de capital humano de alto nivel para las regiones, por el apoyo económico brindado para poder asumir este proceso de formación.

I would like to thanks, to Professors Alberto Viani and Jakub Novotny, for allowing me to enter in the Materials Analysis laboratory of the the Institute of Theoretical and Applied Mechanics of the Czech Academy of Sciences. Their knowledge, friendship and constant support allowed to develop the research internship, which was decisive in the concretion and culmination of this doctoral process.

Abstract

Chemically bonded phosphate ceramics (CBPC) have high mechanical strength, some exceeding the mechanical strength of Portland cements, such as magnesium phosphate cements (MPC). However, obtaining these cements involves the treatment of metal oxides through thermal processes with high energy consumption. Likewise, the most used chemical precursors is the orthophosphoric acid, which increase the costs in the synthesis of these cements. One approach to address the present problem includes the use of unconventional raw materials, which can provide the required ions in the acid-base reactions of these types of cements. EAF and BOF steel slags contain significant amounts of divalent metal oxides like wüstite (FeO) and divalent-trivalent metal oxides like magnetite that can act as formers of iron phosphate compounds. Likewise, the phosphoric rock used to obtain phosphate compounds and which in some regions of the world is underutilized because it does not have the content of P_2O_5 for industrial use processes, is presented as an important option in the formation of these cements. For this reason, this work evaluates the behavior of steel slag (EAF - BOF) and phosphoric rock as potential raw materials to form CBPC for possible applications in construction materials.

Initially, a literature review is carried out to elucidate the advantages and disadvantages of phosphate cements in comparison with existing technologies and the mechanical possibilities of these cements as materials for applications as construction materials.

Slag was collected from different steelworks in Colombia following standard sampling practice. The different raw materials were characterized by granulometric analysis, SEM / EDS, FTIR, XRD and XRF. The cements obtained were analyzed by XRD, SEM-EDS, FTIR, XPS, ICP-OES, ICC,

TGA and compressive strength tests, the chemical stability of these compounds was also investigated to establish their durability.

Three different types of CBPC were synthesized from the type of anionic precursor used, as they are: i) by using aqueous solutions of orthophosphoric acid, ii) by using concentrated phosphoric rock leached with H_2SO_4 and iii) by using potassium dihydrogen phosphate (KDP) KH_2PO_4. From the aqueous solutions of otophosphoric acid, multiphase phosphate cement was obtained with a glassy structure for the iron phosphate phases and a crystalline structure for the calcium phosphate phases, compressive strengths of up to 20 MPa were recorded for the different compositions evaluated, with short setting times. The use of phosphoric rock showed the formation of Brushite type calcium phosphates, the mechanical strengths recorded are mainly attributed to the abundant amount of anhydrite and gypsum present in the binder. To induce a greater formation of iron phosphates, the reaction of EAF slag and KDP is promoted, thus allowing the description of the kinetic model in the formation of slag-based phosphate cement, amorphous products were observed in the form of metal phosphate hydrates and a fraction of calcium silicate hydrates, similar to those found in Portland cement, the phosphate matrix allows the effective immobilization of heavy metals in the slag, such as Cr and As, mechanical tests showed a compressive strength of 15-25 MPa.

The oxides contained in the slags (EAF-BOF), especially CaO and FeO act as alkaline components in acid-base reaction systems for the synthesis of CBPC, the cements thus formed show moderate mechanical strength and facilitate possible applications as construction materials, the type of acid component used influences the developed microstructure, showing amorphous structures, with a prevalent formation of iron phosphates as the main phase of these cements, conditioning the mechanical strength and improving the durability of the cement. The variety of oxides contained

in slags affects the cement formation rate, limiting the type and quantity of formed cementitious products.

EAF slag-based phosphate cement is presented as a possible real field application in mortars or structural bricks, which describes a new way of recycling slag to obtain cement, while reducing the environmental impact of phosphate cement synthesis, because it eliminates the high energy consumption required for the calcination of alkaline compounds, allowing in turn its use without restrictions as a construction material.

Research Output

The thesis is a summary of the following papers:

Engineering applications of chemically-bonded phosphate ceramics. *Carlos Andrés Cárdenas-Balaguera and Maryory Astrid Gómez-Botero*. Ingeniería e Investigación, volume. 39 No. 3, December - 2019 (10-19). http://dx.doi.org/10.15446/ing.investig.v39n3.81424

Characterization of steel slag for the production of chemically bonded phosphate ceramics (CBPC). *Carlos Andrés Cárdenas-Balaguera and Maryory Astrid Gómez-Botero*. Construction and Building Materials, volumen 241, April 2020 (1-11). https://doi.org/10.1016/j.conbuildmat.2020.118138

Multiphase phosphate cements from steel slags. *Carlos Andrés Cárdenas-Balaguera and Maryory Astrid Gómez-Botero*. Journal of Sustainable Cement-Based Materials, December 2020. https://doi.org/10.1080/21650373.2020.1863275

Assessment of phosphoric rock and electric arc furnace slag (EAF) as raw materials for the formation of chemically bounded phosphate ceramics (CBPC). *Carlos Andrés Cárdenas-Balaguera and Maryory Astrid Gómez-Botero*.

In preparation.

Formation, properties and microstructure of a new Steel slag - based phosphate cement. *Carlos Cárdenas, Petra Mácová, Maryory Gómez, Lucie Zárybnická, Radek Ševčík, Alberto Viani*.

Accepted for publication. ASCE's Journal of Materials in Civil Engineering. DOI 10.1061/(ASCE)MT.1943-5533.0003958

Congress and meetings in the thesis subject:

Carlos Andrés Cárdenas-Balaguera and Maryory Astrid Gómez-Botero. XIX Congreso Internacional de Materiales – CIM 2017. “Caracterización de materias primas colombianas para la obtención de materiales cementantes ecoeficientes”.Barranquilla, Colombia, 2017

Contributions of this thesis

The main contributions of this thesis are presented, to the assessment of steel slag and phosphoric rock to obtain iron phosphate cements for applications in building materials.

The first contribution was the exhaustive bibliographic review of the engineering applications of phosphate cements, to provide a clear frame of reference for these cements and performance possibilities as a potential building material. Details of this review are in Chapter 1.

The second contribution is the characterization of industrial waste and Colombian raw materials, foreseeing possible applications in CBPC, under the acid-base reaction system, particularities of these characterizations are found in chapters 2 and 4.

The third is the proposal of models to obtain an optimal composition of steel-slag based phosphate cements, using linear regression models for each type of slag and different factors, expressed from the mathematical calculation with the compressive strength as the response variable. These models are shown below, additional details can be found in Chapter 3.

C-EAF 1 = -62.7425 + 1.6308*b + 45.6422*c -1.0360*b*c

C-EAF 2 = -62.7425 -34.3347 + 1.6308*b + 45.6422*c + 0.6628*b + 0.7622*c -1.0360*b*c

C-BOF = -62.7425 -53.3492 + 1.6308*b + 45.6422*c + 0.5028*b + 17.1200*c -1.0360*b*c

C-FINE = -62.7425 -46.4100 + 1.6308*b + 45.6422*c + 0.8087*b + 4.9000*c -1.0360*b*c

The fourth contribution is the description of the formation, properties and microstructure of a new environmentally friendly steel slag-based phosphate cement, with medium mechanical strengths, suitable for bricks and masonry mortar applications (according to standard ASTM 270-07/ASTM C62), It is proposed to obtain these products with low energy consumption, eliminating in their synthesis the intervention of high temperatures for the treatment of their raw materials. In addition,

the durability and ability to encapsulate hazardous elements is evaluated. Corresponding details are in chapter 5.

The fifth contribution makes mention of the description of the kinetic model in the formation of steel slag-based phosphate cement details on the dissolution of raw materials and phenomena associated with the reaction of ions in the acid-base system can be found in chapter 5.

The sixth contribution corresponds to an approach to the description and understanding of the amorphous structures present in the developed cements, in the form of metal phosphate hydrates and a fraction of calcium silicate hydrates. This phenomenon has recently taken interest since its presence substantially affects the performance of cement and that for steel slag-based phosphate cements it corresponds to its main phase. Attributing to the amorphous phase as responsible for the main mechanical strength reported. Likewise, this amorphous phase contributes to improving the durability of the cement. Details corresponding to the main reaction products, kinetics, phase quantification, among others, are observed in chapters 3 and 5.

The last contribution is the reuse of industrial waste such as steel slag for the formation of CBPC. Reuse away from conventional applications including, but not limited to: storage and stockpiling, application in road construction as aggregates and use for partial replacements in different cementitious systems, details of this are contained in chapters 2, 3, 4 and 5.

Table of Contents

Introduction

ACID-BASE CEMENT AND PHOSPHATE CEMENT

Acid-base cements emerged in the mid-19th century as dental cements and are defined as a mixture of basic powders and acidic liquids, with a rapid hydration, forming solid substances with various applications [1], in this type of cements, phase diagrams are not useful to describe the course of their formation, since it is doubtful to reach the conditions of thermodynamic equilibrium in fast-setting cements [1]. Chemically bonded phosphate ceramics (CBPC) were discovered and developed as acid-base reaction cements, between an aqueous solution of orthophosphoric acid and an oxide or silicate at room temperature, which are formed as cements but share properties and structural characteristics with ceramics [2]. Iron phosphate cements with a predominantly amorphous structure [2], originate as mixtures under the acid-base reaction system, between aqueous solutions of orthophosphoric acid and iron oxides, among which are wüstite (FeO) and magnetite (Fe_3O_4). Hematite (Fe_2O_3) is the most stable and abundant compound of iron oxides, but it does not react to form CBPC, in contrast wüstite and magnetite have a sufficiently high solubility to form coherent ceramics [3]–[6]. Considering iron as the third most abundant element in the earth's crust, the participation of iron oxides is important as an available raw material in the formation of CBPC; in addition to the above, it is presumed that the existence of other mineral compounds and industrial wastes rich in soluble iron oxides can act as CBPC formers.

It is difficult to explain the formation of phosphate cements from Portland chemistry, where the formation mechanisms differ from those used in acid-base reaction systems, although they exhibit similar physical characteristics [7]. Properties such as rheology, magnesia-to-phosphate molar ratio (M/P), liquid-to-solid ratio (L/S), reactivity of powders, effect of retardants such as boric

acid, borax, sodium, tripolyphosphate, sodium sulfonate and citric acid, particle size distribution, durability, reactivity, fluidity and strength, have been widely studied in phosphate cements [7]–[11].

An important bibliographic review is presented in this research, compiling relevant information with special emphasis on the engineering applications of CBPC, in order to understand the performance of phosphate cements in the context of building materials, finding that the main phosphate cements with relevant applications are calcium, iron, and magnesium phosphates, the latter highlighting for its greater development.

Due to its wide range of applications, magnesium phosphate cement (MPC) is the greater diffusion and researching phosphate cement [2], [7], the most relevant findings to explain the formation mechanisms of phosphate cements are observed in research at MPC [12]–[16]. The analysis of the reaction kinetics shows, that it is directly influenced by the reactivity of MgO and its grain size, impacting the dissolution rate of MgO and substantially affecting the formation of amorphous and crystalline phases in MPC [15]. Amorphous and crystalline reaction products have been identified in this type of cement, initially show the formation of an amorphous orthophosphate hydrate precursor and a more amorphous second phase, whose chemical nature is not fully disclosed and with some similarities to the MPC, such as the crystalline networks of magnesium potassium phosphate $MgKPO_4 \cdot 6H_2O$ (MPC) which are attributed as responsible for mechanical strength [7]–[10]. The formation of amorphous phases compromises a significant amount of water, hindering the crystallization of the MPC and affecting the mechanical strength of the cement [11]. The setting reactions of the amorphous precursors are in analogy with the sol-gel processing of ceramics, crystallization processes of calcium phosphates and zinc phosphates [16]. The formation of the amorphous phase of MPC has taken more interest recently, because its presence substantially

affects the microstructure and performance of cement [9], [12]. Through the use of various techniques such as NMR and X-ray micro tomography, it has been possible to elucidate the role of water in the formation of the microstructure of magnesium phosphate cements, allowing to understand that at stoichiometric ratios or in a lower proportion of water, they originate high levels of saturation of the MgO grains, triggering reactions far from thermodynamic equilibrium, thus favoring the formation of amorphous phase that fills the volume of the solid and directly influences crystallization, the water in excess to respect to stoichiometry of MPC reaction, favours crystallization of platelet over acicular crystals and is likely related to a change in reaction mechanism [13].

Given the advances in the understanding of the mechanisms of formation of magnesium phosphate cements, the scarce transfer and verification of these models in other types of phosphate cements is notorious, especially the explanation and research on the phenomenon of formation of amorphous phases, phenomenon of clear presence and relevance in iron phosphate cements as mentioned above. The presence of amorphous phases modifies the structural behavior of phosphate cements, especially when some researchers suggest that amorphous phases should theoretically be the main phases in acid-base reaction cements and that their presence in the matrix must be the majority [1], also associating these structures as one of the reasons for the improvement of the chemical resistance of these cements [10], [14], influencing their durability.

STEEL SLAG

The chemical composition of steel slag shows an abundant presence of iron and calcium oxides [17]–[19], mainly wüstite (FeO), synthesized thanks to the high production temperatures of the slags (at 1600 °C), these oxides are forming main phases or in solid solution in other compounds

[20]; therefore, in the presence of various types of oxides and other components in the slags, the result to be obtained in possible mixtures to form CBPC is uncertain, probably inducing formations of multiphase phosphate compounds with the concurrence of calcium oxides and iron oxides mainly. In recent years, the addition of steel slag as a raw material for the production /synthesis of magnesium phosphate cement has been observed as a partial replacement for magnesium oxides [21]–[23], in an attempt to reduce the consumption of resources associated with the high calcination temperatures of MgO, making its use possible in CBPCs. However, few studies have been conducted where iron phosphate cements are synthesized with only steel slag as the alkaline component of the system [24], this approach would imply environmental and economic benefits.

PHOSPHORIC ROCK

On the other hand, the alkaline components commonly used in the formation of phosphate cements are acid phosphates of the type monopotassium phosphate (KH_2PO_4), ammonium acid phosphate [$(NH_4)H_2PO_4$] and orthophosphoric acid (H_3PO_4) [2], where the soluble P_2O_5 content provides the phosphate anions required for acid-base reaction systems. These compounds are originally derived from phosphate minerals such as phosphoric rock with typical presence of fluorapatite ($Ca_{10}F_2(PO_4)_6$) [25]–[27]. The mining and exploitation of phosphate minerals is subject to techniques to solubilize the mineral, currently different techniques are used to produce soluble phosphates [26]. However, in some countries such as Colombia, an important part of the production of phosphate rock is underused as acid soils amendments, mainly due to its low level of exploitation (<30%) [25], in addition to the release of heavy metals in their treatment such as As, Pb, Cd, Cr, F, Zn, Cu [28], [29], factors that invite to seek exploitation routes as raw material for obtaining CBPC, allowing the solubilization of this mineral at the same time as the encapsulation of the dangerous elements, thus guaranteeing the rational use of this resource.

PORTLAND CEMENTS, RAW MATERIALS AND ENVIRONMENTAL IMPACT

The environmental impact caused by the production of traditional cementitious compounds [30], [31], is of significant importance, great efforts have been made to reduce the environmental impacts of this type of materials [32], [33]. In this sense, alternative materials have been tested with that reduce the environmental impact, among them are phosphate cements, in particular, magnesium phosphate cements whose superior mechanical properties in contrast to Portland cement [34], [35], offer important possibilities as an environmentally friendly material; however, the processing of raw materials such as MgO with calcination temperatures similar to Clinker Portland [36], substantially influence production costs and consequently the consumption of resources for its synthesis.

In the synthesis of environmentally friendly cementitious materials, the use of raw materials with low environmental impact is important. The reduction of energy consumption through the reuse of industrial wastes, added to the rational use of natural resources through innovative methods of formulation and production of cements, are established as important pillars for the achievement of eco-sustainable materials for construction applications [37]. Raw materials such as steel slag and Phosphoric Rock offer interesting potential as possible components for the formation of CBPC, but, the use of these entails important technological and scientific challenges for their exploitation. The presence of metal oxides in the chemical composition of steel slag is exceptional, including oxides of different metals not forming CBPC [2], [3] that significantly affect the solubility and kinetics of these cements, condition that induces the application of complex slag transformation processes to reach the alkaline elements necessary for the synthesis of phosphate cements. Likewise, the lack of solubility and the presence of abundant gangue minerals in the structure of phosphoric rock [38]–[40] induces processes of benefit and refinement to find acid compounds for

acid-base systems, with properties corresponding to construction materials, without incurring additional costs and processes.

Consequently with the above, this research proposal contributes to understanding the relationship between the properties of unconventional raw materials and the properties of iron phosphate cements, synthesized from these raw materials, such as: workability, curing times, mechanical strength, chemical composition, microstructure, porosity and shrinkage. In this doctoral thesis CBPC were developed, using raw materials scarcely referenced in the literature for the formation of CBPC, such as: EAF, BOF and LF steel slags that act as an alkaline component for acid-base reactions; and aqueous solutions of H_3PO_4, potassium dihydrogen phosphate KH_2PO_4 and phosphoric rock as an acid component. The synthesis of Steel Slag–Based Phosphate Cement has not been reported to date, so that knowledge about their behavior is non-existent. This research proposes an environmentally friendly alternative, which represents an opportunity for the reuse of industrial waste, taking advantage of the high potential for formation of acid-base cements and the residual hydraulic activity of calcium silicates. The content of each of the chapters of this thesis is described below.

Document Overview:

Chapter 1. Presents the review on the basic concepts and structural applications of phosphate cements, commonly known as chemically bonded phosphate ceramics (CBPC). Analysis of the mechanical strength achieved by the different phosphate cements, visualizing their relevance and potential use is showed. Commercial products of this type of cement and the immobilization of radioactive waste and hazardous elements as the most frequent application are also assessed.

Chapter 2. The chemical, morphological and mineralogical characterization of different steel slags is presented, and their physical properties are also described. The high presence of iron oxides and calcium oxides, present in the form of dicalcium silicates, dicalcium ferrites and wüstite as the main phases in the slags, are manifested as definitive characteristics, forming CBPC. Preliminary mixtures of steel slag and aqueous solutions of orthophosphoric acid are made, evaluating their mechanical behavior and chemical stability.

Chapter 3. Results are presented on the application of the Design of Experiments (DoE) methodology, to make viable the variables in the formation of slag-based phosphate cements. Four types of cements were synthesized from steel slag and aqueous solutions of orthophosphoric acid, evaluating the different proportions of acid and alkaline components, as well as additives to obtain CBPC. The cements obtained mainly exhibited amorphous structures for iron phosphate ($Fe(H_2PO_4)_2$) or ($FeHPO_4$) and crystalline phases for dihydrogen phosphate of calcium hydrate ($Ca(H_2PO_4)_2 \cdot xH_2O$) and brushite ($CaHPO_4 \cdot 2H_2O$). Mechanical strengths between 10 and 19 MPa with short setting times were observed for the different cements obtained.

Chapter 4. The results of the evaluation of the physical, chemical and mineralogical characteristics of phosphoric rock are presented, showing an important presence of P_2O_5, as a possible source of phosphate anions. EAF slag is used as an alkaline component for the formation of cements, due to its higher content of iron oxides for the synthesis of possible iron phosphates. Procedures are shown to upgrade and concentrate phosphoric rock, in order to make its use viable in the formation of CBPC. An incipient formation of brushite-type calcium phosphate binder is evidenced, the scarce formation of which is mainly inhibited by the presence of gypsum and anhydrite.

Chapter 5. The formation of phosphate cements based on EAF slag and potassium dihydrogen phosphate (KH_2PO_4) is presented, both fresh and after cured. The reaction mechanisms are described from the evolution of synthesis reactions of amorphous products such as metal phosphate hydrates and hydrated calcium silicates, using In-Situ techniques. The matrix formed allows the immobilization of heavy metals such as Cr and As. The chemical stability and mechanical strength of cements are analyzed, allowing to elucidate possible applications such as mortars and bricks as building materials.

Research hypothesis:

Phosphoric rock and steel slag are sources of phosphate anions and metal cations within the acid base system for the synthesis of iron phosphate cementitious materials, with potential mechanical, physical and chemical properties for use as building materials.

Scientific research problem:

How does phosphoric rock and steel slag influence the synthesis of iron phosphate cements and the properties of these cements for their potential use as building material?

Objectives:

General Aim

- Establishing the effect of phosphoric rock and steel slag (EAF-BOF) on the synthesis of iron phosphate cements and their properties for possible applications as building materials.

Specific Aims

- Establishing the influence of chemical, microstructural and physical properties of phosphoric rock and steel slag (EAF-BOF) in the synthesis of iron phosphate cements.
- Describing the synthesis reactions of the iron phosphate cements by using good resolution techniques in order to optimize them.
- Evaluating the effect of different ratios of the acidic and basic components, as well as of additives in the chemical composition and the performance of the iron phosphate cements.
- Analyzing the physical, mechanical, morphological and microstructural properties of the iron phosphate cements, both in-situ and after curing.

Achievement of goals and Methodology aspects:

General Aim	Specific Aims	Methodology aspects
Establishing the effect of phosphoric rock and steel slag (EAF-BOF) on the synthesis of iron phosphate cements and their properties for possible applications as building materials.	Establishing the influence of chemical, microstructural and physical properties of phosphoric rock and steel slag (EAF-BOF) in the synthesis of iron phosphate cements.	**Chapter 1.** Analysis of the mechanical strength achieved by the different phosphate cements, **Chapter 2.** Characterization of different steel slags. Preliminary mixtures of steel slag and aqueous solutions of orthophosphoric acid are made, evaluating their mechanical behavior and chemical stability. **Chapter 4**. Evaluation of the physical, chemical and mineralogical characteristics of phosphoric rock.
	Evaluating the effect of different ratios of the acidic and basic components, as well as of additives in the chemical composition and the performance of the iron phosphate cements.	**Chapter 3.** Application of the Design of Experiments (DoE) methodology, to make viable the variables in the formation of slag-based phosphate cements.
	Analyzing the physical, mechanical, morphological and microstructural properties of the iron phosphate cements, both in-situ and after curing.	**Chapter 4**. Chemical, morphological and mineralogical characterization of EAF slag and phosphate rock-based binders. **Chapter 5.** Chemical, morphological and mineralogical characterization of EAF slag-based cements and potassium dihydrogen phosphate (KH_2PO_4)
	Describing the synthesis reactions of the iron phosphate cements by using good resolution techniques in order to optimize them.	**Chapter 5.** The formation of phosphate cements based on EAF slag and potassium dihydrogen phosphate (KH2PO4) is shown. The reaction mechanisms are described from the evolution of synthesis reactions of amorphous products such as metal phosphate hydrates and hydrated calcium silicates. The chemical stability and mechanical strength of cements are analyzed to elucidate possible applications such as mortars and bricks as building materials

1. Engineering applications of chemically-bonded phosphate ceramics

This chapter corresponds to the article: http://dx.doi.org/10.15446/ing.investig.v39n3.81424

Abstract: Phosphate cements originated more than a century ago for specific applications to the field of dentistry. These cements have other applications including: biomaterials with bone applications, stabilization of hazardous waste, and structural cements. However, the applications in civil infrastructure are recent and not widely known. Therefore, this review analyzes phosphate cements, presenting the most significant findings of the research to address their mechanical behavior of these cements. It also describes the impact and application of phosphate cements as a structural product (pastes, mortars and concretes), in addition to typical values of mechanical strength, workability, commercial applications, etc. As a result, the review allows to elucidate advantages and disadvantages in comparison with existing

technologies and the mechanical possibilities of these cements as biomaterials and for the immobilization of radioactive waste.

1.1 Introduction

Ceramic and hydrated cements are the most recognized products of inorganic solids. Ceramics are obtained by compaction of powders and subsequent sintering at high temperatures, resulting in hard and dense ceramics with good properties. Its structure is usually highly crystalline with vitreous phases, presenting ionic and covalent bonds. Hydrated cements are chemically-bonded materials with hydrogen bonds that are formed by the chemical reaction of water with some characteristic powders that harden at room temperature, obtaining a product with sufficient compressive strength, to be used in structural applications [2]. These cements are usually united by Van der Waals forces, exhibiting a non-crystalline, very porous structure. It is worth noting that the most noticeable difference between ceramics and hydrated cements lies in their consolidation process as a material. To obtain ceramic hard products, materials must be exposed to high temperatures. In contrast, hydrated cements reach hardness at room temperature [2], although raw materials are subjected to high temperatures for their manufacture and considerable energy consumption is needed to obtain the clinker [31], which is the main component of conventional Portland cement.

However, there is an intermediate product among those mentioned above, which consolidates similarly to a hydraulic cement, but resists and behaves structurally as a ceramic. As it presents bonds of the ionic and covalent type, its structure varies from very crystalline to vitreous, showing compressive strengths similar to conventional cement and setting times faster than hydraulic cements [2]. This intermediate product that contains crystalline or non-crystalline phases and sets

at temperatures close to that of the environment is known as chemically-bonded ceramics (CBC) [41]; [42].

The chemically-bonded phosphate ceramics (CBPC) are a specific type of chemically-bonded ceramics (CBC), formed from reactions of phosphate anions with metal cations. The CBPC have had an important development in the last two decades, mainly due to the search for environmental alternatives for the manufacture of cements [42].

A significant environmental impact in terms of energy consumption and generation of greenhouse gases is a widely known result of the production of conventional Portland cement [30], [33]. Therefore, the search for different cement alternatives that are friendly to the environment has led researchers to coin the term "eco-efficient cements" or "green cements". Magnesium phosphate cements are recognized as eco-efficient commercial products, due to their low environmental impact, in addition to their good mechanical performance, availability of raw materials and manufacturing facility. Under the names of "Ceramicrete" and "Grancrete", these types of cements are some of the more promising eco cements [37].

There is a positive impact of phosphate cements in the environmental context [42]. This article reviews the mechanical performance of phosphate cements and their structural requirements in contrast to Portland-type conventional cements.

1.2 Basic concepts of phosphate cements

1.2.1 Acid-base reaction system of chemically-bonded ceramics (CBC)

Chemically-bonded ceramics are structured as an acid-base reaction. These reactions originate from a base, usually powders of a metal oxide or a silicate, with an acid. The product of the reaction is a complex salt that acts as binding agent or cementing matrix, besides the presence of water.

The excesses of the alkaline base that do not react become part of the cement fillers. The great majority of these reactions are fast and mainly exothermic [43].

The process for forming cements under the acid-base reaction system is described below [43] and illustrated in Figure 1 [44].

• Dissolution of the alkaline base in an acid solution, to facilitate the formation of cations.

• Interaction of anions and cations in the solution to form neutral compounds.

• Gelification of the compound and saturation of the solution with the compound.

• Precipitation of solids in the saturated gel solution forming connected networks of the types: crystalline, semicrystalline and disordered solids.

In the specific case of phosphate cements, the reactions to combine the cations and phosphate anions can take place in solution at normal or hydrothermal pressures or by combinations at high temperatures to overcome the kinetic barriers. The transformations of phosphates into new structures can be achieved thermally or through ion exchange reactions [45].

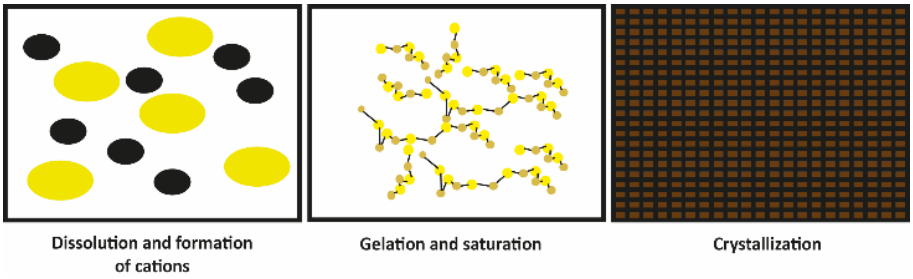

Figure 1. Steps in the formation of chemically-bonded ceramics.

Source: Adapted from Wagh (2004).

1.2.2 Chemically-bonded phosphate ceramics (CBPC) or phosphate cements

Phosphate cements are essentially an acid-base system that reacts at room temperature [2]. These cements are formed by the reaction of phosphoric acid or an acid phosphate with metal oxides,

where the acid component contributes to the phosphate anions and the basic component to the metal cations, necessary for the cement shaping reaction (Figure 2).

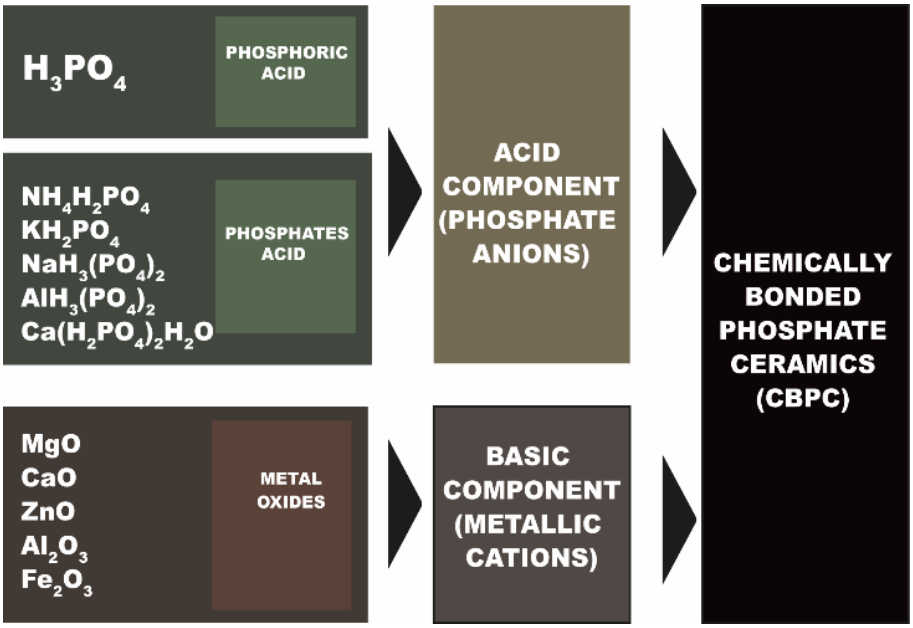

Figure 2. Components in the formation of phosphate cements.

Although phosphate cements are more expensive than Portland cements, the former are projected as one of the special cements with the highest development potential [45], [46]. Some of the main reasons are the ease and safety to handle their reagents and that they are non-toxic and stable at high temperatures (1000 °C) [45] and have a wide pH range, available raw materials and low environmental impact, in addition to good reported mechanical properties. Five types of cement are recognized as typical phosphate cements: magnesium phosphate, calcium phosphate, zinc phosphate, aluminum phosphate and iron phosphate. Among them, magnesium and calcium phosphate cements stand out for having the highest development in structural applications. Some of the reactions and main products responsible for the mechanical properties in phosphate cements have been presented by Wagh (2016) and [47], and are listed in Table 1.

Table 1. Typical reactions and products of phosphate cements

Phosphate cement	Chemical reaction	Main formed product	Reference
Calcium Phosphate	$CaSiO_3+H_3PO_4+2H_2O \leftrightarrow SiO_2{\cdot}H_2O+CaHPO_4{\cdot}2H_2O$	Brushite	[48]
Zinc Phosphate	$3ZnSO_4{\cdot}7H_2O+2NaHPO_4{\cdot}2H_2O \rightarrow Zn_3(PO_4)_2{\cdot}4H_2O+H_2SO_4+2Na_2SO_4+21H_2O$	Hopeite	[49]
Aluminum Phosphate	$Al_2O_3 + 2AlH_3(PO_4)_2{\cdot}H_2O \rightarrow 4AlPO_4 + 4H_2O$	Berlinite	[50]
Iron Phosphate	$Fe_2O_3 + Fe + 6H_3PO_4 \rightarrow 3Fe(H_2PO_4)_2 + 3H_2O$	Iron Dihydrogen phosphate	[51]
Magnesium Phosphate	$Mg_3(PO_4)_2{\cdot}4H_2O \rightarrow NH_4MgPO_4{\cdot}6H_2O$	Struvite	[52]

1.2.3 Environmental impact of phosphate cements and Portland cements

It is unfeasible to establish a definitive relation of the environmental impact of phosphate cements compared with Portland, due to the low development of the former. However, some of the phosphate cements with the highest impact and development are magnesium phosphate cements, which can be used as reference, specifically the commercial application Ceramicrete with the addition of fly ash, for a comparison with Portland cements. Production of greenhouse gases for Ceramicrete consists mainly in carbon dioxide, under two premises. First, there are greenhouse gases produced in the transformation of raw materials, that is, by the decarbonization of limestone and dolomite, called direct emissions. Second, some gases are associated with the combustion of fossil fuels in different stages of the process, such as calcination, milling, screening, transport and packaging among others. These are called process emissions, in addition to the energy consumed in the transformation processes to obtain the cements [42]. Wagh (2013) establishes a first approach to the environmental impact of the phosphate cements. Table 2 presents a parallel comparing the environmental impact of the two technologies. This parallel allows to conclude that the energy consumed and the greenhouse gases released by the processes of magnesium phosphate cement are approximately 40% less, in comparison with conventional Portland technology [2].

Table 2. Environmental impact of the production of phosphate cements

Product	Composition	Energy consumption (MJ/ton)	Greenhouse gases (ton/ton)	Main process
Ceramicrete	$MgKPO_4 \cdot 6H_2O$ + Fly ash	2 186	0.32	Calcination, release of CO_2 and chemical process.
General purpose Portland cement	Mixture of oxides, sulphates and silicates.	4 800	0.85	Calcination, CO_2 release and mechanical processes

Source: Adapted from Wagh (2016).

In addition, phosphate cements can be referred to as eco-efficient or eco-friendly products. Several authors have tried to link alternative raw materials and additives of low environmental impact in the formation of cements. The review of some researches evidenced the use of substitute raw materials that reduce manufacturing costs and reuse of industrial waste as source of raw materials [24], [53]–[55]. This fact has a substantial impact, since it allows to diminish the environmental impact produced by the exploitation and transformation of conventional raw materials.

1.2.4 Biomaterials of phosphate cements

There is a group of phosphate cements that exhibit relevant mechanical properties, although it is not completely applicable in civil engineering. These cements have generated a great scientific interest in recent years [56]–[58]. The applications are confined to the human body due to biocompatibility, among other reasons. This group of phosphate cements is identified in the group of biomaterials, briefly described below.

1.2.5 Dental cements: Zinc phosphates

Zinc phosphate cements are the oldest known dental cements, as they were developed in 1880. Although at present they are not widely used in comparison with new materials that have emerged [58], they still find a subsistence niche in cemented restorations.

Dental cements of zinc phosphate are obtained by mixing phosphoric acid and zinc oxide. Due to the strong reaction that originates, aluminum hydroxide has been used to neutralize the reaction. These cements have reached compressive strengths between 71 and 131 MPa and tensile strength between 4.3 and 8.3 MPa [2]. Dental porcelain cements consisting of alumina, vitreous silica, calcium oxide, sodium oxide, fluorine, zinc oxide and phosphoric acid are probably the inorganic cements with the highest reported mechanical strength. They have a compression strength of 255 MPa, bending stress of 24.5 MPa and tension of 13.6 MPa. However, the fracture tenacity of 0.12 to 0.3 MPa/m^2 indicates the fragility of this cement [2].

1.2.6 Cements for orthopedic applications: Calcium phosphates

Calcium phosphate cements mainly precipitate as hydroxyapatite, which is a basic mineral constituent of the bones. That is why this type of cement will always be one of the main alternatives of use in this field. In addition, these cements are easily grafted with rapid hardening in the bones of the human body and minimal intrusion implications. These cements are used in special applications such as bone augmentation, bone reinforcement, metal implant fixation and spinal fractures [59]. The cortical bone is the external part of the bone that represents its main mechanical properties. Table 3 describes these properties compared to calcium phosphate cement. The main aspect is the similarity in the density of these two materials, which is inferior when compared with typical metal prostheses such as titanium [44]. There are also great similarities in compression strength and Young's modulus. Advances in future research are expected to improve biocompatibility, resistance to stress and fracture.

Table 3. Mechanical properties of calcium phosphate cements.

Property	Cortical bone	Calcium phosphate cement
Specific Gravity (g/cm^3)	1.7-2.1	1.7 – 2.0
Tensile Strength (MPa)	60 - 160	2.1 - 14
Compressive strength (MPa)	13 - 18	20 - 91
Young's Modulus (GPa)	3 - 30	35 - 105
Fracture energy (J/m^2)	390-560	----------
Resistance to fracture (MPa/m^2)	2 - 12	0.3 – 0.8
Composition	Inorganic + organic	Inorganic

Source: Adapted from Wagh (2004).

1.3 Phosphate cement for structural applications

Research in phosphate cements began at the start of the 20th century and resulted in the main development of dental cements and biocements. In the year 2003, Wagh, Grover and Jeong published a literature review of abstracts of articles from the years 1988 - 2002 (Table 4). They described the low percentage of research developed in structural applications. Only 5.6% of applications are structural, perhaps due to the difficulty of industrially scaling this type of cement, where production volumes are considerable. However, the low percentage can also suggest an important development potential.

Table 4. Phosphate Cement Research

Items	Percentage
Articles on biomaterials and dental cements	68 %
Structural materials	5.6%
Refractory materials	12.6%
Structure of materials, properties, etc.	13.9%
Total number of articles found relevant to low temperature phosphate cements and ceramics (2 264)	100%

Source: Adapted from Wagh (2004).

The first cements for structural purposes were developed at Brookhaven National Laboratory (BNL) in the United States (1970). Looking for applications of magnesium phosphate cements, aluminum, Pb and Fe phosphates were also researched without finding practical applications at the structural level. From the Argonne National Laboratory research in the decade of 1990, the possibilities of application of magnesium phosphate cements for structural uses were extended, specifically in the immobilization of dangerous and radioactive waste [2]. The research developed in the Argonne National Laboratory, which is evidenced by numerous publications and patents, is substantially important to describe the progress of this type of material.

Trying to define a frame that contains the generalities of the mechanical properties of the phosphate cements is a complex challenge, because phosphate cements have a great variability of compositions, offering a wide range of mechanical properties. However, the significant development experienced by magnesium phosphate and calcium phosphate cements can be used as reference to explain the mechanical behavior of these compounds. Table 5 presents a general framework of phosphate cements, with the purpose of contrasting their main differences and similarities. In many cases, phosphate cements show mechanical properties superior to the conventional Portland cements. However, producing phosphate cements as commercial products (pastes, mortars and concretes) is more expensive than producing a conventional cement. Therefore, specific applications with added value are projected as commercially viable possibilities [42].

1.3.1 Magnesium Phosphate Cements

1.3.1.1 Phosphate cement pastes

Phosphate cement pastes comprise the reaction between the acidic and basic components without other additional components. This frames the fundamental model for the analysis and understanding of these cements. However, in practical terms, making cements with only these components promotes additional costs that oppose to the approach of making products of this type of cements more commercially available. Below significant findings are explained on their mechanical properties.

The proportion of raw materials is an important factor that requires differences in terms of mechanical strength. A. Wang, Yuan, et al. (2013) calcined the MgO (1200 °C) for 3 hours and dried particles of KH_2PO_4 (100 °C) as acidic component for 6 hours. Then, by grinding, they pre-mixed the two components and dried them for 3 hours forming a powder compound, that was mixed with deionized water in different proportions. The optimum liquid - solid ratio was 1:7, keeping the mixture under stirring until solidification, and the optimum ratio for the MgO/KH_2PO_4 was 4:1, registering compressive strengths close to 40 MPa [60]. These same authors studied the liquid - solid relations. They used KH_2PO_4 and MgO in a weight to weight ratio of 1:1, which constituted the solid component, and used deionized water as liquid component, reporting the formation of cements for liquid (milliliter)-to-solid (grams) ratio of 1:4, 1:3, 2:5, 1:2, 3:5 and 2:3, with compressive strengths between 8 MPa and 22 MPa . The study showed that the compressive strength increased as the water content decreased, linking low porosities with high mechanical resistance [61].

Formosa et al. (2008) proposed the evaluation of a magnesium phosphate cement, composed of potassium hydrogen phosphate (KH_2PO_4) and magnesium oxide (MgO), with contribution percentages between 65% - 45% (MgO) and 45% - 35% (KH_2PO_4) and a water/solids ratio between 0.24 – 0.28. The authors found that increasing the water content and/or magnesium oxides

decreases the compressive strength. They also show that the increase of the curing time is not a significant parameter to increase the mechanical strength, however an increase in the compressive strength is obtained between 10-12% (28 days) reaching values of 79 MPa. The increase of the porosity is due to a greater amount of water and MgO, influencing a decrease in the mechanical strength [53].

Table 5. Features of phosphate cements

Phosphate	Main applications	Main features	Typical ranges of compressive strenght (MPa)	Ref.
Zinc Phosphate	Biomaterial: dental cement	Exothermic reactions, low scale production.	50 - 130	[58] [2]
Calcium Phosphate	Biomaterial: bone cement, structural products in addition to Wollastonite	Exothermic reactions, high manufacturing cost.	20 – 150	[62] [48] [63] [2]
Aluminum Phosphate	Dental porcelain, products resistant to corrosion at high temperatures, refractories and electric insulators	Products superior to most phosphate cements, difficulties to scale products industrially.	30 – 110	[64] [65] [2]
Magnesium Phosphate	Encapsulation of radioactive materials and hazardous waste, sealant in oil wells, corrosion protection coatings, road repair.	Cement of greater development and projection as structural material, wide range of applications from Ceramicrete	20 – 90	[66] [67] [50] [61] [60] [68]
Iron Phosphate	Encapsulation of radioactive material and hazardous waste.	Availability of raw materials at low cost, broad spectrum in the reuse of waste materials	20 -50	[51] [69] [24] [6] [2]

1.3.1.2 Composite cements (mortars, concretes and others)

Phosphate cements also form composite materials similar to Portland cement mortars and concretes. Del Valle et al. formed a composite material from the magnesium phosphate cement

matrix and hemp fibers (Hemp) as a structural phase. The researchers added proportions of hemp with respect the total weight of solids of 8, 12, 16 and 20%; although the additions with 20 % do not substantially outperform mechanical performance. They offer improvements to those found in the literature [68]. Maximum strength σ_{MAX} = 0.71 MPa was recorded. The researchers highlight the excellent thermal and hygroscopic properties of this fiber demonstrated during the tests.

The modulus of elasticity has also been studied for the mineralogical phases of the reaction of magnesium phosphate cement, Morales et al. (2015) analyzed the mechanical behavior of the different minerals present in the cement using the Statistical Nanoindentation Technique (SNT) and Scanning Electron Microscope equipped with Energy Dispersive X-ray analysis (SEM-EDX). The elastic modulus that registered a greater resistance corresponds to the Periclase (MgO). It is a phase of aggregation or filler significantly higher than the K-struvite ($KMgPO_4 \cdot 6H_2O$) that is, the cement matrix. It is worth noting the fundamental role of Periclase for the development of mechanical strength of cement [70].

Some reactive materials that are part of the acid-base system in phosphate cements, in some circumstances, can provide material that do not react by generating phases of the source material, which behave as filler, These phases of material that do not react contribute significantly to the resistant activity of the cements, classifying these mixtures as mortars [71].

Various composite materials have been developed from the matrix of magnesium phosphate cement. Lu, Hou, Ma, Fan, and Li (2016) added different proportions of graphene oxide in order to increase their mechanical strength, determining an ideal proportion of 5 wt.% of graphene. The addition of graphene oxide decreases the workability of the magnesium phosphate cement paste, modifying setting times from 15 minutes to 11 minutes. Likewise, fluidity decreases with the

increase in graphene oxide. This is attributed to the addition of Graphene oxide that accelerates the hydration of cement by possessing a larger specific area, thus absorbing more water and generating an aggregation of the phosphate cement. The addition of graphene oxide has a negative effect on the workability, similar to what happened in Portland cement. However, the compressive and flexural strength improves, with values of 40.61 MPa and 6.82 MPa, respectively. This can also be explained by the decrease in porosity and a greater degree of hydration of the paste [72]. Reactive mineral admixtures as in Portland technology are also used in phosphate cements. Hou, Li, Tong, and Zhang (2012) used calcined coal gangue (with 58.73% SiO_2 and 26.48% Al_2O_3) and calcined magnesia as active addition to obtain magnesium phosphate cements. The addition of calcinated coal gangue increases the setting times from 6.5 to more than 8 minutes, since it decreases the concentration of the used acid phosphate ($NH_4H_2PO_4$). With the addition of the coal gangue, the initial compressive strength (24 hours) increases slightly, then decreases. However, considerable increases in resistance are reported after day 28, reaching resistance of 95 MPa after 360 days with percentages of 10% coal gangue. The authors attribute this phenomenon, to the hydration of the gangue due to the high contents of amorphous silica and alumina [73].

Donahue and Aro [74], applied Ceramicrete (magnesium phosphate cement binder, perfected and patented by Argonne Laboratories) and aggregates such as fly ash, OSB (oriented standard board), fiberboard chip and paper pulp waste to develop consolidated boards under pressure. Physical and mechanical properties were evaluated, complying with all the minimum requirements of the standards for low density boards, except for the modulus of rupture (MOR). The authors showed the great potential of the boards for specific applications.

1.3.1.3 Additives in magnesium phosphate cements

One of the characteristic factors of phosphate cements is the fast setting time, Formosa et al. (2015) contrasted the setting times and the mechanical properties in phosphate cement pastes added with boric acid. The cement was prepared from magnesium oxide (MgO), monopotassium phosphate (KH_2PO_4) and boric acid (H_3BO_3) as retardant. The results showed that the modulus of elasticity increased with the curing time for each formulation, but decreased in the measure that the additive (H_3BO_3) increased. Therefore, increasing the H_3BO_3 decreases the strength [36]. Likewise, applying statistical techniques such as Design of Experiments (DoE), the same authors refined the findings mentioned above, defining ideal additions of 60 wt.% magnesium oxide (MgO), 40 wt.% monopotassium phosphate (KH_2PO_4) and boric acid between 0.5 wt.% and 1.0 wt.%, with a liquid - solid ratio of 0.24. They obtained a cement with good workability reaching final setting times of up to 60 minutes, with constant compressive strengths since the seventh day setting higher than 40 MPa [71].

1.3.2 Calcium Phosphate Cements

Calcium phosphate cements for applications in civil engineering, have been generalized under the name of IPC (Inorganic Phosphate Cement), which are made with an initial mixture of wallastonite ($CaSiO_3$) source of calcium and phosphoric acid (H_3PO_4) source of phosphorus. These compounds react mainly forming brushite ($CaHPO_4 \cdot 2H_2O$), in addition to amorphous silica. Alshaaer, Cuypers, Mosselmans et al [47], researched the mechanical response of calcium phosphate cement for high temperature applications. The researchers reported that for a temperature range between 80 and 200 ^oC the flexural strength decreases from 14 MPa to 7 MPa. This attributed to the appearance of microcracks due to the dehydration of brushite, a situation that does not affect the compressive strength. Between 800 and 1 000 ^oC, an increase in resistance is observed reaching

values of 80 MPa and 12 MPa for compressive and flexural strength, respectively. This occurs due to the healing effect when reaching glass transition temperatures for some phases of the cement. Similarly, the aging effect at room temperature is described, registering an increase in compressive strength of up to 50 %. Continuing with the line of research, Alshaaer [75] proposed a new , hydrothermal post curing (HTPC) system to provide a solution to problems of dimensional and chemical stability of the IPC. With the application of the HTPC, the cement changes phase to monetite, which describes a decrease in the compressive strength of about 60 %. This occurs due to the change in the pore structure, which is a situation that positively affects the flexural strength increase by 30 %.

Cements reinforced with fiberglass can present problems of durability due to the chemical attack on the fiber by the hydroxide ions present in alkaline environments. Calcium phosphate cements (IPC) do not present an alkaline environment, favoring the durability of fiberglass. Cuypers et al. (2006) researched the phosphate cement matrix added with fiberglass to study typical damage mechanisms in relation to mechanical properties. After performing simple tensile tests, Portland cement and a calcium phosphate cement (IPC) were compared, both reinforced with fiberglass. It was reported that Portland cement resistance decreased to 50 % of the initial strength after an accelerated aging for 90 days, opposed to phosphate cement that maintained 90-95 % of its initial resistance [76].

Colorado, Hiel and Han [77] mixed nano graphite platelets into a phosphate cement paste composed of powders of wollastonite ($CaSiO_3$) and phosphoric acid (H_3PO_4). They formed a composite material of IPC by a very rapid exothermic reaction that produces bubbles, which promote porosity and negatively affect mechanical strength. In addition to evaluating the effect of graphite, the authors provide information on alternative mixing methods (RAM, Resonant

Acoustic Mixer), which reduce the formation of bubbles and therefore result in better mechanical characteristics. The research reported mean flexural strengths of 23 MPa and good thermal stability at high temperatures (600 ºC).

Functional ceramics that exhibit additional properties to those commonly studied are also analyzed in calcium phosphate cements. Colorado et al. (2015) added on a matrix of IPC, barium titanate ($BaTiO_3$) selected for its good dielectric properties and high thermochemical stability. They effectively showed that the dielectric constant increased as the ($BaTiO_3$) load increased. At the same time, compression strengths of approximately 150 MPa for addition values of $BaTiO_3$ between 15-30 wt.% were reported [48].

1.4 Phosphate Geopolymers

The geopolymeric cements include a series of materials in which a reactive source of alumina and silica is mixed with an activator, in an aqueous solution such as sodium or potassium hydroxide and silicate solution [46]. The alkaline activation of aluminosilicates, such as fly ash or metakaolin, is widely registered to obtain inorganic products known as geopolymers. Similar to conventional geopolymers, phosphate geopolymers have been developed. These materials have a tetrahedral molecular structure of PO_4^{5-}, together with AlO_4^{3-} and SiO_4^{4-} as their basic components [64].

From metakaolin and silica fume reacted with phosphate monoaluminate (mixture of different acidic aluminum phosphates, $Al(H_2PO_4)_3$, $AlPO_4$, $Al_2(HPO_4)_3$. Y.S. Wang et al. (2017) performed a geopolymer with mechanical setrength at 7 and 28 days of 7 MPa and 30 MPa, respectively. They also showed good mechanical behavior at high temperatures (1000 ºC) [64]. This geopolymer can be described as an aluminum phosphate cement.

1.5 Commercial products and frequent applications of phosphate cements

1.5.1 Commercial applications

There are two types of phosphate cements in structural mechanical applications that register commercial products: potassium magnesium and potassium cements. They are developed by Argonne laboratories, who have patented a binder known as Ceramicrete and a calcium phosphate cement, widely studied by the University of Vrije Brussels, which in combination with fiberglass has resulted in a composite material that was patented under the name of VUBONITE.

The Ceramicrete has been widely disseminated in the immobilization of hazardous waste and as a material sprayed on sheets of polystyrene foam to produce housing walls that rise in record time, known as Grancrete [2]. Related to the Ceramicrete matrix, Qiao Chau, and Li (2010) evaluated mortars of magnesium phosphate cements as possible material for the repair of potholes or patches on the roads. They payed special attention to the relations (M/P) magnesium oxide (MgO) and potassium dihydrogen phosphate (KH_2PO_4), in addition to their corresponding ratio (S/B) sand and binder. They showed that these relationships influence the mechanical properties and setting times of mortars. Magnesium phosphate cement mortars showed superior bond strengths to those of mortars and Portland concretes. The pull-off tests showed flexural strengths of up to 5 MPa (28 days) in contrast to Portland mortars that reached 2 MPa at 28 curing days [78].

The composite material, VUBONITE has had various applications in civil buildings at a structural level [79] used this material for the construction of modular bridges, which took advantage of the tensile strength provided by fiberglass, added to the resistance to corrosion and fire of phosphate cements. In spite of the relatively low rigidity of the material, much lower than for steel or reinforced polymers, a cost-effective, resistant and easy-to-assemble bridge was made.

1.5.2 Immobilization of radioactive waste and hazardous elements

One of the main applications of phosphate cements has been the immobilization of radioactive waste and hazardous elements (such as Pb, Cd, As and Cr). A good number of authors have reported research in this field, in addition several to patents registered in this regard. Some of the researches carried out are cited below.

In a patent, Singh, present a method to produce phosphate cements and immobilize large amounts of waste of low radioactivity and hazardousness. They reported compressive strengths of 30 MPa obtained in a potassium magnesium phosphate cement [5]. The patents of Wagh and Singh [66] and Wagh Singh and Jeong [80] disclose processes for using phosphate ceramics to encapsulate wastes, recording compressive strengths for magnesium phosphate ceramics and phosphate and magnesium ceramics of the order of 20 MPa and 46.4 MPa) respectively. In U.S. Patent No. 5.830.815 (1998), the inventors describe a method for producing phosphate-bonded structural products for high volumes of benign waste [80].

Colorado and Singh [81] stabilized nuclear waste streams with high sodium content by means of magnesium phosphate cement, elaborated from anhydrous monobasic sodium phosphate (NaH_2PO_4), magnesium oxide (MgO), waste, water and fly ash as filler, the authors recorded compressive strengths obtained between 40 MPa and 5 MPa depending on the monobasic sodium phosphate concentration, with observed higher strength at higher concentrations. The nuclear regulation commission (NRC) establishes a minimum compressive strength of 3.45 MPa for cements for immobilization of waste. In the same line of research, Choi et al. [24] intervened the final waste of the processing of nuclear fuels, through the development of phosphate iron cements obtained mainly from the reaction of basic steel slag (BOF Slag) and phosphoric acid (H_3PO_4).

The slag / acid weight ratios used were 1:1.5, 2 and 2.5, registering compressive strengths between 16 MPa and 19 MPa.

Likewise, in a calcium phosphate cement matrix, lead was added to evaluate its ability to block gamma rays. The powders constituted by wollastonite ($CaSiO_3$) and lead (in proportion of solids weight of 2%, 10% and 50%) reacted with phosphoric acid in a powder-to-acid ratio of 100:120, forming a calcium phosphate cement. The authors reported excellent gamma-ray attenuation coefficients, in addition to compression strengths close to 80 MPa for mixtures with 10 % lead dust [63].

1.6 Conclusions

In civil building applications, magnesium phosphate cement and calcium phosphate cement stand out. The mechanical strength reported in phosphate cements with synthesis conditions optimized, is important due to most of them have compressive strengths with values equal to or higher than Portland cements used for structural purposes . Besides, their low environmental impact makes cements of phosphate an important material for structural works in Civil Engineering. The final cost of phosphate cements as product is higher than the cost of a traditional Portland cement. However, new applications in specific environments, in addition to the use of fillers, can potentiate this type of cements as commercially viable products.

Phosphate cements that exhibit the best mechanical response at elevated temperatures are calcium phosphate cements, registering much higher values of compressive strength at 1000 °C than other cements. However, they present problems of dimensional instability.

In the synthesis of composite materials with phosphate cement matrix, the reinforcement materials showed significant support to improve the mechanical resistance, while influencing the decrease in cement costs.

The presence of water is necessary for the formation of phosphate cements, especially in the dissolution of acidic compounds and it helps to provide an aqueous environment for the dissolution of the alkaline bases. The amount of water present in the mixture substantially affects the mechanical strength. Lower water contents increase the resistance to compression and produces low porosities. Water also influences as a retardant in setting. Although the curing time is not a factor of wide interest and frequent research in the available literature, it increases the compression resistance, especially after 28 curing days, and there are no significant changes for curing times of less than 7 days.

One of the most used additives is boric acid. This setting retardant, in adequate proportions, increases the fluidity of cement, improving its workability. The use of this additive does not significantly influence the mechanical strengths of the cement. The durability of the phosphate cements is superior to the Portland cements, and it is another positive aspect of these materials. It presents an environment with neutral pH, which favors the inactivity of other materials present in the cement.

The most frequent application of phosphate cements is the immobilization and neutralization of hazardous and radioactive waste, in which the demands of mechanical resistance of 3.45 MPa are not so stringent (500 psi) [82].

Phosphate cements have made important contributions to be considered as an alternative use material to conventional materials, the evaluation of new components in the acid-base reaction

system can allow to visualize new applications of chemically-bonded phosphate ceramics as a construction material.

2. Characterization of steel slag for the production of chemically bonded phosphate ceramics (CBPC)

This chapter corresponds to the article: https://doi.org/10.1016/j.conbuildmat.2020.118138

Abstract: This chapter studies the use of steel slag as a source of metallic oxides for the synthesis of chemically bonded phosphate ceramics (CBPCs). Analysis of different slags revealed characteristics, relating to alkaline character, granulometry and metallic oxide content, which could enable their use other than as construction aggregates. Steel slags from an electric arc furnace (EAF) and basic oxygen furnace (BOF), as well as ladle furnace basic slag (LFS), were collected from steel plants in Colombia following the ASTM D75 standard practice for aggregate sampling. The slags were analysed through techniques such as SEM/EDS, FTIR, XRD and XRF,

finding considerable quantities of CaO and iron oxides that provide the necessary metallic cation in acid-base reaction systems. The formation of phosphate ceramics was achieved from steel slags, compression strengths of up to 20 MPa were reached at 35 days and the chemical stability of the cements obtained was evaluated. Additionally, physical properties important to the formation of chemically bonded phosphate ceramics (CBPCs), such as specific gravity, grain size and pH, were determined.

2.1 Introduction

Chemically bonded ceramics (CBCs) are among the plethora of materials subject to chemical reaction. This group of new materials has been developed in recent decades, and has grown in importance. Chemically bonded ceramics are a group of materials that share characteristics with ceramics structured by sinterization with increased temperature, as well as conventional cements [2]. The chemically bonded ceramics group includes chemically bonded phosphate ceramics (CBPCs). These latter are typically formed by a process known as an acid-base type reaction, which allows reactions combining metallic oxide cations with phosphate anions, producing water and salts. These reactions can take place in solutions under normal pressure and hydrothermal conditions [45], [83]. Chemically bonded phosphate ceramics are also referred to as phosphate cements. Acid-base (AB) cements have been known since the 19th century and are an alternative to polymerization for the formation of macromolecular materials. These cements are quick setting and some possess unusual properties such as adherence and translucency. Their applications range from biomedical to industrial. [43]. The first AB cement, of zinc oxychloride, was reported by Sorel in 1855, and was used in dentistry without significant acknowledgment [43]. Another form of AB cement, synthesized from zinc oxide and phosphoric acid, was developed at the turn of the

20th century. Difficulties were encountered in the formation of these cements, which led to research being focused on the reduction of the strong formation reactions, through calcination of the zinc oxide and the use of zinc hydroxide and aluminum to neutralize the phosphoric acid. These cements are currently used in dental restoration. The development of CBPC is linked to the discovery of zinc phosphate cements, which is the main reason for their significance [2].

The best-known phosphate compounds include magnesium phosphate ceramics, calcium phosphate, iron phosphate, zinc phosphate and aluminium phosphate. Magnesium phosphate ceramics have a particularly significant industrial impact, as they are currently sold under various trade names for applications in civil engineering. Similarly, bioceramics derived from magnesium phosphates are a new alternative biomaterial, due to the biological importance of magnesium ions in enzyme activation, and cellular growth and proliferation [84]. Other useful biomaterials include the zinc phosphate cements mentioned above, and calcium phosphate cements, which have been investigated as bone replacements for some time.

Due to environmental considerations of increasing importance worldwide, a lot of research has focused on the development of eco-efficient materials with minimum impact on the environment. At present there are significant efforts to find ways to reuse industrial waste, in order to reduce its environmental impact. Various studies on chemically bonded phosphate ceramics have had a positive influence in this respect. The Argonne National Laboratory in the USA synthesized a phosphate cement named “ferroceramicrete” from red sludge, a waste product of aluminium production from bauxite. This process utilized the high content of iron oxide (hematite) present in red sludge. Partial quantities of this hematite were reduced in order for it to be subsequently activated with phosphoric acid, thereby obtaining cement suitable for use in the production of bricks, blocks and concrete for construction [85]. The development of ceramics using slag as a

source of iron oxide has also been recorded. He et al. [69] developed an iron phosphate cement using copper slag rich in iron oxide (FeO) and an acid phosphate such as monopotassium phosphate (KH_2PO_4), recording compression resistances of 44.78 MPa. Similarly, Choi et al. used BOF slag for the formation of iron phosphate ceramics, obtaining compression resistance in the order of 19 MPa [24]. These cements have been used in the immobilization of dangerous waste. Attempts have been made to use silicates from mining tailings and waste to obtain chemically bonded ceramics [55], although extracting the silicates from the mining tailings has proved challenging. In addition, it is important to highlight the synthesis of phosphate ceramics with good compression resistance from silicates such as wollastonite ($CaSiO_3$) [86][63]. Meanwhile, Hou et al. bonded calcined carbon gangue as an active addition to magnesium phosphate (MPK) cements, modifying the setting time and mechanical properties of the cement. These results showed that calcined coal gangue extended the final setting time and improved the early strength of the cement [73]. Li et al. reported that the addition of Class F fly ash can improve water and salt resistance in magnesium phosphate cements without altering mechanical resistance [67]. Similarly, Wagh et al. proved that the addition of class C and F fly ashes doubles or triples the compression resistance of phosphate cements. This increase can probably be explained by the additional reactions of the amorphous silica of the ashes with the acid phosphates [3]. The compatibility shown with fly ash and other types of industrial waste evidences the solidity in the formation of phosphates in the presence of impurities. This allows for variation in the raw materials [7] and, added to the fact that one of the areas with the greatest advances in research is the formation of phosphate cements in the presence of heavy and dangerous radioactive wastes [80], demonstrates that these waste particles do not prevent or limit the formation of chemically bonded phosphate ceramics.

It is important to state that the large majority of phosphate ceramics are obtained from reactive grade compounds obtained commercially under a range of specifications [1]. However, a great opportunity exists to form phosphate ceramics from industrial wastes such as steel slag, which have a high content of precursor oxides for the acid-base reactions in phosphate ceramics [42], [55], [87].

Steel slag is a waste product of steel production, which is primarily carried out using electric arc furnaces (EAF), basic oxygen furnaces (BOF) or ladle furnaces (LFS). Black steel slag (electric arc furnace slag) is derived from primary metallurgy or scrap melting in electric arc furnaces [17]. White steel slag (ladle furnace basic slag) originates from molten liquid from electric arc furnaces, which is poured into a ladle furnace subject to constant stirring by argon gas, allowing the elimination of heavy metal oxides and desulphurization of the molten liquid. BOF slag is obtained via steel refinement in basic oxygen furnaces. In these, the liquid metal (pig iron) is introduced together with lime and dolomite into a basic oxygen converter, into which oxygen is pumped at high pressure in order to eliminate impurities such as silicon, manganese or phosphorus, since these combine with the calcium to form slag which can then be removed.

Most steel slags are composed principally of CaO, MgO, SiO_2 and FeO, the total concentration of these oxides being in the range of 88 – 92% [17]. For this reason, steel slag can be a rich source of oxides for the generation of chemically bonded ceramics with significant cementing properties and potential commercial viability. However, the concentration of these oxides and of the other secondary components varies between different batches of slag depending on the raw materials, furnace type and technology available, directly affecting the mechanical and cementing properties of the ceramics formed. Therefore, in the search for new materials derived from steel slag it is important to achieve accurate representation of the raw materials through normalized sampling

methods, ensuring universalization of the components and the most detailed possible description of the raw materials, with the assistance of the engineering and materials science disciplines.

The present chapter provides a state of the art study of the use of industrial waste to obtain chemically bonded phosphate ceramics, specifically using steel slag, a process rarely reported in the literature. The objective of this study is to describe and compare different types of Colombian steel slags that are potential precursors to chemically bonded phosphate ceramics, through analysis of their physical, chemical and mineralogical properties, as well to demonstrate the formation and description of phosphate ceramics using steel slags.

2.2 Materials and methods

2.2.1 Conditioning of steel slags

Four types of slag were analyzed: two EAFs, one BOF, and one FINE. These were provided by Colombian steel mills. The slag used in this study named EAF-1 come from a national steel producer while the EAF-2, BOF and FINE slags are from another steel producer. Both of the plants where the slags originate are located in the department of Boyacá in Colombia. The FINE slag is a mix of EAF, LFS and BOF slags, the last of these being the largest component. This slag is obtained as a final waste product after a process of magnetic separation. All the slags were subjected to a stabilization process with the addition of water, and subsequent cooling at room temperature.

The slags were sampled in accordance with the ASTM D75M-14 and ASTM C702M-11 standards. To reduce its size, the slag was ground using jaw crushers, knee mills and ball mills of the following specifications: BRAUN CHIPMUNK primary jaw crusher with 7cm entry opening, 3 cm discharge opening and 270 rpm speed, equipped with a motor of 1710 rpm speed, 1.5 Kw,

and 60 Hz frequency; CONSOLIDATED STRUTEVANT MILL CO knee mill with maximum opening of 3.5 cm, minimum opening of 0.1 cm, equipped with a motor of 835 rpm, ½ HP and 60 Hz frequency; SIEMENS SINAMICS ball mill with a frequency range of (0 - 60) Hz, loaded with spheres of 26 mm, 19 mm and 13 mm of diameter.

2.2.2 Physical analysis of steel slags

The pH was determined via potentiometric procedure using a HANNA HI8424 digital pH meter with a BAECO BA17 glass electrode, calibrated with pH buffer solutions of 4.00, 7.00 and 10.00. 30 g of each slag sample was placed in solution with 80 ml deionized water for one hour, and the solution was stirred before the measurements were taken.

The apparent specific gravity, bulk specific gravity and absorption percentage were determined using 50 g of saturated surface dry sample of each slag. These samples were weighed with an analytical balance (Mettler Toledo, UMX5 comparator) with 0.1 mg sensitivity. The volume was determined using 100 ml pycnometers. All assays were carried out according to the ASTM C-128 standard.

Particle size distribution (granulometry) was carried out dry on each slag, according to standard ASTM C-136. 300 g of sample of each slag was sieved in a PINZUAR brand sieve stirrer (ROT-TAP) of 1725 rpm, 1/3 HP and 60 Hz frequency, equipped with sieves N^{o} 4, 8, 14, 20, 35, 60, 100, 200 and 400, normalized according to ASTM E11-95.

2.2.3 Chemical and mineralogical analysis of slags

Semiquantitive analysis of the oxides was achieved through X ray fluorescence spectrometry, carried out with Omnian mode standardless analysis, calculated by Epsilon. This was performed

using slags manually crushed into power in a plastic holder, using an Epsilon 1 PANalytical device with excitation capacities ranging from 10 kV to 50 kV, silicon drift detector (SDD), 50 kV X ray tube generator and silver anode. In the percentages determined the loss on ignition (LOI) was considered. For the quantitative analysis of the oxides, 0.7 g of each sample was prepared in duplicate. Loss on ignition tests were repeated until the weight was stabilized. A mix of lithium tetraborate ($Li_2B_4O_7$) and lithium metaborate ($LiBO_2$) 66/33 was used as a fluxing agent, to obtain a disc in a platinum crucible at 1100 °C of the molten mass (pearly). This was analyzed by XRF spectrometry in a Thermo ARL Optim'X WDXRF device.

Fourier transform infrared spectroscopy (FT-IR) was performed using a Shimadzu IRTracer-100 device with a scan range of 400–4000 cm^{-1}. The analysis technique used was attenuated total reflectance (ATR), which was applied to all the slags.

All the slag samples were analyzed by X ray diffraction (XRD) using an EMPYREAN diffractometer with Co source ($K\alpha_1$=1.78 Å) ($K\alpha_2$=1.79 Å). The X ray diffraction patterns were acquired in the interval 2θ (10.01-99.98º), with a minimum step size of 0.026 º/s. The software High Score Plus was used to identify the minerals present in the samples via the Inorganic Crystal Structure Standard Database (ICSD) and Crystallography Open Database (COD). Similarly, the High Score Plus software was used for the quantitative analysis of the crystalline and amorphous fractions. This was performed using Reitveld refinement, using the internal standard method with additions of rutile (TiO_2) of 20%. The parameters considered to validate the adjustment of the Rietveld refinement for each sample analyzed were as follows: R expected (Re), R profile (Rp), Weighted R profile (Rwp) and Goodness of Fit (GOF) [88].

Scanning electron microscope analysis was carried out using an SEM Jeol JSM-6490 LV device with acceleration voltage of 20fV, coupled to an EDS detector used to analyze the elemental chemical composition of the different slags through X ray energy dispersive spectroscopy.

2.2.4 CBPC development using steel slags

Phosphate cements were prepared in duplicate from the EAF-1, EAF-2, BOF and FINE slags. The particle size was 150 μm and the liquid-solids ratio was maintained at 1: 1.5 for each sample. For this, 5 g of slag reacted with 7.5 ml of H_3PO_4 solution. The H_3PO_4 was dissolved in deionized water in concentrations of 60 %. H_3BO_3 was added in proportions of 1.5 % by weight, as a retardant additive to the mixture. The mixing of the components was performed in polypropylene containers, in order subsequently to form cylindrical samples of 16 mm x 32 mm in PVC molds. These molds were cured in environmental laboratory conditions (T = 22 ± 2 °C and $H_{relativa}$= 60 ± 5 %) for 7 and 35 days.

Compression resistance tests were performed on the prepared specimens according to the ASTM C 39 standard. The compression resistance tests were carried out in a SHIMADZU Autograph AGSX universal testing machine with loading capacity of 50 KN and loading speed of 0.25 MPa/s.

Samples with the previous composition were also prepared in order to evaluate the chemical stability of the cements formed. Once the cements were cured, the samples were submerged in 500 ml of deionized water and 500 ml of Na_2SO_4 with concentration of 1 M. These were removed after 7 and 21 days (see figure 3), dried for 24 hours at 60 °C, and subjected to compression tests in order to establish the effect of the immersion solutions on the mechanical properties of the cements. The pH of the water and the solution were analyzed at 0,1,7, and 21 days. The product

of the leaching of the cements submerged in H_2O and Na_2SO_4 solution was filtered and dehydrated for 24 hours in order to evaluate its composition by XRF. Table 6 shows the basic conditions of the curing of the ceramics and the immersion tests to evaluate chemical stability.

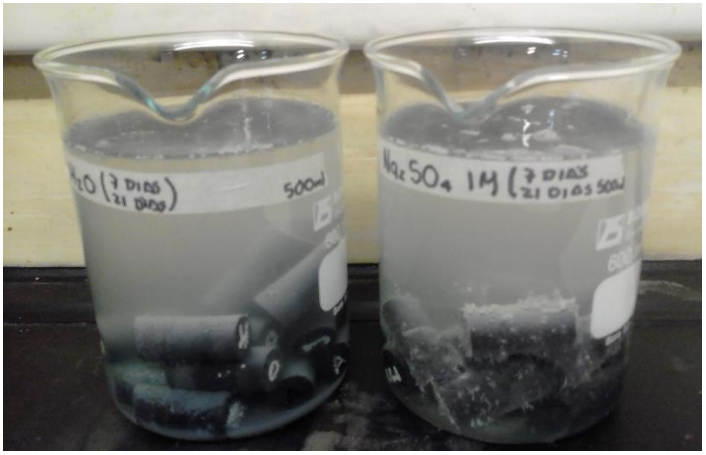

Figure 3. Leaching test for slag cement in H_2O and Na_2SO_4.

Table 6. Experimental tests to evaluate mechanical resistance and chemical stability of CBPCs.

C- Slag	Treatment	Samples
C – EAF 1	Compression tests after curing (laboratory environmental conditions)	
C – EAF 2	7 and 35 days	16
C – BOF	Compression tests after Immersion (H_2O) 7 and 21 days	16
C – FINE	Compression tests after Immersion (Na_2SO_4) 7 and 21 days	16
	TOTAL	48

2.3 Results and discussion

2.3.1 Physical properties

The pH results found for the EAF1, EAF2, BOF and FINE slags are presented in table 7. The high alkalinity levels correspond mainly to the high CaO content reported for all the slags. The higher alkalinity in the BOF and FINE slags is a direct result of the higher CaO percentages in these slags,

as will be discussed later. A fundamental aspect in the formation of chemically bonded ceramics is the basicity of metallic oxides which react with various acidic compounds to form consolidated ceramics [2]. Steel slags can act as a metallic cation source via metallic oxides, consolidating their role as the basic component in these chemical reaction systems [89]. Basicity values are defined for EAF 1, EAF2, BOF and FINE slags of 2.4, 2.1, 5.0 and 4.1 respectively, classifying these slags as basic with B values > 2, favoring their use in cements. Beside above, the hydraulic index of the slags is also defined with values of: 1.6, 1.6, 0.9 and 0.7 for the slags EAF 1, EAF2, BOF and FINE respectively, values that classify binders for the manufacture of ceramic products in general, presenting a theoretical hydraulics for the manufacture of fast and slow cements.

Table 7. Physical properties of the slags.

Physical properties	EAF 1	EAF 2	BOF	FINE
Color	Dark gray	Dark gray	Dark Sephia	Dark Sephia
pH	11.80	11.78	12.93	12.97
Relative Density	3.82	3.65	3.51	3.37
Bulk Density	3.70	3.44	3.43	3.32
Absorption (%)	0.89	1.72	0.68	0.44
Particle Size Distribution				
D_{60} (mm)	0.21	0.22	0.20	0.23
D_{30} (mm)	0.12	0.11	0.13	0.13
D_{10} (mm)	0.08	0.06	0.09	0.08
Coefficient of uniformity (CU)	2.65	3.66	2.22	2.87
Coefficient of curvature (CC)	0.85	0.91	0.93	0.91

The values for the relative densities of the slags show high similarity, although they are slightly higher for the EAF slags. These relative densities, presented in table 7, are slightly higher the relevant value for Portland cement (3 g/cm^3), indicating that the use of slags as a reactive material for the formation of chemically bonded ceramics would provide a physical load for the mix similar to or slightly higher than that of a conventional cement. The values recorded for bulk density were

very similar for all four slags, which may be due to their mineral composition. This confirms the low absorption of the slags of around 1%, which directly contributes to their plasticity and porosity, and also guarantees adequate conditions for their use in a potential mix, since the quantity of water required for the mix would be minimal and so better control could be achieved of the proportions of the other raw materials. In figure 4 the appearance of the slags after the crushing and grinding process is shown.

Figure 4. Steel slags subjected to crushing and grinding.

The data recorded for the particle size distribution of the slags is shown in table 7 and figure 5, enabling their use as an aggregate to be considered. Granulometric analysis demonstrates similar grain size for these materials, showing that 60 % of the particles of each slag studied present a size below 300 µm approximately, although a difference in particle size between 0.25 mm and 2.36 mm can be observed for the EAF1 slag in relation to the other particle sizes, this difference is not significant, while the shape of the size distribution curves of the particles shown in figure 5 varies in a narrow range, tending towards smaller sizes that correspond to a fine aggregate (ASTM D-75/D75M). Based on the uniformity and curvature coefficients obtained for the EAF1, EAF2, BOF and FINE slags, these samples are classified as poorly graded fine sands according to the USCS (United Soil Classification System). The reaction of the slags with the other components that results in chemically bonded ceramics requires relatively low grain size (fine sands) [2], making it necessary to crush and grind the slags to bring them to the desired particle size.

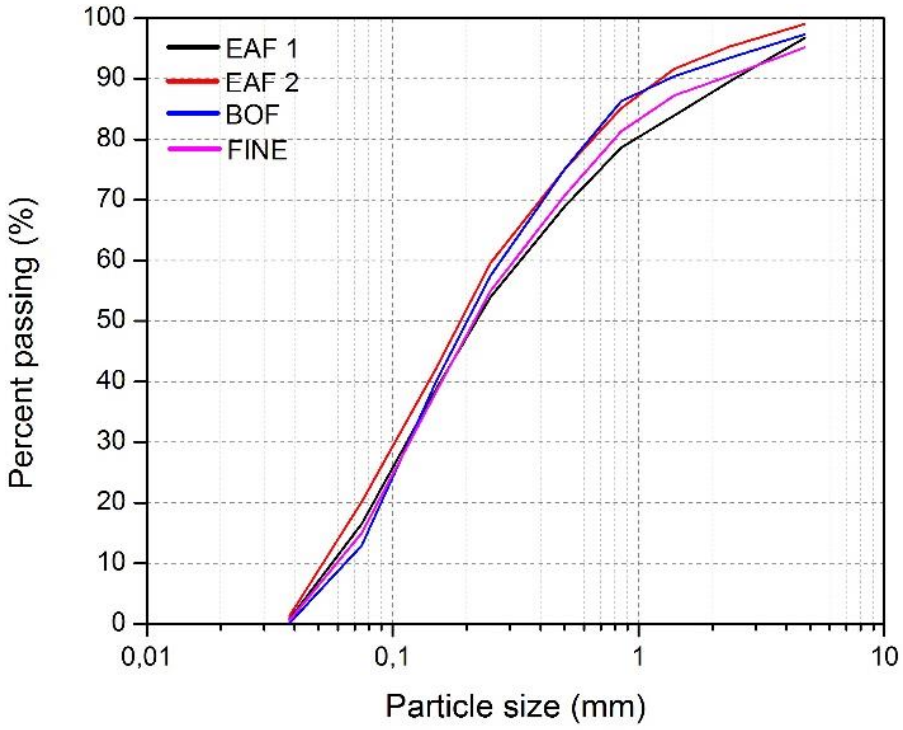

Figure 5. Granulometric analysis of the slags.

2.3.2 Morphological, chemical and mineralogical analysis of the steel slags

2.3.2.1 SEM/EDS, XRF

The SEM analysis carried out on the slag samples is presented in figure 6. This shows heterogenous morphology with a wide variety in particle size, between 0.1 µm and 100 µm. In general, particles with irregular and angular shape are observed, due to the crushing and grinding processes applied. Additionally, agglomeration is observed for the smallest particles [90], for the four slags analyzed. Table 8 shows the EDS results for the semiquantitive elemental composition of the slags, which in general identify Ca, O, Fe and Si as the elements in greatest proportion. This is corroborated by XRF results which show CaO, Fe_2O_3 and SiO_2 as the predominant oxides. However, the results obtained from XRF for some oxides, for example Fe_2O_3, do not enable us to determine the corresponding type of iron oxide. However, this oxide can be present as FeO, Fe_2O_3 or Fe_3O_4.

Table 9 shows significant quantities of CaO, Fe_2O_3, SiO_2, MgO, Al_2O_3 and MnO. These oxides can participate in the formation of chemically bonded ceramics [2]. Divalent oxides such as CaO, MgO and MnO are the principal candidates for the formation of coherent ceramics. Meanwhile, trivalent oxides such as Fe_2O_3 y Al_2O_3 can also form CBPCs, but must be subjected to reduction or calcination processes at medium temperatures [42]. SiO_2 has low solubility and therefore does not participate in the formation of ceramics serving instead as a filler, improving mechanical resistance and helping to reduce the setting time [1].

The different origins of the EAF slags is observed to be of little significance, given that they present very similar compositions. The FINE slag is a refinement of BOF slag, where a part the iron has been removed by a process of magnetic separation, as shown by XRF analysis. Meanwhile, the addition of LFS slag to FINE slag is demonstrated by EDS analysis, as the Si percentage is higher than in the BOF slag, Si being a very significant element in LFS slags [91], [92].

The presence of certain elements such as Cr, Mn and P is due principally to the circumstances of the steel production. Electric arc furnaces, which produce EAF slags, are fed with scrap from various sources that contains a significant presence of alloyed metals such as Cr and Mn [17]. Also, percentages of P are found in the iron mineral that feeds the oxygen steel working process (basic oxygen convertor). Phosphorus is an inconvenient element in the composition of steel and so dephosphorization processes of the liquid pig iron are required, a characteristic determinant in the production of BOF type slags [93].

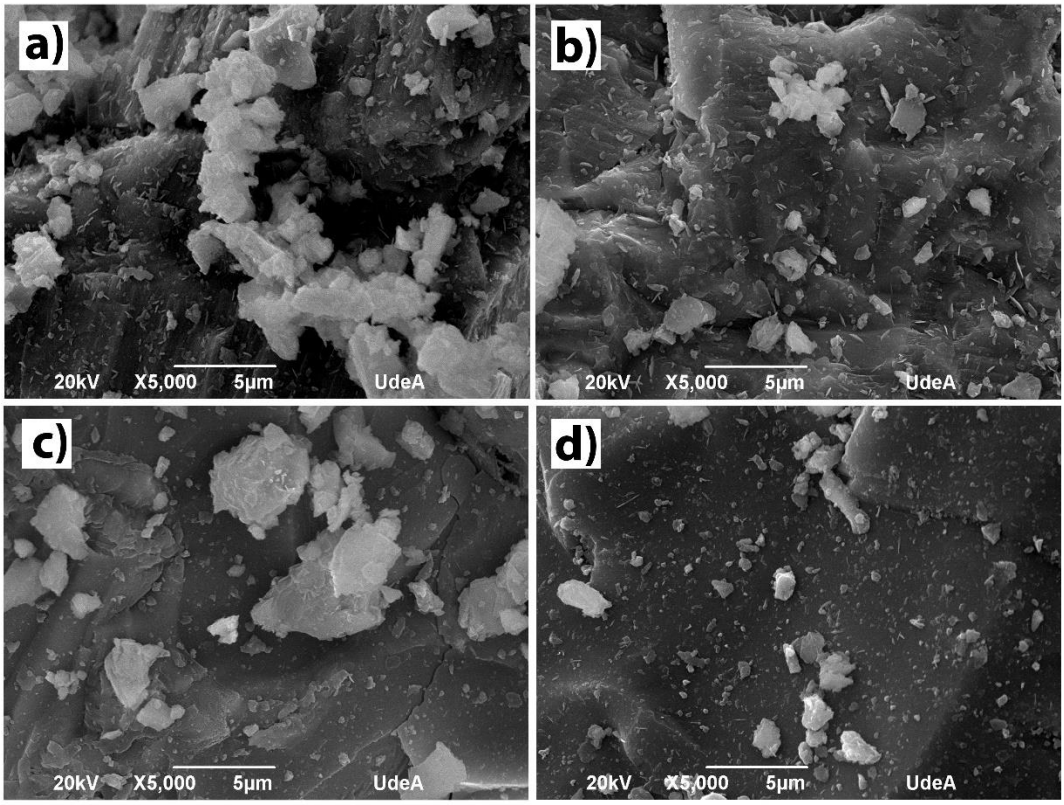

Figure 6. SEM images of the slags: a) EAF-1, b) EAF-2, c) BOF and d) FINE.

Table 8. Semi-quantitative analysis by EDS of the elementary composition of slags (wt %).

Element	EAF 1	EAF 2	BOF	FINE
C	4.15	2.64	3.22	3.62
O	36.69	27.48	20.34	37.95
Al	4.67	4.79	0.75	0.33
Si	9.44	8.12	3.64	10.69
Mg	1.02	0.66	0.37	---
P	---	---	2.38	5.74
Ca	29.59	30.16	39.00	40.45
V	---	---	0.44	---
Fe	11.36	19.64	18.72	1.22
Ti	0.54	0.70	---	---
Cr	0.57	3.29	---	---
Mn	1.97	2.51	11.14	---

Table 9. Chemical analysis (XRF) of the slags (wt %).

ÓXIDE	EAF 1	EAF 2	BOF	FINE
Na_2O	0.28	0.30	0.26	0.15
MgO	7.68	2.82	1.93	2.17
Al_2O_3	1.55	2.73	0.33	0.93
SiO_2	12.22	13.35	8.45	10.83
P_2O_5	0.61	1.37	7.14	7.53
SO_3	0.58	0.65	0.71	0.64
CaO	25.08	30.91	41.68	46.03
TiO_2	0.37	0.50	0.16	0.20
Cr_2O_3	0.80	0.84	0.14	0.13
MnO	5.87	4.10	8.70	8.32
K_2O	0.35	0.32	0.58	0.68
Fe_2O_3	38.51	37.89	29.49	23.38
TOTAL (%)	93.96	95.84	99.70	101
LOI∗	0.00	0.00	+0.07	+0.04

∗ Loss on Ignition at 900 °C
Correction factor (FC) = 1

2.3.2.2 FTIR

The bands observed in the FTIR spectra in figure 7 present chemical composition of some similarity for all the slags. The bands for the EAF slags are very similar, while the BOF and FINE bands present differences to these. There are frequent peak overlaps that make identification of the bands difficult, but the results corroborate to a great extent those found by the SEM/ EDS and XRF analyses. In general, the area from 1200 to 900 and 500 to 800 is identified as corresponding respectively to the deformation of the stretching and bending bands of Si-O [94]. This indicates the presence of silicates as the most abundant compounds in the slags, given that this is one of the most significant visual areas in the graphic.

Specifically, bands at 1112 cm^{-1} and 993 cm^{-1} are observed, corresponding to the vibrations of the Si-O bond that are typical of silicates [95], [96]. The asymmetric stretching vibration of Si-O at 970 cm^{-1}, clearly visible for the EAF slags, indicates the presence of silicate chains [94]. The bands at 1112 cm^{-1} and 847 cm^{-1} relating to the bending vibration of SiO^{4-} associated with dicalcium

silicate β (Ca_2SiO_4) larnite, are visible for the EAF slags, and may form shoulders in the BOF and FINE slags [95], [97]. The bands at 1012 cm^{-1} and 1051 cm^{-1} present for the BOF and FINE slags are assigned to the P-O stretching modes [98]–[100], corresponding to the typical phosphates for these types of slag. The band at 584 cm^{-1} is associated with the (Fe-O) vibration of magnetite [95], observable for the EAF slags. The band present at 1478 cm^{-1} corresponds to the (MgO) vibration visible for the EAF slags. The band at 712 cm^{-1} visible for all four slags corresponds to the CO_3^{2-} ion of calcite [101], [102], which is likely to be present in very low proportions in all the slags. The wide band at 1418 cm^{-1} relates to the metallic stretching of the Fe-Ca bond which, together with the band at 875 cm^{-1}, indicates the stretching of the Fe-O bond [103]. This demonstrates the presence of calcium ferrites, possibly brownmillerite (Ca_2FeAlO_5) or srebrodolskite ($Ca_2Fe_2O_5$), in the greatest proportion for the BOF and FINE slags. The bands present in the range from 450 cm^{-1} to 650 cm^{-1} are commonly associated with simple metallic oxides, but due to the complexity in the composition of the slags, interpretation of the results in this area is difficult.

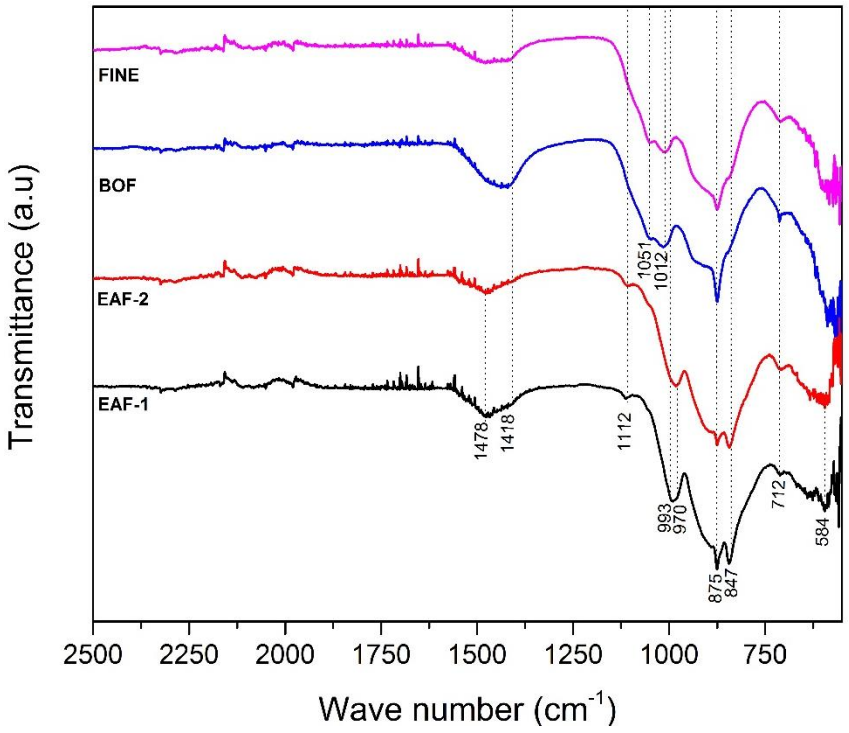

Figure 7. FTIR analysis of slags.

2.3.2.3 XRD

Steel slags present a vitreous phase which is produced from the cooling of the slags with water. In the present analysis, the vitreous phase was considered and quantified through Rietveld refinement with the addition of internal standard (TiO_2). XRD analysis shows a crystalline phase corresponding to approximately 40 % of the total weight in all the slags, with a mineralogical phase largely corroborated through the chemical composition observed by FTIR. Moreover, values of around 60 % by weight corresponding to the amorphous phase are observed for all the slags. In figure 8, the mineralogical composition of the steel slags, according to the COD and ICSD databases, are presented in percentage values by weight, quantified through Rietveld, table 10.

The adjustment criteria of the Rietveld refinement calculated from the residual values (R_e, R_p, R_{wp}, and GOF), which quantify the difference between the experimental and calculated profiles, are

shown in table 11. The statistical values for $R_{p,}$ and R_{wp}, are considered acceptable when under 10 %. R_e evaluates the quality of the data and, theoretically, (R_{wp}) can never be better than (R_e) [104]. GOF compares (R_{wp}) y (R_e), and a perfect refinement for GOF would present values close to 1. However, in practice, values lower than 5 represent an optimum refinement [105].

In general, the composition of the slags can be defined through the silicates and iron oxides shown in table 10. The chemical composition of the EAF slags is very similar, regardless of the steel mill that they originate from. In these slags, it is observed that silicates predominate over iron oxide, and the participation of dicalcium silicate β with a crystalline formation similar to larnite (Ca_2SiO_4) is significant. Formation of alite (Ca_3SiO_5), present in some slags subject to rapid cooling, is not observed, confirming the slow cooling process for this type of slag [19]. Iron oxides are principally represented by wuestite (FeO) and magnetite (Fe_3O_4), while appearing lower proportions in crystalline combinations such as brownmillerite (Ca_2FeAlO_5) and srebrodolskite ($Ca_2Fe_2O_5$). Additionally, there is a compositional participation of chromium oxide and manganese in spinel form (FeO·MnO·MgO) Cr_2O_3. The content of free lime and free magnesia is practically negligible in the composition of EAF steel slags.

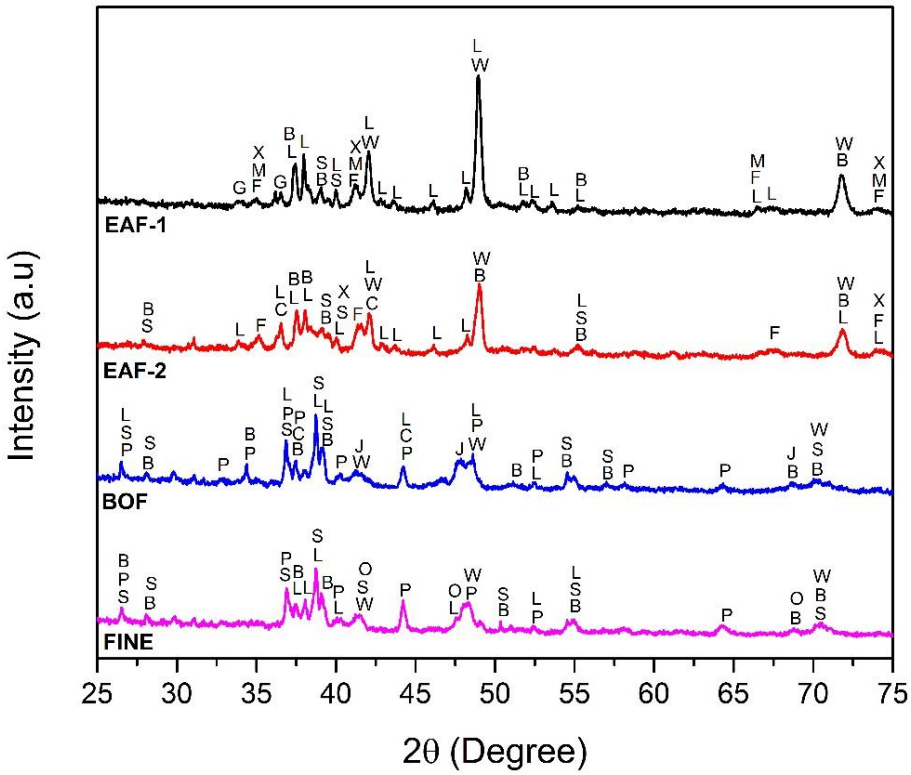

Figure 8. Diffractograms of the slags studied. Calcium oxide (C), Dicalcium silicate- Larnite, Calcium Phosphate V (L), Silicocarnotite (P) Gehelenite (G), Brownmillerite (B), Srebrodolskite (S), Wuestite (W), Magnesiowuestite (M), Magnetite (F), Ferrous Manganese Oxide (J), Manganese Oxide (O), Spinel (X).

The BOF and FINE slags present similar composition to one another and show significant differences to EAF slags. Iron oxides are distributed in the BOF and FINE slags, principally in wuestite and forming compounds in dicalcium ferrites such as brownmillerite and srebrodolskite. The results of the XRF, SEM/EDS and FTIR analyses demonstrate the presence of phosphate, which is also evidenced by XRD analysis through the formation of silicates with phosphate contents in their structure. Various authors explain the presence of phosphate as an impurity or forming a solid solution which establishes itself in the form of dicalcium silicates or silicocarnatite [106][19]. Another important difference is the presence of manganese oxides, alone or in combination with iron in the form of ferromanganese oxide. In general, very low content of free lime is observed, since most of this is combined in the form of silicates or with iron oxide to form

calcium ferrites, due to the high temperatures in the order of 1600 ºC required to melt steel. The FINE slag show the highest content of free lime, which can be explained by the significant presence of CaO in slags from ladle furnaces (LFS) [91]. Many of the phases described through XRD have also been identified in previous studies, corroborating the findings in this study [18], [107], [108]

The chemical and mineralogical analyses are consistent with the SEM/EDS, XRF, FTIR and XRD results, showing good availability of metallic oxides as possible precursor compounds to chemically bonded phosphates. Steel slags contribute mainly to the formation of calcium phosphate, iron phosphate and manganese phosphate cements. Due to the complex and varied chemical composition of steel slags, it is considered that these contribute to the formation of multiple phases or multiphase cements in the following way: Dicalcium silicates possibly contribute to the formation of cements with significant calcium phosphate phases in all the slags, and compounds like brownmillerite or srebrodolskite, wuestite and magnetite can help in the formation of iron phosphate cements [2]. Manganese oxides can form manganese oxide phases with additional temperature or reduction treatment. Equally, it is important to highlight that BOF and FINE slags can, as a result of their high CaO content, generate cements with very rapid setting time due to the rapid dissolution reactions that this oxide presents, negatively affecting the workability of the cement formed [51].

Table 10. Mineralogical composition of steel slags by Rietveld refinement.

Mineral phase	Code	Formula	EAF 1	EAF 2	BOF	FINE
Lime (%)	COD 96-900-6730	CaO	---	0.5	0.5	2.2
Dicalcium silicate – Larnite (%)	COD 96-901-2791	Ca_2SiO_4	17.7	16.6	---	---
Dicalcium silicate – Calcium Phosphate V (%)	ICSD 98-008-1098	$Ca_{15}P_2SiO_{32}$	---	---	1.7	6.6
Silicocarnotite (%)	ICSD 98-002-3641	$Ca_5P_2Si_6O_{12}$	---	---	18.6	7.8
Gehelenite (%)	ICSD 98-008-7144	$Al_2Ca_2SiO_7$	1.4	---	---	---
Brownmillerite (%)	ICSD 98-009-7626	Ca_2FeAlO_5	2.7	1.0	14.4	15.6
Srebrodolskite (%)	ICSD 98-002-6474	$Ca_2Fe_2O_5$	---	2.7	3.5	3.7
Wuestite (%)	COD 96-900-9771	FeO	14.3	10.7	6.9	7.0
Magnesiowuestite (%)	COD 96-900-6045	$Mg_{2.4}Fe_{1.6}O_4$	0.2	---	---	---
Magnetite (%)	ICSD 98-016-4814	Fe_3O_4	0.9	4.2	---	---
Ferrous Manganese Oxide (%)	ICSD 98-006-0690	$Fe_{0.09}Mn_{0.9}O$	---	---	0.7	---
Manganese Oxide (%)	COD 96-101-0394	MnO	---	---	---	0.3
Spinel (%)	COD 96-900-5292	$Mn_{9.54}Cr_{14.46}O_{32}$	0.8	0.1	---	---
Amorphous (%)			62.1	64.2	53.6	56.9

Table 11. Agreement Indices of the Rietveld refinement.

Agreement Indices	EAF 1	EAF 2	BOF	FINE
R_e	2.79	3.00	2.96	3.00
R_p	2.53	3.10	2.75	3.13
R_{wp}	3.29	4.11	3.64	4.45
GOF	1.39	1.87	1.51	2.19

2.3.2.4. Amorphous

Due to the high amorphous content in the slags (quantified through Rietveld refinement), it is important to specify their content. For this, XRF data corresponding to the quantitative elemental composition of the slags by oxide weight, and XRD data on the crystalline phases quantified through Rietveld were used. The determination of the amorphous oxide content consisted in subtracting the oxide weight determined through XRD from the total oxide content of the slags

obtained through XRD [109]. A mass balance was used to estimate the amorphous content and to determine which compounds could exist within it. In table 12, the approximate composition of the amorphous components of CaO, Fe_2O_3 and SiO_2 is calculated. These results are a first approximation, since it should be considered that while the calculations performed under the assumption that the detected phases have an ideal composition, the phases in solid solution, such as those described above, can generate imprecision, and in addition the minority phases have been ignored.

Table 12. Mass balance of the content of amorphous and crystals in steel slag (wt%).

Slag	Oxides	Crystalline phases	Amorphous	% TOTAL FRX
EAF1	CaO	13.41	11.67	25.08
	Fe_2O_3	11.43	27.07	38.51
	SiO_2	5.09	7.12	12.22
	TOTAL	29.93	45.86	75.81
EAF2	CaO	11.06	19.85	30.91
	Fe_2O_3	10.84	27.05	37.89
	SiO_2	5.72	7.63	13.35
	TOTAL	27.62	54.53	82.15
BOF	CaO	22.78	18.9	41.68
	Fe_2O_3	12.64	16.85	29.49
	SiO_2	4.62	3.83	8.45
	TOTAL	40.04	39.58	79.62
FINE	CaO	21.13	24.9	46.03
	Fe_2O_3	14.24	9.14	23.38
	SiO_2	3.27	7.56	10.83
	TOTAL	36.64	41.6	80.24

2.3.3 Chemically bonded phosphate ceramics (CBPC).

From the reaction of H_3PO_4 and the steel slags, the formation of coherent ceramics is shown. These ceramics are principally formed through the reaction of the base component (steel slags) with the

acid component (aqueous solution of H_3PO_4). The cements formed with EAF1, EAF2, BOF and FINE are referred to as, C-EAF1, C-EAF2, C-BOF and C-FINE, respectively.

2.3.3.1 Morphological and chemical analysis of the cements formed

The SEM image in figure 9 shows the principal phases present in the cements formed from the steel slags after they were subjected to compression, prior to immersion tests. In general, two clearly distinguishable phases are observed in the SEM images: one crystalline phase with formations with ordered tendency, in external laminate shape, and an amorphous vitreous phase which describes the cement matrix. From the EDS corresponding to the micrographs (figure 10), Ca, Fe and P are observed as the principal elements in greater proportion, suggesting a probable composition of calcium phosphates and iron phosphates. The crystalline phase is associated principally with calcium phosphates formed through the reaction of calcium silicates and phosphoric aqueous solution [48], [110]. The amorphous phase corresponds to an iron phosphate, originating from the iron oxides present principally in the Wuestite, dicalcium ferrites in reaction with phosphoric acid solution, a compound already identified by Wagh and Singh for iron phosphate cements, known as vitrocrystalline ceramics [2], [5].

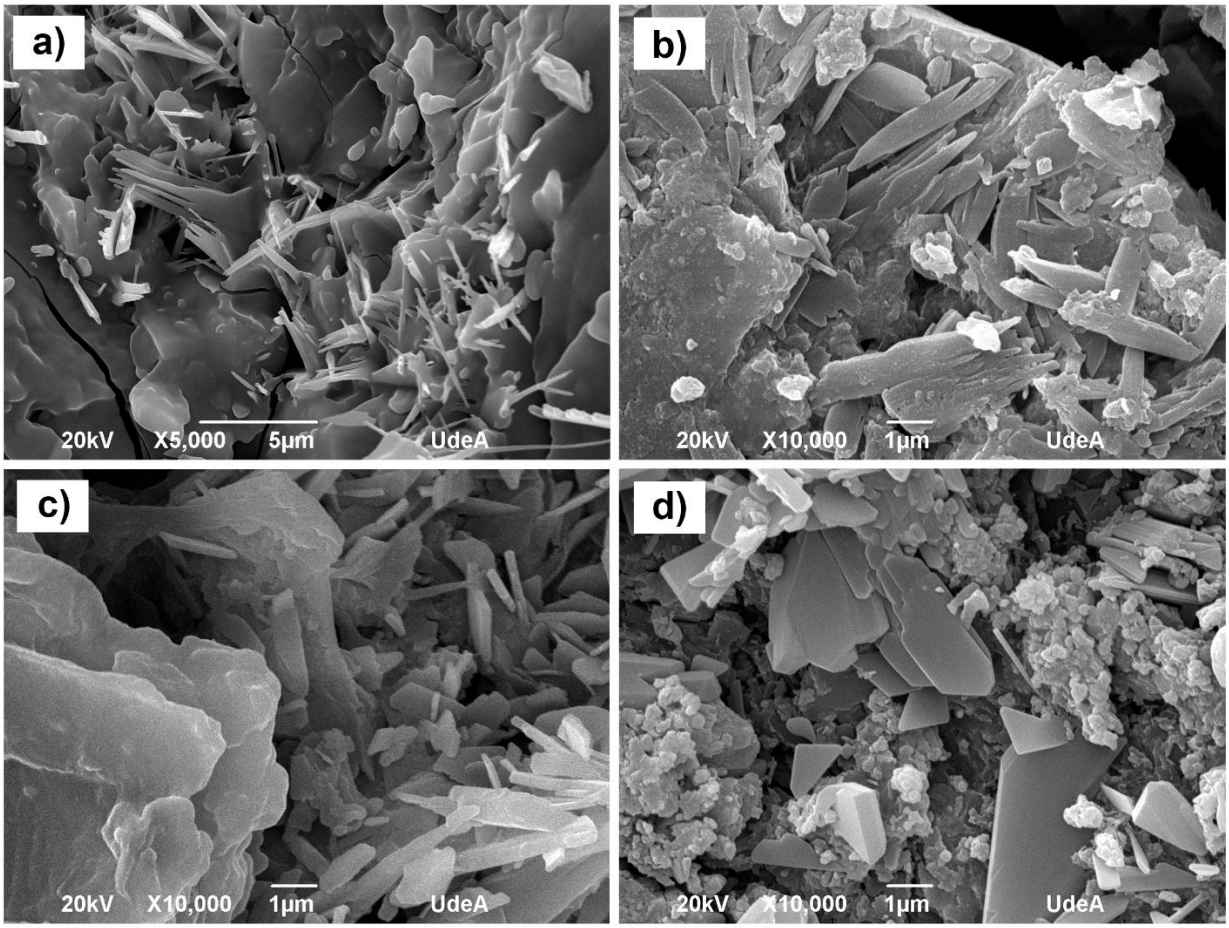

Figure 9. Morphology of cements obtained from steel slag.

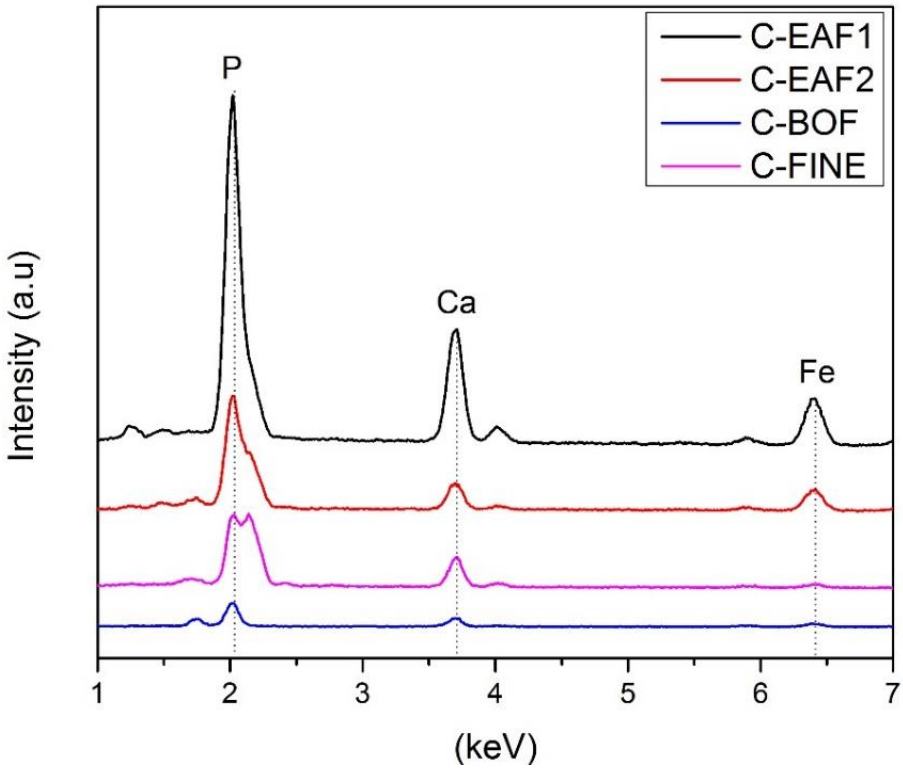

Figure 10. EDS of cements obtained from steel slag

Figure 11 shows the diffractogram of the cements formed from steel slags analyzed. Two calcium phosphate compounds corresponding to the crystalline phases that are present in the four cements are mainly identified: Calcium Dihidrogenophosphate Hydrate $Ca(H_2PO_4)_2 \cdot xH_2O$ and Brushite $CaHPO_4 \cdot 2H_2O$, confirming the described previously in SEM/EDS. The figure also shows a greater Brushite phase formation for C-BOF and C-FINE, possibly explained by the higher content of CaO present in the BOF and FINE slag composition. In addition to a considerable formation of calcium dihydrogen phosphate hydrate for C-EAF. Likewise, an amorphous phase is present, which is not identified in XRD, which can be associated mainly with iron phosphates as mentioned above and residues of amorphous raw material that did not participate in the chemical reaction of cement.

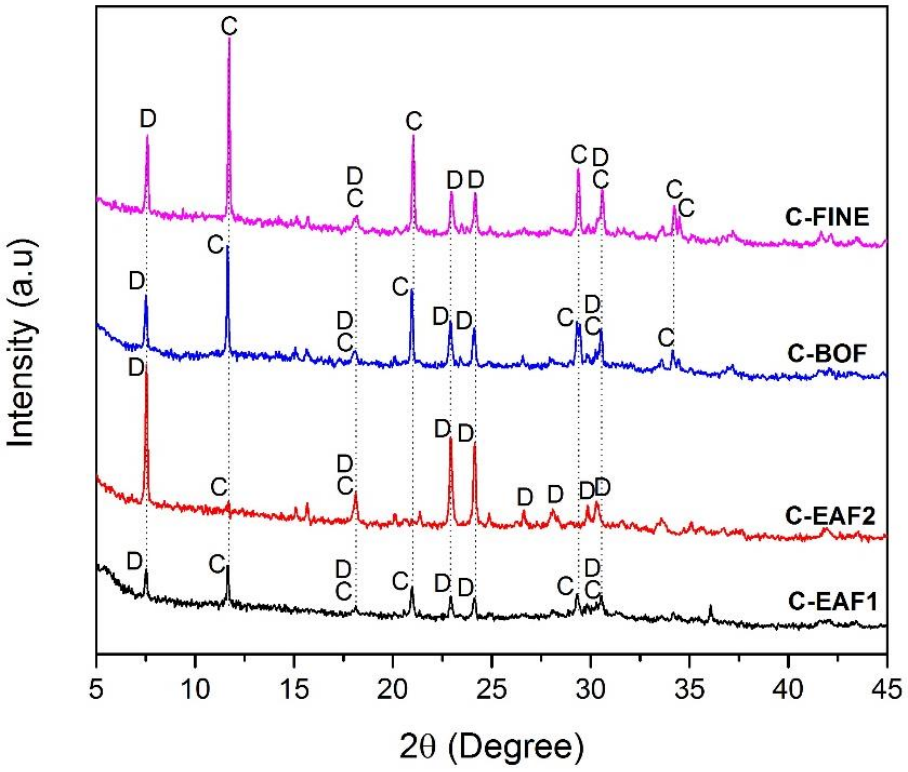

Figure 11. Diffractograms of the cements formed: (D) Calcium Dihidrogenophosphate Hydrate, (C) Brushite.

2.3.3.2 Compression Strength

In Figure 12 the mechanical behavior of the cements formed from steel slags prior to immersion in H_2O y Na_2SO_4, is observed. Compression resistances for the four compositions of between 5 - 20 MPa are observed. With regard to the development of the early compression resistances (7 days), with the exception of C-EAF1, all show similar resistances at 7 and 35 days. The reactions of quick setting and early high resistance are associated with behavior typical to phosphate cements [111]–[113]. Greater compression resistances are observed in the C-BOF and C-FINE cements (15 - 20 MPa). This is possibly associated with the greater percentages of calcium oxide (CaO) present in their composition, which forms phosphate cement phases associated with greater mechanical resistance [47], [75].

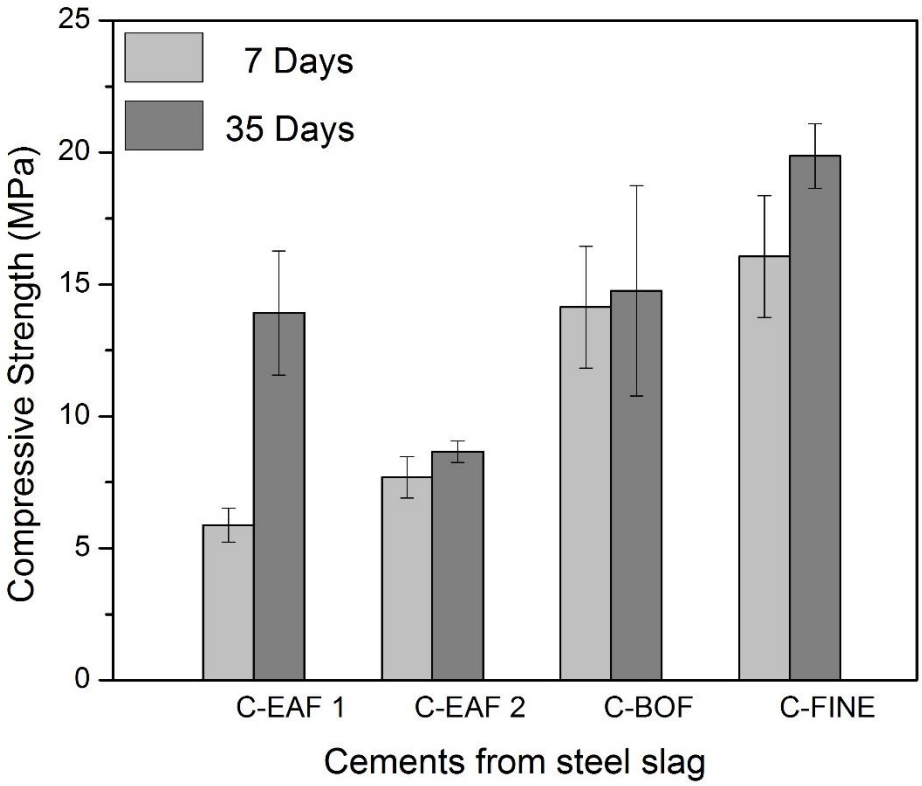

Figure 12. Compressive strength of CBPC at 7 and 35 days of curing.

2.3.3.3 Chemical stability

Some studies have recorded poor chemical resistance on the part of phosphate cements, specifically in the case of magnesium phosphates. The authors describe how their compression resistance diminishes when they are immersed in water or subjected to a humid environment [114], [115], affecting their mechanical properties. Also, it has been described how these cements are affected by components which have not reacted and are highly soluble in water, generating pores which affect the morphology of the cements and reduce their mechanical resistance [111]. Therefore, the compression resistance of the different compositions after immersion of the samples in H_2O and Na_2SO_4, was evaluated. In this process, degradation of the test tubes was observed, as well as leaching products in the samples (figure 3), associated primarily with Fe, Ca and P,

registered via XRD analysis (Table 10). This indicates the degradation of calcium phosphates and iron phosphates as possible principal phases in the ceramics formed. The attack of sulphates on the surface is evident, producing efflorescence and slight expansion on the samples in Na_2SO_4 solution (figure 13). In Figure 14a, reduction in resistance for the cements of the samples immersed in H_2O for 7 days in the order of 68 % to 77 % is observed, with a slight increase in resistance at 21 days. For samples immersed in Na_2SO_4, resistance is reduced between 65 % and 85 %, with an increase in resistance at 21 days (figure 14b). The mechanical resistances decreases substantially, principally affecting the samples immersed in H_2O and the C-EAFs. In general, the cements show a similar behavior for the samples immersed in H_2O, however, for the samples immersed in Na_2SO_4 a greater deterioration is observed in the C-EAFs than the C-BOF and C-FINE.

The reduction in resistance associated with the C-SLAG is principally due to the leaching of the constituent elements, as can be observed in the XRF analysis of the leaching products (table 13). This could be associated with the loss of resistance to water penetration, related with a structure of low density and high porosity. It is also important to highlight the small volume of the test tubes immersed in water, which have a greater area of exposure to leaching and sulphate attack.

Table 13. Elements present in leaching C-Slag (XRF) wt %.

	Na	Al	Si	P	S	Ca	Mn	Fe
Leached in H_20	---	0.85	0.05	16.38	---	5.21	2.21	23.79
Leached in Na_2SO_4	10.57	0.90	0.04	11.93	6.32	2.95	1.25	12.23

Moreover, consistently with the XRD results, the presence of free lime (f –CaO) is common, in the order of 0.5 % to 2.2 %, which favors the hydration of f –CaO, causing an increase in volume

and, in turn, an increase in the internal pressure and therefore damage to the structure [116]. Equally, possible carbonation cannot be ruled out, the high quantities of Ca in the composition and the alkaline environment of the slags can favor the capture of CO_2, causing modification to the chemistry of the cement and, and possibly explain the slight increase in compression resistance at 21 days immersion in H_2O or Na_2SO_4 solution [117].

In Portland cement mixtures which incorporate steel slags as aggregate, it has been recorded how these can affect the workability of conventional cements [116], [117]. Similarly, cements synthesized from slags and H_3PO_4 solutions present low workability, attributed to the angular shape of the slag particles, which reduces the flow of the mixture [118], in turn resulting in the reduction of mechanical resistance since good distribution of the particles in the mold is not enabled.

The release of dangerous metals by leaching in steel slags can cause environmental problems and be a potential risk to human health. Signs of dangerous elements in steel slags such as Cadmium, Chrome, Mercury and Lead have been reported in various publications. However, recently, a study has been published on the leaching of dangerous metals in slags, in which steel slags were ruled out as a dangerous waste product, as none of the elements cited exceeded the concentration limits of the tests forming part of the TLCP (Toxicity Characteristic Leaching Procedure) [119]. The levels of Chrome in steel slags reported in this study and quantified by XRF are around those referenced in the literature [120] and do not exceed 1 wt %.

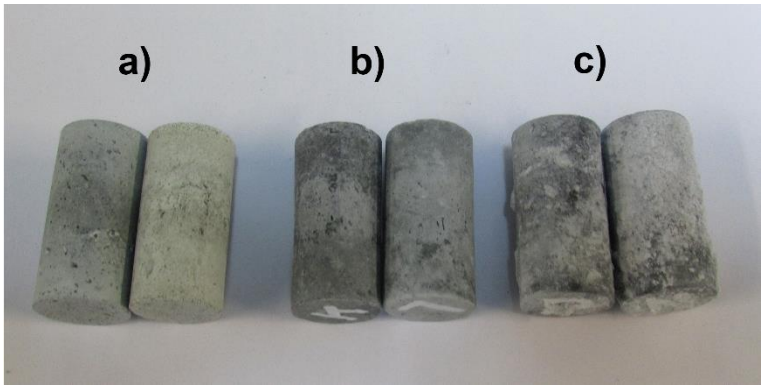

Figure 13. a) Samples without leaching treatment, b) Samples immersed in H_2O after 21 days, c) Samples immersed in Na_2SO_4 after 21 days

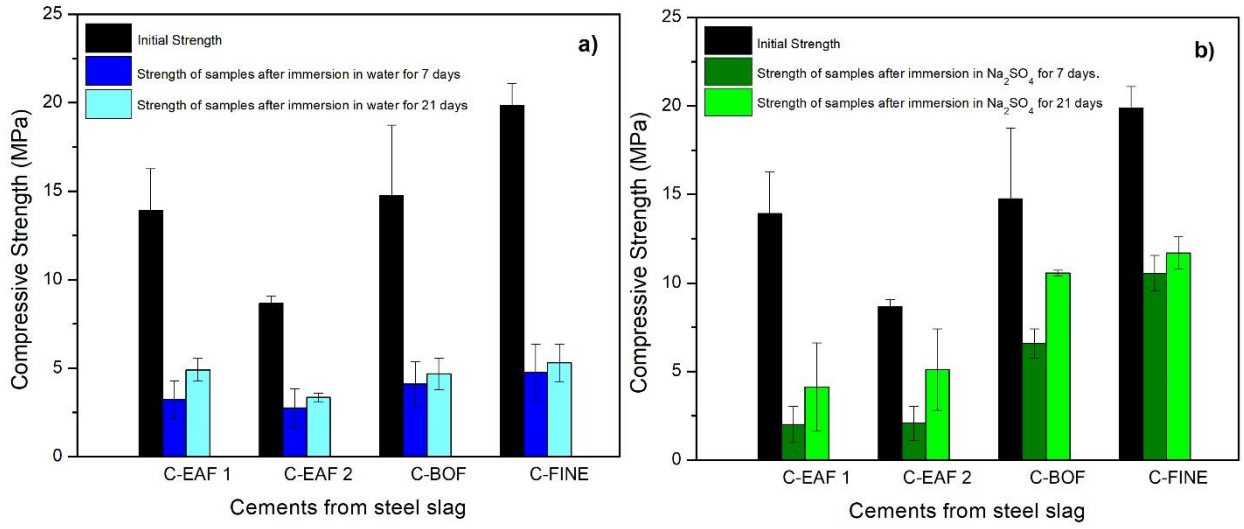

Figure 14. Compressive strength of CBPC at 7 and 21 days of immersion.
a) Immersed in H_2O, b) Immersed in Na_2SO_4

2.4. Conclusions

The alkalinity, relative density and granulometry of the analyzed slags were adjusted to parameters rendering them suitable for use as precursors of ceramic phosphates.

The chemical, morphological and mineralogical analyses describe compounds potentially suitable for the synthesis of chemically bonded phosphate ceramics (CBPC). The principal mineral phases present in all the analyzed slags were: wuestite, dicalcium silicate, srebrodolskite and

brownmillerite, all of which are rich in calcium oxide and iron oxide, which can provide the metallic cation necessary for acid-base system reactions.

In general, it is considered that the four slags analyzed can form phosphate cements. The EAF slags, with significant content of iron oxide and CaO, can contribute principally to the formation of iron phosphate cements and secondary phases of calcium phosphates. The calcium oxide (CaO) content found in the BOF and FINE slags may allow the formation of calcium phosphates, or at least constitute one of the principal phases in the formation of a chemically bonded phosphate ceramic (CBPC). However, the rapid dissolution reactions shown by CaO at certain pHs can make the formation of coherent ceramics difficult, especially for slags like BOF and FINE which have high CaO content.

A good percentage of oxides that form phases with other elements is found for the analyzed slags. These minerals, which dissolve with difficulty to provide the metallic cation, form compounds that do not react and may participate as fillers in the recently formed cements, together with other minerals corresponding to the gangue.

Early compression strengths (7 days) are common for the four types of cements formulated with ranges between 6 and 16 MPa, in addition to compression strengths (35 days) of up to 20 MPa for C-FINE.

The diverse chemical composition present in the steel slags with significant percentages of compounds susceptible to the formation of CBPCs makes it necessary to consider the application of adequate methods for the treatment or use of this material. Steel slags considered as industrial waste have a wide potential for use as components in chemically bonded phosphate ceramics (CBPCs).

3. Multiphase phosphate cements from steel slags

This chapter corresponds to the article: https://doi.org/10.1080/21650373.2020.1863275

Abstract: The use of industrial waste in the synthesis of phosphate ceramics opens the door to new ways of production and marketing of this kind of product, as well as contributing to the reduction of the environmental impact of industrial waste. In the present study, chemically bonded phosphate ceramics (CBPC) were synthesized from steel slags (electric arc furnace slag (EAF), basic oxygen furnace slag (BOF), and ladle furnace basic slag (LF) and aqueous solutions of H_3PO_4. A chemical analysis was performed of the steel slags, which were selected through standard sampling before being ground and milled to obtain the appropriate granulometry. In the evaluated slags, iron oxides and calcium oxides, present both in their free state and in compounds with other elements, were identified as the elements with the greatest presence and potential to form CBPC. Design of experiments (DOE) was applied to form multiphase cements, in order to make the variables present in the

obtainment of cements workable, thereby allowing the formation reactions of cement to be better understood. The cements obtained were analyzed through XRD, SEM-EDS, FTIR, XPS and mechanical compressive strength tests. The synthesized cement exhibited mainly vitreous structure for the iron phosphate phases ($Fe(H_2PO_4)_2$) or ($FeHPO_4$), and mainly crystalline structure for the calcium phosphate phases, present as dihydrogen phosphate of calcium hydrate ($Ca(H_2PO_4)_2 \cdot xH_2O$) and brushite ($CaHPO_4 \cdot 2H_2O$). Compression strength between 10 and 19 MPa was recorded for the different compositions evaluated, with short setting times.

3.1 Introduction

Chemically bonded phosphate ceramics (CBPC) can be explained based on the acid-base reaction system. Here, the alkaline component is generally represented by metallic oxides (leachable cation powders that accept protons), which act as mono, binary or ternary component acid decomposition systems; and the acid component is represented by soluble phosphates or dilute phosphoric acid (proton donor liquid). In the acid-base reaction at room temperature, complex salts are formed that correspond to phosphate cement obtained through exothermic reactions [121]. To produce coherent ceramics through acid-base reactions, it is of fundamental importance to consider the solubility conditions of the reagents; low solubility does not provide enough ions for a tridimensional structure, while excessive solubility leads to crystalline precipitates that cannot form a tridimensional network [2]. Therefore, the selection of raw materials with adequate reaction rates is a high priority in the synthesis of phosphate cements.

Wagh proposes oxides that are sources of metallic cations, such as ZnO, CaO, Al_2O_3, MgO and Fe_2O_3, as raw materials for the formation of CBPC; and soluble phosphates or phosphate acids, as well as aqueous solutions of H_3PO_4, as a source of phosphate anions. Many of these soluble

phosphates and phosphate acids can be obtained commercially as fertilizers, including monopotassium phosphate (KH_2PO_4); magnesium dihydrogen phosphate [$Mg(H_2PO_4)_2 \cdot H_2O$]; ammonium acid phosphate [$(NH_4)H_2PO_4$]; diammonium phosphate; [$(NH_4)_2HPO_4$] aluminum hydrophosphate [$AlH_3(PO_4)_2 \cdot H_2O$] [2]; and, most commonly, monopotassium phosphate (MPC), which forms magnesium phosphate cement in reaction with MgO. This binder has been a focus for research and development [36], [71], [122], notably for its use in environmentally friendly alternative cements, which facilitate the bioreceptivity of organisms and promote sustainability due to their lower pH to Portland cements [123]. Recently, wollastonite ($CaSiO_3$) has begun to be used as a source of calcium ions and aqueous solutions of phosphoric acid (H_3PO_4) in the synthesis of calcium phosphate cements [47], [48], [112], [124].

It is important to highlight that, in the phosphate cement formulations mentioned above, the raw materials that have been used are mainly of reagent grade, of a specific stoichiometry, and have been subject to a meticulous synthesis process to enable them to participate in the formation of CBPC. However, there is a large amount of industrial waste that, despite being processed at great scale without a significant level of purity management, can be used in the formation of phosphate cements, thereby helping to reduce their environmental impact. There have been some successful attempts to formulate CBPC with the use of industrial wastes. Wagh et al. synthesized iron phosphates with applications in the manufacture of bricks, adding bauxite as a source of iron oxides [85], and finding that the addition of fly ash increases the compression strength of phosphate cements by two or three times [42]. Hou et al. added coal gangue to magnesium phosphate cement, thereby improving its mechanical properties [73]. Garner et al. demonstrated that the addition of ground blast furnace slag (GBFS) and fly ash (FA) improved the mechanical properties and performance of magnesium potassium phosphate cements (MPCs), and led to both chemical

and structural changes. This enabled a better understanding of the function of these additives, given that they did not only act as inert fillers in the MPC matrix, but were responsible for the modification of its physical and chemical properties [54]. The examples cited above demonstrate the potential for the reuse of industrial wastes in the formation of CBPC.

Two byproducts of interest for this study are obtained from integrated steel production: (i) blast furnace slags, particularly granulated blast furnace slags (GBFS); and (ii) steel slags, including electric arc furnace (EAF) slag, basic oxygen furnace (BOF) slag, and ladle furnace basic slag (LF). Granulated blast furnace slags (GBFS) are widely used as an active additive to Portland cement, due to their vitreous structure and latent hydraulicity, which give them significant cementitious properties [17]. However, it is important to clarify that these additives correspond specifically to the Portland cementitious system; and a number of studies have demonstrated the low hydraulic reactivity exhibited by EAF, BOF and LF slags, due to the presence of dicalcium silicates as principal phase, and to the scarcity or absence of tricalcium silicates. As such, EAF, BOF and LF steel slags are considered to be weak clinkers for Portland cements [17].

The main advantage of the use of industrial wastes such as EAF, BOF and LF-type steel slags is that they act directly as the alkaline component in the formation of CBPC. However, this type of reaction in the formation of CBPC has not been widely referenced. Choi et al. used BOF slag as an alkaline component for the formation of CBPC for use in the immobilization of the final waste products of the processing of radioactive fuels. They developed iron phosphate cements primarily through the reaction of basic steel slags (BOF) and phosphoric acid (H_3PO_4), and focused their investigation on the potential capacity of the cements to immobilize radioactive residue solutions, given that the mechanical strength conditions were not crucial [24]. Jiang et al. added steel slag powders (SSP) to magnesium phosphate cement mortar, evaluating the workability, mechanical

properties, and water resistance. Here, steel slag powders were used as an addition without totally replacing the MgO, which continued to be the alkaline reaction component [22].

This chapter proposes the development of chemically bonded phosphate ceramics (CBPS), using raw materials scarcely referenced in the literature as CBPC formers, such as: EAF, BOF and LF steel slags as base component for acid-base reactions; and aqueous solutions of H_3PO_4 as the acid component, in which the slags provide the metallic cations necessary for the formation of ceramics. Moreover, the mechanical strength of the cements developed is investigated, and an initial approach is made towards understanding their structure, morphology and chemical behavior steel slag-based phosphate cement.

3.2 Materials and methods

3.2.1 Design of Experiments (DoE) and Statistical analysis

Design of experiments methodology has been widely used as a tool to find the optimum model to explain the interaction of variables in experimental procedures. A wide range of variables participate in the synthesis of cement phosphate from steel slags, which include: proportions of acid and base; concentration of H_3PO_4; chemical composition of the slags; grain size; curing time; retardant additives; type of mixture; reaction speed; and reaction temperature. Therefore, in order to synthesize chemically bonded phosphate ceramics, prior experiments were made to evaluate the previously mentioned variables. This made it possible to clarify which of these were controllable, thereby limiting the number of variables to use, and optimizing the performance of the controlled variables.

Analysis of the design of experiments results is based on variance analysis (ANOVA), which enables it to be determined whether the effects (changes observed in the response variable due to

a change in the level of a factor) on the response variable are statistically significant. The DoE selected was response surface methodology (RSM), where the response variable is influenced by a range of factors, and the objective is to optimize this response [125]. This technique was used to investigate the behavior of the H_3PO_4 concentration and the proportion of liquid-solid components on the compressive strength of the cements formed from the different types of slag used, as well as verifying the existence of interactions between the variables and determining how these affect the response variable.

Three (3) factors were considered: type of slag, concentration of H_3PO_4; and liquid-solid proportion. A 4 x 3 x 2 mixed-level factorial design and three replicas were selected, for a total of 72 experimental runs. A randomization process was performed for the runs, in order to reduce the systematic error in the DoE analysis. The following were evaluated: four (4) types of slag (EAF1, EAF2, BOF and FINE), the last of these being a combination of EAF, BOF and LF; three (3) concentrations of H_3PO_4 (50%, 55%, 60%); and two (2) liquid-solid ratios (1.5:1, 2:1), calculated from the percentage by weight of the H_3PO_4 diluted with deionized water, divided by the percentage by weight of the slags (Table 14). The proposed objectives were to optimize the response variable and determine the optimal operation conditions of the system. R Studio software version 1.0.143 was used to generate, execute and analyze the experimental designs.

Table 14. DoE parameters and response variable

Replica 1					Replica 2					Replica 3				
Run order	Slag type	H_3PO_4 (%)	L/S Ratio	Resis. (MPa)	Run order	Slag type	H_3PO_4 (%)	L/S Ratio	Resis. (MPa)	Run order	Slag type	H_3PO_4 (%)	L/S Ratio	Resis. (MPa)
1	EAF2	55	1.5	14.1	25	FINE	50	2	7.31	49	BOF	60	2	12.23
2	FINE	55	1.5	16.04	26	BOF	60	1.5	10.91	50	FINE	50	1.5	11.65
3	EAF1	60	2	3.31	27	FINE	55	1.5	14.45	51	EAF1	55	1.5	13.87
4	BOF	55	2	14.69	28	EAF2	50	1.5	7.79	52	BOF	60	1.5	13.3
5	BOF	50	2	7.25	29	EAF2	60	2	7.73	53	EAF1	50	1.5	10.94
6	FINE	55	2	17.28	30	EAF1	60	1.5	9.2	54	EAF2	60	2	8.05
7	EAF1	50	1.5	12.42	31	FINE	60	2	11.53	55	EAF1	50	2	6.06
8	BOF	50	1.5	5.24	32	EAF2	50	2	9.29	56	EAF2	55	2	8.51
9	FINE	60	2	16.11	33	EAF1	60	2	3.67	57	BOF	55	2	15.61
10	EAF2	55	2	7.42	34	EAF1	50	1.5	7.19	58	FINE	60	2	12.17
11	FINE	50	2	8.97	35	BOF	50	2	14.99	59	EAF1	55	2	3.43
12	EAF1	60	1.5	8.62	36	EAF1	50	2	5.94	60	EAF2	50	2	4.94
13	EAF2	60	2	8.98	37	BOF	55	2	13.2	61	BOF	55	1.5	15.26
14	EAF2	50	1.5	5.33	38	BOF	60	2	12.12	62	FINE	60	1.5	17.81
15	EAF1	55	1.5	9.13	39	EAF1	55	2	4.07	63	EAF2	60	1.5	13.54
16	EAF2	50	2	8.6	40	FINE	60	1.5	20.9	64	EAF2	50	1.5	8.9
17	EAF1	55	2	4.43	41	EAF2	60	1.5	16.67	65	FINE	55	2	11.63
18	EAF1	50	2	4.31	42	EAF2	55	2	7.79	66	BOF	50	2	14.96
19	BOF	60	1.5	8.46	43	EAF1	55	1.5	10.3	67	FINE	55	1.5	13.16
20	BOF	60	2	10.37	44	BOF	55	1.5	17.22	68	EAF1	60	1.5	7.85
21	FINE	60	1.5	20.95	45	EAF2	55	1.5	15.71	69	EAF1	60	2	3.28
22	FINE	50	1.5	14.41	46	FINE	50	1.5	8.9	70	FINE	50	2	10.64
23	EAF2	60	1,5	18.72	47	BOF	50	1.5	3.11	71	EAF2	55	1.5	18.14
24	BOF	55	1.5	13.3	48	FINE	55	2	13.66	72	BOF	50	1.5	2.6

The estimated model was verified in terms of residuals based on the assumptions of normality, independence and homoscedasticity, in which it is presumed that the errors of the model are random variables that follow an independent and normal distribution with a mean of zero and constant variance (σ^2). If these assumptions are satisfied, the procedure of variance analysis is an exact test of the hypothesis that there are no differences in the means of the treatments [125]. The Shapiro-Wilk and Anderson-Darling tests were applied for normality; Levene and Breusch-Pagan

(variables) tests for constant variance, and Durbin Watson tests for independence. It was found that the p-values in each of the tests were greater than the defined level of significance $\alpha = 0.05$, meaning that the model is verifiable for normality, independence and homoscedasticity.

3.2.2 Raw materials

Cements were synthesized from aqueous solutions of H_3PO_4, as a source of phosphate anions, and four types of slag, as sources of the metallic cations necessary for the base reaction. 85% ortho-phosphoric acid from PANREAC was used. Technical grade boric acid (H_3BO_3) of 99% purity from PROTOKIMICA was used as a retardant agent for the reaction. The slags used were from Colombian steel factories. The FINE slag is classified as the final waste from the factory and is made up of a mixture of LF, BOF and EAF slags. The slags were cooled with water and air. ASTM D75M-14 and ASTM C702M-1 standards were used for slag sampling. Slags were ground to decrease their particle size, which for all slags was determined as passing through sieve # 100 (150 μm), standardized according to ASTM E11-95.

The chemical composition of the slag was analyzed by XRF spectrometry on a Thermo ARL Optim'X WDXRF device. The XRD analyses were performed using an EMPYREAN diffractometer, with Cu source, ($K\alpha_1$=1.54 Å) ($K\alpha_2$=1.54 Å) with a range of 2θ (5.00 º-95.00º) and a step size of 0.013 º/s.

The quantification of the metallic oxides present in the slags observed through XRF (table 15), suggests that phosphate ceramics could be formed through the chemical composition of these slags, due to the predominant presence of oxides such as CaO and Fe_2O_3. These oxides favor the synthesis of phosphate cements based on slags, as they are iron phosphates and calcium phosphates [126]. According to the various studies compiled by Wagh [2], these cements are mainly formed

by monovalent or divalent oxides that have adequate solubility in the presence of phosphate acid solutions. For iron oxides, appropriate solubility conditions are presented; while the solubility of calcium oxides is too high for acid-base synthesis reactions, so while they can produce small quantities, large quantities are very difficult to obtain [42].

Table 15. Chemical composition of slags (FRX).

	Na_2O	MgO	Al_2O_3	SiO_2	P_2O_5	SO_3	CaO	TiO_2	Cr_2O_3	MnO	K_2O	Fe_2O_3	LOI*
EAF1	0.28	7.68	1.55	12.22	0.61	0.58	25.08	0.37	0.80	5.87	0.35	38.51	0.00
EAF2	0.30	2.82	2.73	13.35	1.37	0.65	30.91	0.50	0.84	4.10	0.32	37.89	0.00
BOF	0.26	1.93	0.33	8.45	7.14	0.71	41.68	0.16	0.14	8.70	0.58	29.49	+0.07
FINE	0.15	2.17	0.93	10.83	7.53	0.64	46.03	0.20	0.13	8.32	0.68	23.38	+0.04

* LOI Loss on Ignition at 900 °C
Correction factor (FC) = 1

From the results of the mineralogical analysis carried out by XRD (table 16), the principal phases present in the slags are identified as: dicalcium silicate (Ca_2SiO_4); brownmillerite (Ca_2FeAlO_5) and wüstite (FeO). FeO, as a divalent oxide, favors the formation of iron phosphate cement, while compounds such as dicalcium silicate (Ca_2SiO_4) and brownmillerite (Ca_2FeAlO_5) can provide the metallic cations necessary for the formation of calcium phosphate cements when they are dissolved in the acid environment. Other compounds referenced through XRD and present in the slags, although not in a generalized manner, are lime (CaO); silicocarnotite ($Ca_5P_2Si_6O_{12}$); gehlenite ($Al_2Ca_2SiO_7$); srebrodolskite ($Ca_2Fe_2O_5$), magnetite (Fe_3O_4; ferromanganese oxide ($Fe_{0.09}Mn_{0.9}O$) and manganese oxide (MnO), which can act as an alkaline component in the formation of CBPC through their dissolution as compounds.

Table 16. Main phases of slags identified in XRD.

Phase	Formula	EAF 1	EAF 2	BOF	FINE
(U) Lime	CaO	---	X	X	X
(L) Dicalcium silicate	Ca_2SiO_4	X	X	X	X
(P) Silicocarnotite	$Ca_5P_2Si_6O_{12}$	---	---	X	X
(G) Gehelenite	$Al_2Ca_2SiO_7$	X	---	---	---
(B) Brownmillerite	Ca_2FeAlO_5	X	X	X	X
(S) Srebrodolskite	$Ca_2Fe_2O_5$	---	X	X	X
(W) Wuestite	FeO	X	X	X	X
(F) Magnetite	Fe_3O_4	X	X	---	---
(J) Ferrous Manganese Oxide	$Fe_{0.09}Mn_{0.9}O$	---	---	X	---
(N) Manganese Oxide	MnO	---	---	---	X

3.2.3 Formulation and synthesis of the (CBPC) specimens

Controllable and uncontrollable factors affect the reactions involved in the synthesis of phosphate cements from steel slags. Uncontrollable factors include the reaction speed, reaction temperature, and the chemical composition of the slags. Controllable factors include the liquid to solid proportion, H_3PO_4 concentration, type of slag, grain size, curing time, mixture type and retardant percentages. To obtain the cements, preliminary assays were carried out in order to reduce and fix the number of levels of the controllable factors. Cements were synthesized with the variables observed in table 17.

Table 17. Variables of synthesized cements.

Factor	**Level**
Liquid-Solid ratio	1.5:1, 2:1
H_3PO_4 concentration (%)	50, 55, 60
Slag Type	EAF1 – EAF2 – BOF - FINE
Particle size	Passing #100
Curing time	28 days
Agitation Type	Manual
Retardant Percentage H_3BO_3 (wt. %)	2

72 specimens were developed, corresponding to 24 different types of mixture prepared in triplicate from the slags, aqueous solution of H_3PO_4, and retardant (H_3BO_3), according to the liquid-solid ratios considered. Deionized water was used to adjust the concentration of the phosphoric acid solution to 50%, 55%, and 60%. The mixing of the components was carried out in plastic recipients by manual stirring for 3 minutes, in order to form cylindrical samples of 1.6 cm diameter and 3.2 cm width in plastic molds. These were unmolded on the fifth day after their preparation and subsequently cured under laboratory environmental conditions (T = 22 ± 2 °C and $H_{relative}$= 60 ± 5 %) for 28 days, before finally being subjected to compression strength tests. The prepared specimens showed rapid setting with strong exothermic reactions, and a slight growth or expansion was observed on the part of the specimens made with EAF slags, at 60% H_3PO_4 concentration, and 2:1 liquid/solid ratio. Similarly, a slight contraction or reduction in volume was observed in those specimens prepared with 50% H_3PO_4 and 1.5:1 liquid-solid ratio. Both these phenomena could be associated with the quantity of water present in the reaction.

3.3 Characterization of the cements

The ASTM C 39 standard was used for compression strength tests, which were performed after 28 days of curing time on a SHIMADZU Autograph AGSX universal testing machine, with a maximum load capacity of 50 KN and a load speed of 0.25 MPa /s.

Attenuated total reflectance (ATR) Fourier transform infrared spectroscopy (FTIR) was performed using a Shimadzu IR Tracer-100 with a scan range of 4000 – 400 cm^{-1}. For the XRD and FTIR analyses, four samples corresponding to the different compositions of the cements formed from all the slags evaluated were selected. These samples show the highest mechanical strength and an acceptable workability of the cements. In the quantitative analysis of the phases identified by XRD, Rietveld refinement was applied using an internal standard (TiO_2), and the data obtained were

evaluated using the High Score Plus software to identify the minerals present in the samples via the Inorganic Crystal Structure Standard Database (ICSD) and Crystallography Open Database (COD). To validate the Rietveld refinement, the statistical parameters of goodness of fit (GOF) and R profile (Rp) were considered, a GOF close to 1 was considered a perfect fit, while Rp below 10% was considered admissible [88], [104], [105]

The XPS analysis was carried out using an X-ray photoelectron spectroscope (Specs brand) with a PHOIBOS 150 1D-DLD analyzer, using a monochromatic Al-Kα source (1486.7 eV, 13 kV, 100 W), with scan energy of 90 eV for the general spectra in the range 0 – 1400 eV; and 20 eV for the high resolution spectra (C1s, O1s, Fe2p, Ca2p, and P2p). The scan value was 1 eV for the general spectra and 0.1 eV for the high-resolution spectra. 20 measurement cycles were carried out for the high-resolution spectra and 3 cycles were carried out for the general spectra. The XPS lines were calibrated using C1s at 284.8 eV. Scanning electron microscope analysis of secondary electrons was performed using a 20kV Jeol JSM-6490 LV device with acceleration voltage of 20fV, coupled to an EDS detector used to analyze the elemental chemical composition through X ray energy dispersive spectroscopy. For the XPS and SEM/EDS analysis, a sample corresponding to the composition of the cement obtained with the EAF2 slag was considered. A generalized chemical, morphological and structural analysis of the cements obtained is proposed, based on the similarity in composition and formation reactions observed. Internal fragments of the EAF2 cement composition were selected, that had been previously tested by compression. These fragments were dried under normal laboratory conditions (temperature of $23^{o}C \pm 2^{o}C$, relative humidity of 37 % $\pm$ 1 %) and, they were then secured to metallic supports using carbon adhesive type, for the subsequent coating with gold in high vacuum.

3.4 Results and discussion

3.4.1 Mechanical characterization

The influence of the different variables; slag type, H_3PO_4 concentration and liquid-solid ratio, known as factors in DoE, is presented in figure 15. The graph of the means shown in figure 15 indicates the main effects of each individual factor on the response variable. The highest compressive strength of the phosphate cements obtained was with FINE slag; 55% H_3PO_4 concentration and liquid-solid ratio of 1:1.5. The higher mechanical strengths observed for C-FINE can be explained by the number of crystalline phases obtained for this cement (to be observed in the quantification of phases in cements by Rietveld refinement). Meanwhile, the phosphoric acid concentration has been established as a critical factor in determining the mechanical strength of the cement, so an optimum concentration of this exists to develop the maximum mechanical strength [1]. In addition, as has been shown in other phosphate cements, the decrease in the liquid-solid ratio positively/negatively influences the mechanical strength [34], [127], [128]. Therefore, these factors together contribute to improving the mechanical strength.

Table 18 shows the variance analysis (ANOVA), which determines whether the absolute values of the principal effects and interaction effects are a measurement of the importance of their effect on the response variable. The –p value, corresponding to each of the factors and their double interactions, is lower than the significance level chosen (α=0.05), indicating their statistical significance. Therefore, the null hypothesis is rejected in favor of the alternative hypothesis, which is that the slag type, H_3PO_4 concentration, liquid-solid ratio and the double interactions between them, significantly influence the compression strength. Moreover, the effect of the interaction of the two factors is observed when the effect of one factor depends on the level at which the other is found, indicating that the double interactions contribute substantially to the cement strength.

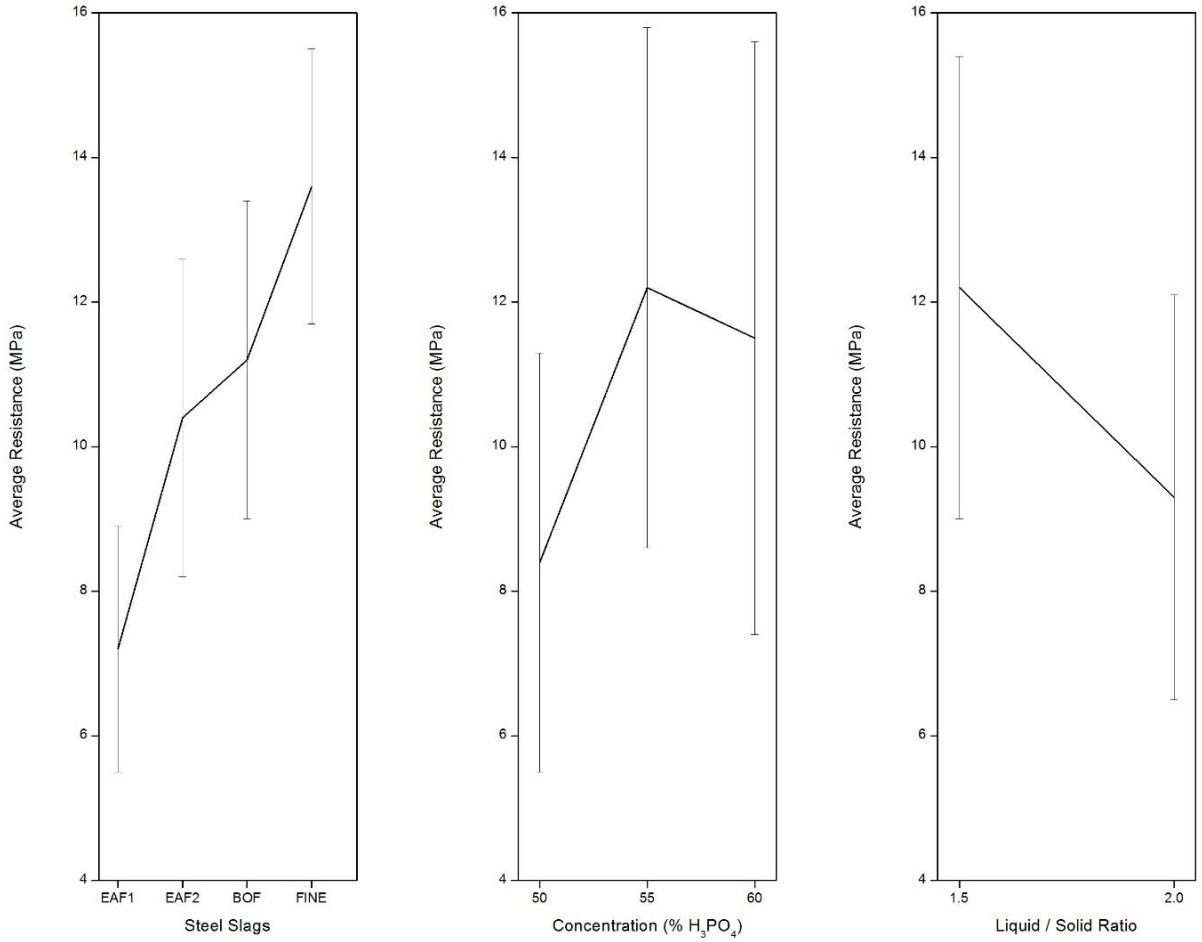

Figure 15. Descriptive statistical analysis.

For the prediction of the response variable, first order regression models were determined whereby the precision of the prediction was measured through the value of the determination coefficient R^2, which is 0.7114, indicating that the model explains 71% of the behavior of the data.

Table 18. ANOVA for compression strength.

Source	Df	Sum Sq	Mean Sq	F Value	Pr (>F)
Slag	3	408.2	136.06	25.528	2.04e-10
Concentration	2	195.3	97.63	18.317	8.47e-07
Ratio	1	143.3	143.26	26.877	3.33e-06
Slag:Concentration	6	165.1	27.51	5.161	0.000295
Slag:Ratio	3	211.4	70.47	13.222	1.38e-06
Concentration:Ratio	2	94.8	47.38	8.889	0.000460
Residuals	54	287.8	5.33		

Equations 1 and 4 present linear regression models for each slag type, expressed from the mathematical calculation with the compression strength as response variable. These models were constructed to obtain the optimal composition of the phosphate cements considering the factors studied. The models are described from the equations, where: REAF1 corresponds to the compression strength for the EAF1 slag; REAF2 to the compression strength for the EAF2 slag; RBOF to the compression strength for the BOF slag; RFINE to the compression strength for the FINE slag; *b* is the H_3PO_4 concentration; and *c* is the liquid/solid ratio.

REAF 1 = -62.7425 + 1.6308*b + 45.6422*c -1.0360*b*c (1)

REAF 2 = -62.7425 -34.3347 + 1.6308*b + 45.6422*c + 0.6628*b + 0.7622*c -1.0360*b*c (2)

RBOF = -62.7425 -53.3492 + 1.6308*b + 45.6422*c + 0.5028*b + 17.1200*c -1.0360*b*c (3)

RFINE = -62.7425 -46.4100 + 1.6308*b + 45.6422*c + 0.8087*b + 4.9000*c -1.0360*b*c (4)

The surface response graphs resulting from the adjustment of the regression models to a set of points in the experimental region are presented in figure 16. The H_3PO_4 concentration affects the strength of all cement types. Generally, higher strength is reported at higher H_3PO_4 concentrations. For C-EAF1, C-EAF2 and C-FINE cements, liquid/solid ratios with minimum values positively affect the response variable, but for the C-BOF cement the high liquid/solid proportions represent

higher strength values. In the surface response figures, the points of maximum strength reported for each cement that do not form part of the model are also represented.

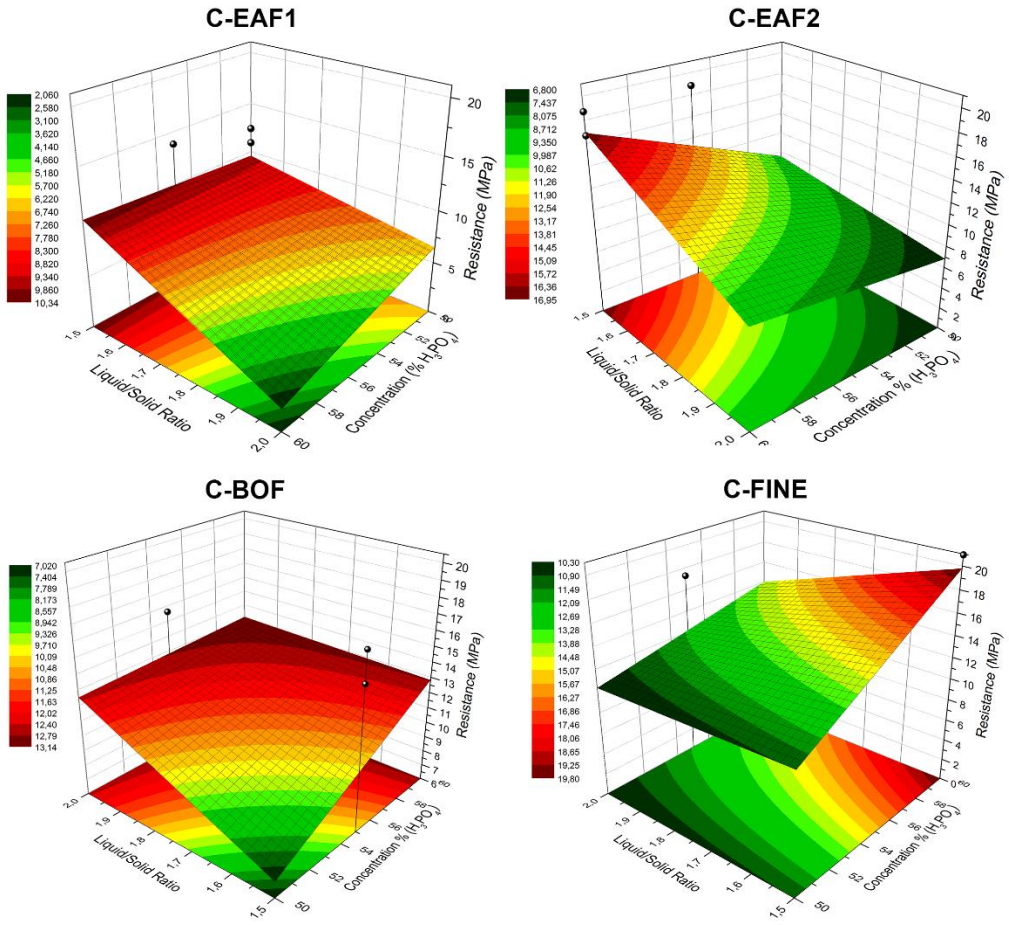

Figure 16. Response surface graphs. Compression strength according to the liquid/solid ratio and phosphoric acid concentration.

3.4.2 Mineralogical, chemical and morphological characterization of the cements

3.4.2.1 XRD

In figures 17a, 17b, 17c and 17d the initial slags (EAF1, EAF2, BOF, FINE) are compared with the cements respectively formed from them (C-EAF1, C-EAF2, C-BOF, C-FINE). The formation of crystalline phases and the presence of a large amorphous phase, possibly a result of the reaction

of the cement and the vitreous compound present in the slags, are identified. It is observed that the initial reagents identified by XRD are almost completely exhausted in the formation of the phosphate ceramics, evidencing the scarcity of the raw materials in the phosphate matrix. Therefore, it is assumed that the reaction takes the time necessary to form a mechanically stable solid material [55]. The principal phases corresponding to the slags analyzed are found on the right of the spectra, with peaks located between (30– 80) $2\theta^{o}$ (black line). Meanwhile, for the cements formed, crystalline phases are described for the peaks located on the left of the spectra, corresponding to the area approximately located between (5 – 30) $2\theta^{o}$ (red line). Various metallic oxides may participate in the formation of CBPS. In the cases where a coherent phosphate ceramic is formed, the reaction products are always mono or dihydrogen phosphate with their respective oxides [3]. XRD describes three common phases for all the cements formed, which are: calcium dihydrogen phosphate hydrate $Ca(H_2PO_4)_2 \cdot xH_2O$; brushite $CaHPO_4 \cdot 2H_2O$; an amorphous phase; and some traces of srebrodolskite, magnetite and dicalcium silicate that did not react (table 19). The amorphous phase is identified by XRD as a hump that is present in all the diffractograms. In figure 17 (a, b) the principal compounds observed from the reaction are wüstite and dicalcium silicate, which could act as precursors in the obtaining of iron phosphate and calcium phosphate, respectively. In figure 17 (c, d) the principal compounds observed from the reaction are dicalcium ferrites and dicalcium silicates, with iron phosphates and calcium phosphates also arising from the reaction. Rietveld quantification with statistical indices between 1 and 2 for GOF (table 19), describes $Ca(H_2PO_4)_2 \cdot xH_2O$ and $CaHPO_4 \cdot 2H_2O$ as minority phases with a range between 10-20%, with an amorphous predominant phase close to 80-90%. For the two crystalline phases identified, and depending on the molar ratio used in the reaction products, brushite or calcium dihydrogen phosphate hydrate can be produced in different proportions [112].

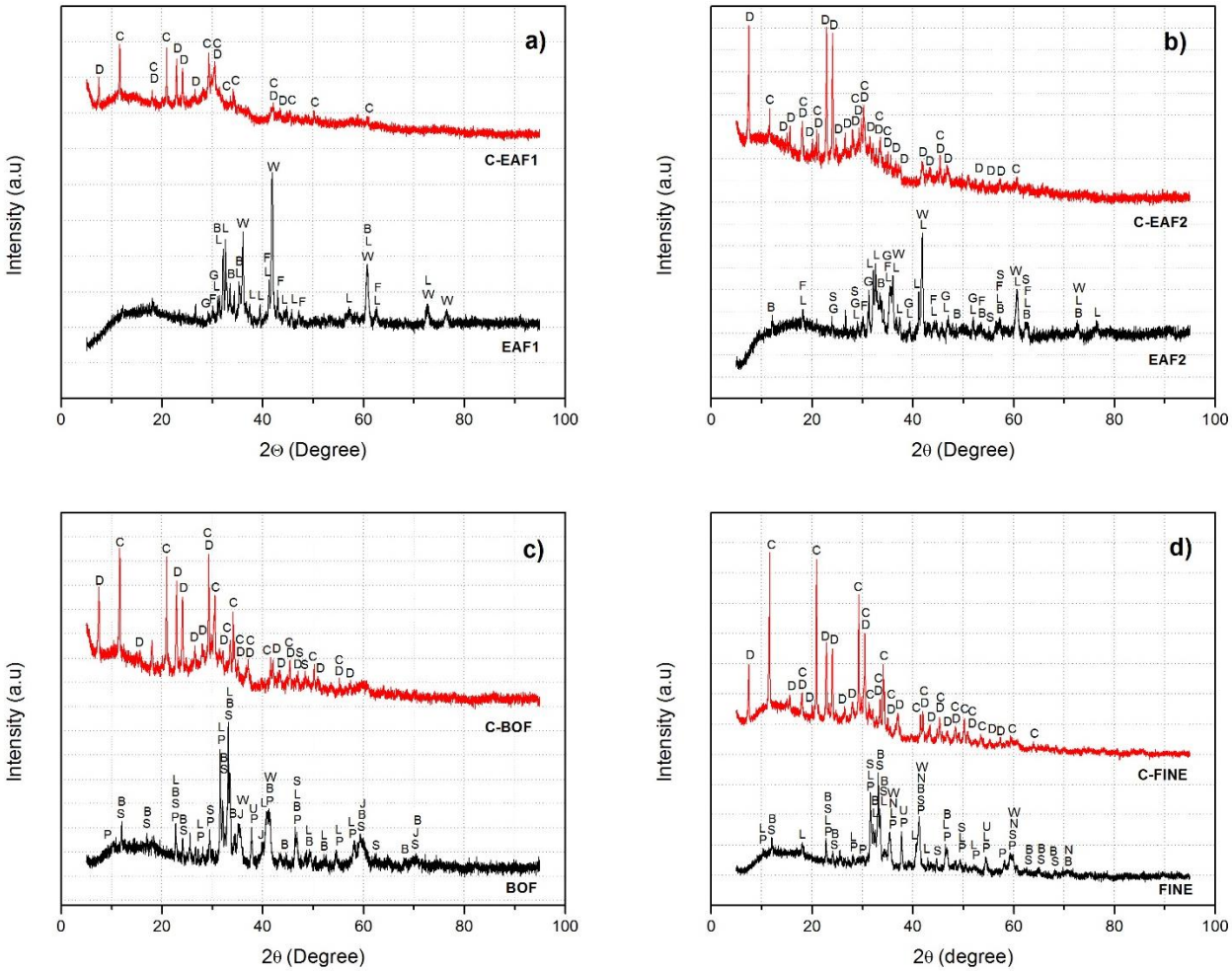

Figure 17. Analysis XRD: a) Comparison EAF1-CEAF1, b) Comparison EAF2-CEAF2, c) Comparison BOF-CBOF, d) Comparison FINE-CFINE. (D) Calcium Dihidrogenophosphate Hydrate, (C) Brushite, (L) Dicalcium silicate, (G) Gehelenite, (B) Brownmillerite, (W) Wüstite, (F) Magnetite, (S) Srebrodolskite, (U) Lime, (P) Silicocarnotite, (J) Ferrous manganese oxide, (N) Manganese oxide.

Table 19. Quantification of phases in cements by Rietveld refinement.

Phase	Formula	C-EAF 1	C-EAF 2	C- BOF	C- FINE
(D) Calcium Dihidrogenophosphate Hydrate %	$Ca(H_2PO4)_2 \cdot xH_2O$	5.4	9.4	9.1	9.2
(C) Brushite %	$CaHPO_4 \cdot 2H_2O$	5.5	1.2	10.2	11.7
Amorphous %	----------	89.0	89.3	80.4	79.0
(F) Magnetite %	Fe_3O_4	0.1	0.1	---	---
(L) Dicalcium Silicate %	Ca_2SiO_4	---	---	0.2	---
(S) Srebrodolskite %	$Ca_2Fe_2O_5$	---	---	0.1	0.1
AGREEMENT INDICES					
R_e		2.05	2.13	2.27	2.28
R_p		1.78	1.89	2.21	2.47
R_{wp}		2.33	2.51	3.16	2.83
Goodness of Fit (GOF)		1.28	1.38	1.54	1.93

The existence of calcium dihydrogen phosphate hydrate ($Ca(H_2PO_4)_2 \cdot xH_2O$) and brushite ($CaHPO_4 \cdot 2H_2O$) in the cements formed can initially be explained by the presence of the $H_2PO_4^-$ and HPO_4^{2-} ions, products of the dissolution of H_3PO_4 in a range (2.15 – 12.37) pH [2], that were identified through FTIR. These ions react with the Ca^{+2} ion, as confirmed through XPS, generating as a result the previously mentioned compounds. Various authors have reported the formation of brushite as a product of the reaction of the aqueous solution of H_3PO_4 and calcium silicate ($CaSiO_3$) [2], [47], [48]. Similarly, the dissolution of dicalcium silicates (Ca_2SiO_4) and dicalcium ferrites (Ca_2FeAlO_5), ($Ca_2Fe_2O_5$) present in the slags generates the Ca^{+2} metallic cation necessary for the reaction with the $H_2PO_4^-$ and HPO_4^{2-} ions, forming the calcium phosphates. The rapid dissolution rate of CaO [2] in compounds such as dicalcium silicates and dicalcium ferrites could lead to very short setting times in cements with strong exothermic reactions, affecting workability in the fresh state.

XRD also shows how the reaction precursors of crystalline nature are transformed into other phases. Equally, the presence of a "hump" is evident in the diffractograms, which could be associated with residues of glassy slag and possible amorphous cements.

3.4.2.2 ***FTIR***

In figure 18, vibrations corresponding to brushite ($CaHPO_4 \cdot 2H_2O$) are observed. This compound appears in all the cements formed, and has four distinct sharp stretching PO/P-O(H) bands in the region between 1150 cm^{-1} and 870 cm^{-1}. These are: 1116 cm^{-1} (shoulder), 1052 cm^{-1}, 980 cm^{-1} and 868 cm^{-1}, and are identified for all four types of cement. Additionally, 789 cm^{-1} and 1648 cm^{-1} (bending vibrations of H_2O); 3485 cm^{-1} and 3543 cm^{1}; (O-H stretching vibration) [100], [129] are identified, as well as a band at 1124 cm^{-1} corresponding to the (P-(OH) stretching vibration for the

HPO_4^{2-} ion [129]. The identification of these bands is consistent with the formation of brushite, a phase whose presence was confirmed through XRD.

The $H_2PO_4^-$ and H_2O ions are assigned to the fundamental vibration units of calcium dihydrogen phosphate hydrate ($Ca(H_2PO_4)_2 \cdot xH_2O$) [130]. The O-H stretching vibration of the $H_2PO_4^-$ ion is associated with the bands at 2926 cm^{-1} and 2336 cm^{-1} (visible especially with the C-FINE). The band identified around 1116 cm^{-1} is assigned to the PO_2 asymmetric stretching (B_1); the band at 958 cm^{-1} (shoulder) corresponds to $P(OH)_2$ asymmetric stretching (B_2); the band at 868 cm^{-1} is assigned to $P(OH)_2$ symmetric stretching (A_1); and the band around 569 cm^{-1} corresponds to the PO_2 bending(B_1) [130].

Some compounds are not identified by XRD, but are assumed to form part of the slag-based phosphate cements. These are the amorphous phases, mainly composed of amorphous iron phosphate, amorphous silica, and amorphous calcium phosphates. Some authors have identified the formation of amorphous silica and amorphous calcium phosphates (ACP) $Ca_x(PO_4)_y.nH_2O$, from the acid-base reaction of wollastonite and aqueous phosphoric acid solution [48], [75], [77], [112]. The main characteristic in the FTIR spectra for the amorphous calcium phosphate (ACP) corresponds to (V_1) for PO_4, the band identified as a shoulder at 950 cm^{-1} [131], which is visible for all the cements synthesized. The corresponding band at 868 cm^{-1}, associated with the HPO_4^{2-} ion, is also assigned to ACP [132]. The amorphous silica can be described by the Si – O – Si vibration, which is associated with short-tailed linear siloxanes, with a band at 1050 cm^{-1} [133] that is present in all the cements formed.

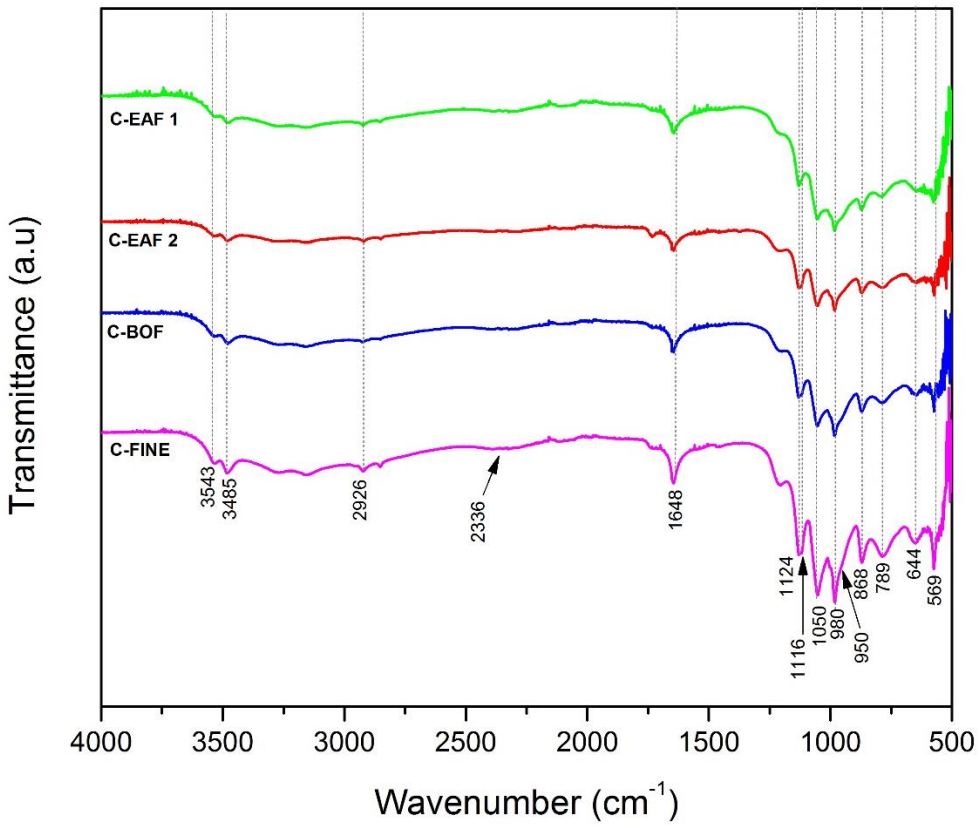

Figure 18. FTIR analysis of the phosphate cements obtained.

3.4.2.3 XPS

In figure 19, two peaks with bond energies of 713.2 eV and 714.5 eV are observed. These correspond to the Fe $2p_{3/2}$ spectra, and can be associated with the presence of iron in Fe^{2+} and Fe^{3+} forms respectively [134]. Additionally, two peaks can be observed with bond energies of 727.2 and 725.3 eV, which are the transition peaks of the Fe $2p_{1/2}$ spectra [135], [136], and which are linked to the main peaks of Fe $2p_{3/2}$ [134]. The presence of the Fe^{2} ions corresponds to the existence of possible amorphous phases of $Fe(H_2PO_4)_2$ and $Fe(HPO_4)$ in the cement formed. In figure 20, peaks are observed at 348.8 eV and 346.7 eV, corresponding to the spectrum of Ca $2p_{3/2}$ for $Ca(H_2PO_4)_2$ and $CaHPO_4$ respectively [121], [137], which in turn correspond to the Ca^{2+} ion. Additionally, a peak at 352.2 is observed, corresponding to the Ca $2p_{1/2}$ spectrum, possibly

associated with $CaHPO_4 \cdot 2H_2O$ [138]. It is important to highlight that the signal corresponding to Fe 2p has higher intensity than that corresponding to Ca 2p. This may explain the greater presence of the amorphous phase for the iron phosphates than for calcium phosphates.

Wagh presented a possible cement formed from the reaction of the aqueous solution of H_3PO_4 with an iron oxide hematite Fe_2O_3 [2]. The product of this reaction was identified as iron (II) dihydrogen phosphate $Fe(H_2PO_4)_2$, or iron (II) hydrogen phosphate $FeHPO_4$. $Fe(H_2PO_4)_2$ is the first compound formed in the reaction of the primary precursors, however, as the reaction continues over the curing time of the cement and in the presence of the reducing agent elemental iron Fe, the product that is finally obtained is $FeHPO_4$. Wagh identifies these cements that form vitreous phases [2].

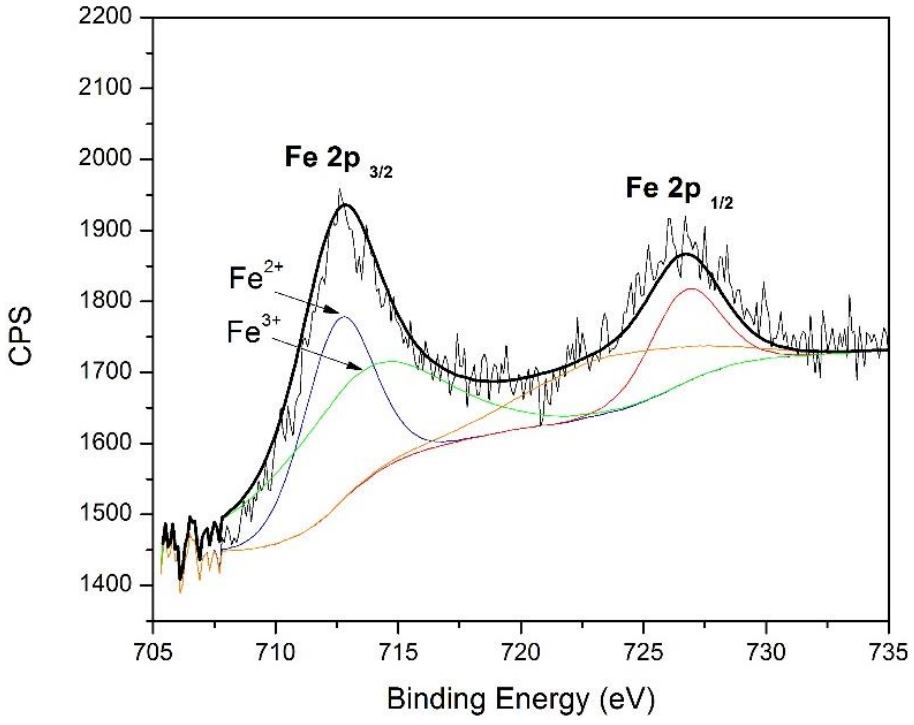

Figure 19. XPS Fe2p spectrum.

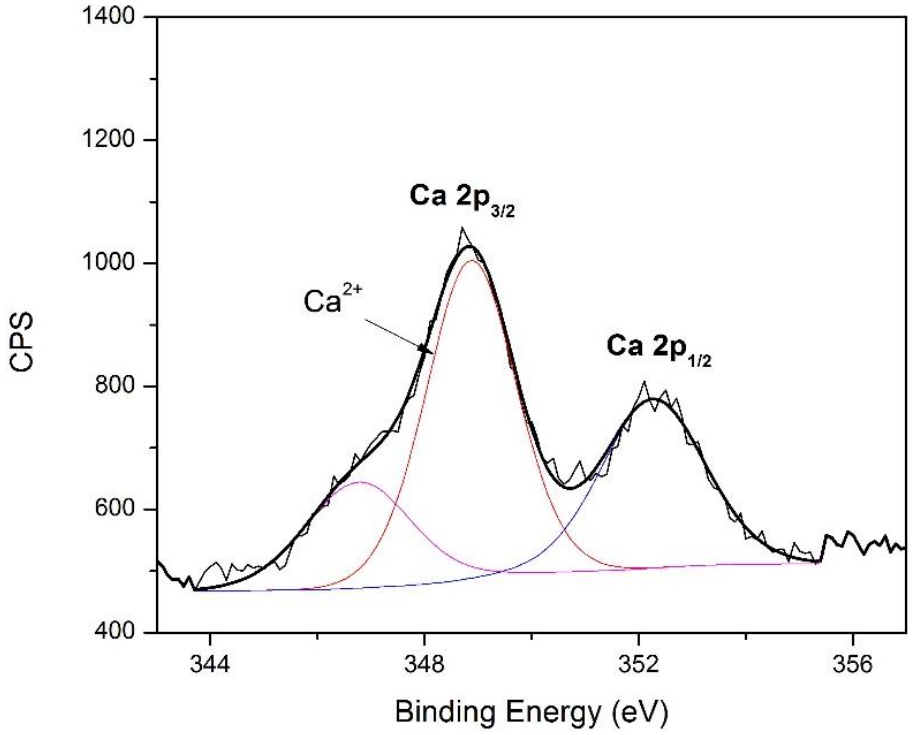

Figure 20. XPS Ca2p spectrum.

The deconvolution of the O1s and P2p can observed in figures 21 and 22, with peaks corresponding to bond energies of 530.3 eV and 133.0 eV, which are associated with $CaHPO_4 \cdot 2H_2O$ [137], [138]. The bond energy at 135.1 eV for P2p indicates that the phosphorus is found in a pentavalent oxidation state, possibly linked as P-O [139], which is the common bond energy for the great majority of phosphate compounds. [140]. The bond energies corresponding to the O1s spectrum for Fe_2O_3 and CaO are 529.6 eV and 529.0 eV, respectively. However, the bond energies corresponding to the O1s spectrum of the cement formed are presented at 528.7 eV and 527.0 eV, which can be attributed to the presence of P-O-Fe and P-O-Ca type bonds, respectively.

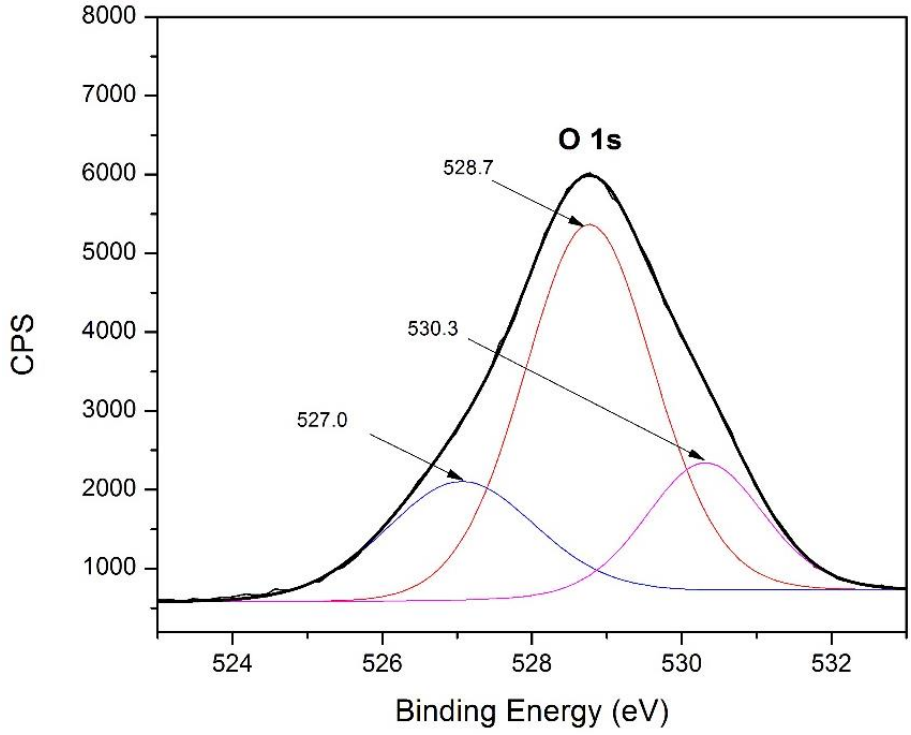

Figure 21. XPS O1s spectrum.

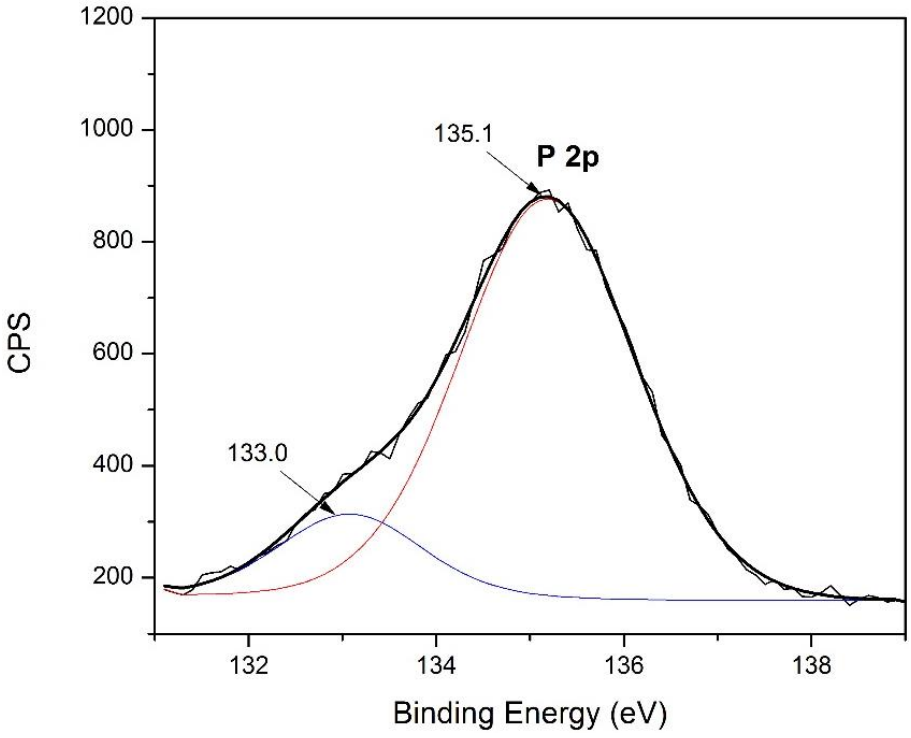

Figure 22. XPS P2p spectrum.

3.4.2.4 SEM/EDS

In figure 23, micrographs for the four cements formed from the analyzed slags can be observed. The presence of two main phases, a crystalline phase and an amorphous phase, are common to all four cements. The formation of calcium phosphates; brushite ($CaHPO_4 \cdot H_2O$) or calcium dihydrogen phosphate $Ca(H_2PO_4)_2 \cdot xH_2O$, can be observed as the incipient formation of columnar-shaped crystals, clearly differentiated from the amorphous phase (figure 24).

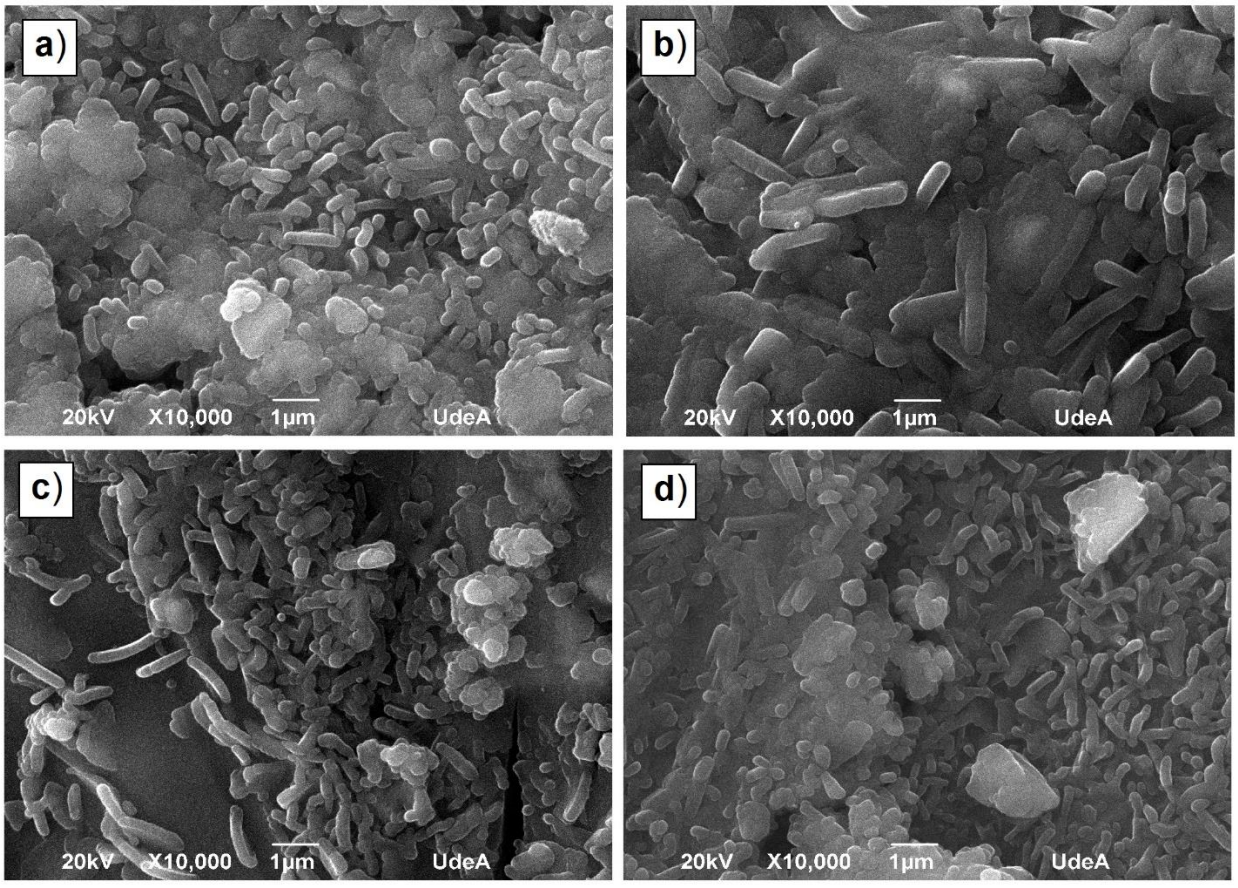

Figure 23. SEM Images of cements obtained from slags: a) C-EAF1, b) C-EAF2, c) C-BOF and d) C-FINE.

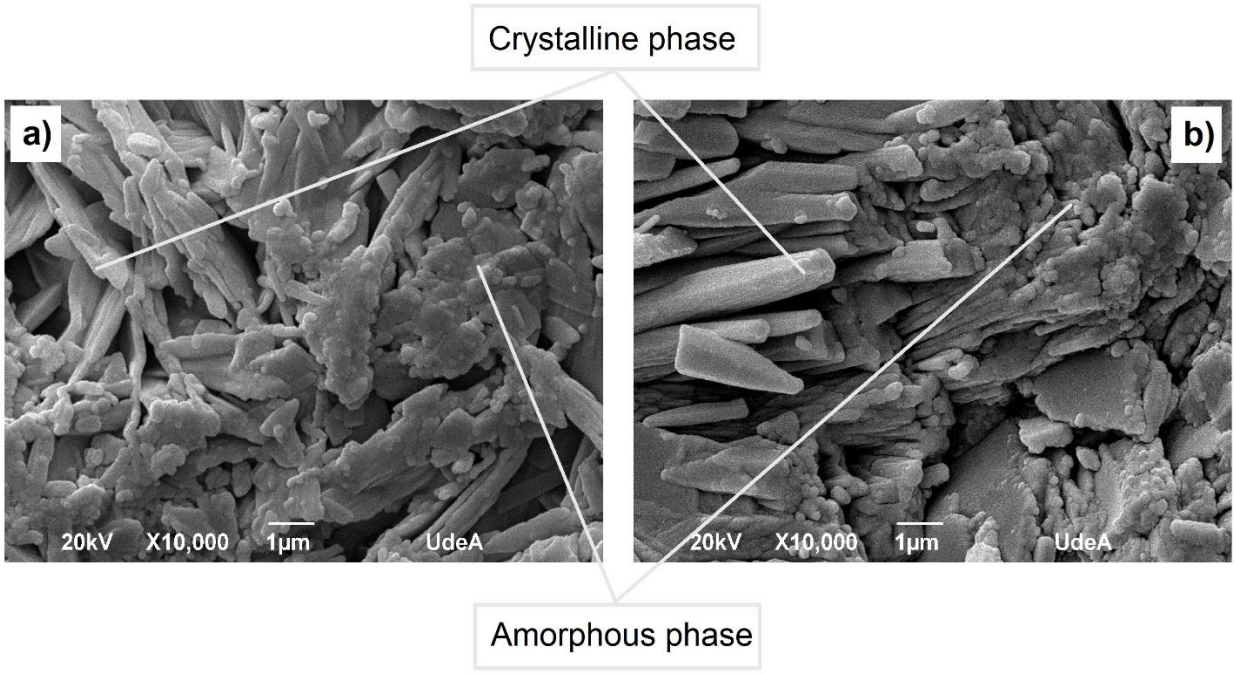

Figure 24. SEM images crystalline phase and amorphous phase, obtained from slags: a) C-EAF1, b) C-EAF2.

To complement the analysis described above, an additional micrograph is presented in figure 25, where the main phases present in the cement formed from EAF2 slag can be observed. From the superposition of EDS elemental composition maps, two phases can be identified as the main hydration products: a crystalline phase composed mainly of calcium phosphates observed on the left side of the CEAF-2 micrograph, and another amorphous phase (not identified by XRD or FTIR, but evidenced by XPS), which is associated with iron phosphates (right side of CEAF-2 micrograph), possibly corresponding to ($Fe(H_2PO_4)_2$) or ($FeHPO_4$) [2] [5]. Moreover, the presence of amorphous calcium phosphates and amorphous silica, possibly originating from the dissolution of dicalcium silicates present in the slags, can be discerned.

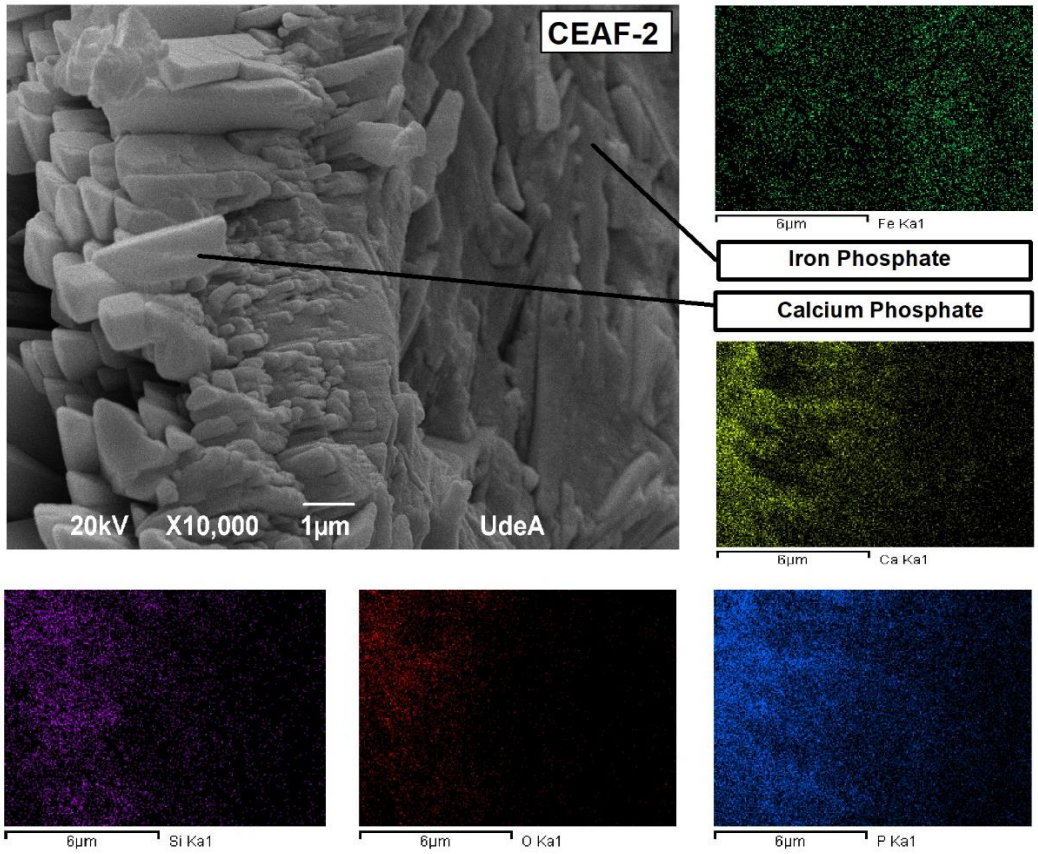

Figure 25. SEM image and composition map of the CEAF-2 cement.

3.5 Amorphous Phase

Different authors have identified amorphous phases in the formation of phosphate cements; Fitch and Sharp describe a "hump", identified through XRD, with amorphous phases between (10-35) 2θ at the baseline, which also coincides with an amorphous phase for slag-based phosphate cement [141], Ding et al. suggests the coexistence of crystalline and amorphous phases in magnesium phosphate cements, whereby the crystalline phase provides the framework for the structure and the amorphous phase is responsible for filling the spaces between the grains [10], C. Shi et al. added waterglass to an MPC paste, which when reacted with the magnesium cation produces an amorphous magnesium hydrate silicate gel compound that fills the pores of the MPC matrix preventing infiltrations in the cement [14], Chong et al. suggests that the presence of calcium ions

in an MPC system induces the formation of amorphous phases [142], Viani et.al explains the formation of two intermediate amorphous phases in MPC, which interfere by partially obstructing the crystallization of MPC. Similar amorphous components are even mentioned in other systems such as calcium and Zinc phosphate cement [11].

A model explaining the presence of amorphous phases and the hydration process of slag-based phosphate cements has not yet been reported. However, the exothermic acid-base reaction system may help partially explain the phenomenon, in the same way, several authors have described the hydration process of magnesium phosphate, which is generally referred to in an attempt to understand the formation of the slag-based phosphate cement described in this investigation. The most widely accepted hydration process for phosphate cement is the dissolution-precipitation model [34]. This can be adapted as follows: i) dissolution of metal oxides in the phosphoric acid solution that allows the release of phosphate anions and metal cations; ii) reaction of anions and cations to form the amorphous metal phosphates hydrates, which in part solidify, forming amorphous compounds or poorly crystalline phases; and iii) partial crystallization of the gel produced forming crystalline networks [2]. Therefore, it can be stated that the phosphates formed from the reaction of the steel slags and the aqueous solutions of H_3PO_4 coexist in crystalline and amorphous phases.

It is important to highlight the high level of amorphous content, quantified through Rietveld refinement (ranging from 80% to 90%), which is found in the cements obtained from the slags. This vitreous phase, is principally associated with amorphous iron phosphates $Fe(H_2PO_4)_2$ or $FeHPO_4$, amorphous calcium phosphate (ACP) and amorphous silica.

The amorphous products are mainly responsible for the mechanical strength reported, given that

they represented 90% of the matrix. Also, it is possible that the majority correspond to iron phosphate, as a large quantity of wüstite and dicalcium ferrites are observed as initial reagents. The iron phosphates are obtained from the reaction of iron oxides such as wüstite (FeO) and magnetite (Fe_3O_4) in aqueous H_3PO_4 solution, as well as from the dissolution of dicalcium ferrites such as brownmillerite and srebrodolskite, and act as donors of the Fe^{2+} cations necessary for the acid-base reaction [2], which is consistent with previous research [46], Liu et al. show the formation of a novel magnesium-iron phosphate cement, from the incorporation of Fe_2O_3 with a magnesium phosphate cement paste (MPC). Although these authors do not specify the type of iron phosphate, they describe this secondary structure as an amorphous phase of iron phosphate gel with a dense microstructure and highly relevant characteristics, notably improved crystallization of the main phase (struvite), mechanical strength and resistance to water [143]. Also, a significant phase of amorphous calcium phosphate, a product of the dissolution of dicalcium silicates and dicalcium ferrites that are donors of Ca^{2+} cations, is expected.

The presence of vitreous phases can be explained initially by the tendency of H_3PO_4 to form completely amorphous hydrogen bond glasses [3]. In an acid-base reaction, when the highly alkaline metallic cations enter the reaction, crystalline structures such as calcium dihydrogen phosphate hydrate and brushite tend to be formed. In contrast, the presence of vitreous iron phosphate structures can be explained by the existence of less basic cations in the reaction, which tend to form amorphous or vitreous structures, given that strongly connected polyhedrons maintain their connection with weaker forces, allowing the formation of more variable and flexible structures [3]. Amorphous calcium phosphates (ACP) are transitional phases during the formation of calcium phosphate in aqueous solutions. ACP normally precipitate from supersaturated solutions which contain calcium cations and ion phosphates [56], although the FTIR signal for the

ACP generally shows wide bands with few distinctive features [56]. It was possible to observe the ACP in the prior FTIR analysis carried out in this study [131]. This analysis also enabled the identification of amorphous silica.

3.6 Conclusions

Chemically bonded phosphate ceramics (CBPC) were synthesized from steel slags (EAF, BOF and FINE). These corresponded to multiphase phosphate cements, with iron phosphates and calcium phosphates being predominant phases.

The crystalline phases found correspond to calcium dihydrogen phosphate hydrate and brushite. Meanwhile, the vitreous phases are attributed to amorphous iron phosphates $Fe(H_2PO_4)_2$ or $FeHPO_4$, amorphous calcium phosphate (ACP) and amorphous silica. The amorphous phase is in a range of 80-90%, so responsibility for the mechanical strength of these cements is attributed mainly to it.

The formation of iron phosphate cements follows mainly from the presence of metallic Fe^{2+} cations present in divalent oxides such as wüstite (FeO), divalent-trivalent oxides such as magnetite (Fe_3O_4), and compounds that dissolve in acid environments such as brownmillerite (Ca_2FeAlO_5) and srebrodolskite ($Ca_2Fe_2O_5$). The formation of calcium phosphate cements is due principally to the formation of metallic Ca^{2+} cations that are predominantly present in dicalcium silicates (Ca_2SiO_4) that dissolve in acid environments, helping in the formation of amorphous silica. In additional, brownmillerite (Ca_2FeAlO_5) and srebrodolskite ($Ca_2Fe_2O_5$) provide the corresponding metallic cation when dissolved.

The highest mechanical strengths correspond to the cements obtained from the BOF slag and the FINE slag (mixture of EAF, BOF and LF slags). The controllable variables considered in this study that have the greatest influence on the mechanical strength of the cements obtained are liquid/solid proportion and H_3PO_4 concentration. It can be stated that the minimum values for the liquid-solid ratios in the mix and the highest concentration of H_3PO_4 positively affect the compression strength. As such, the behavior of the phosphate cements developed is generally predictable; lower quantity of water in the cements contributes to increasing the mechanical strength.

4. Phosphoric rock and electric arc furnace (EAF) slag as raw materials for the synthesis of chemically bonded phosphate ceramics (CBPC)

Abstract: The present chapter seeks to evaluate the possibility of obtaining chemically bonded phosphate ceramics from steel waste products, such as EAF slag, and phosphate minerals, such as phosphoric rock. Chemical, morphological and mineralogical evaluation of the raw materials showed the presence of significant percentages of P_2O_5 and metallic oxides such as Fe_2O_3 and CaO, which are necessary for the formation of ceramics through the acid-base system. XRF, SEM/EDS, XRD, FTIR and TGA techniques were used for the characterization of the raw materials.

For analysis of the formation of the chemically bonded phosphate ceramic and the study of its microstructure, ICP-OES, ICC DRX and SEM/EDS techniques were used, as well as compression tests. The formation of Brushite-type calcium phosphates was mainly observed in the obtained ceramic. The mechanical resistances recorded are mainly attributed to the abundant quantity of anhydrite and gypsum present in the binding agent.

4.1 Introduction

The synthesis of environmentally friendly materials has become a challenge for research. New environmental rules and government policies, as well as evidence of environmental deterioration, mean that the development of new materials must be underpinned by a philosophy of sustainable development. The paradigm of eco-efficiency can be summarized in terms of its two basic pillars: rational use of natural resources and reduction of gases emissions in production processes [31]. This proposal for new cementitious materials is based specifically on these pillars, with the twin aims of significantly reducing the polluting emissions traditionally associated with the cement industry, and improving the use of existing primary materials.

The obtaining of phosphoric acid through leaching of phosphoric rock, generally using H_2SO_4, has significant environmental impacts. These result from the presence of heavy metal waste materials, such as As, Pb, Cd, Cr, F, Zn, Cu, as well as radionuclides in phosphogypsum, the main waste product of the process [28], [29], Moreover, the limitations of the process for phosphoric rocks with low quantities of P_2O_5 [25] as well as the low recycling rates of phosphate (less than 5%)[144], raise concerns over the rational use of phosphoric rock for the synthesis of commercial compounds.

The phosphoric rock found in Boyacá (Colombia) is commonly used for agricultural purposes, such as the obtaining of partially acidulated fertilizers, or as direct application amendments for acidic soils. As this material is relatively insoluble [25], with P_2O_5 content (< 30%), it is not economically feasible for the obtaining of phosphoric acid, meaning that the material is not used to its full potential. Currently, there are no records on the use of phosphoric rock as a raw material for the obtaining of cementitious materials, which is an area with potential for exploration of new uses for this material.

Globally, significant environmental impacts arise from the production of various forms of slag in the steelmaking process [145]. While slags have potential for utilization, EAF slag is significantly under-utilized due to its low hydraulic properties [146] and the presence of leachable elements that can contaminate soils and water sources [120], [126]. The high output of steel slag in Colombia (0.1 to 0.3 tons per ton of steel produced) [147], makes it important to explore new ways of utilizing this material, and thereby enhancing the eco-efficiency of the productive processes.

Phosphate cements, known as chemically bonded ceramics (CBCs) are a focus for research on new eco-efficient materials. These are defined as acid-base reaction systems [11], where the acid component commonly used is phosphoric acid (H_3PO_4), and the base component is provided by metallic oxides. Considering also phosphate rock and steel slag as raw materials, important applications can be seen as precursors of CBCs that warrant further study. The present study explores the obtaining of CBSs from phosphoric acid and phosphogypsum obtained by leaching phosphoric rock from the department of Boyacá and EAF slag.

La roca fosforica al igual que las escorias de aceria no se han considerado como materias primas precursoras de CBPC

4.2 Materials and methods

4.2.1 Raw materials

The raw materials evaluated in the present chapter included: Phosphate rock (phosphorite), commercially acquired under the name "Pesca phosphorite" and subjected to drying, grinding and sieving, with particle size values 104.4 µm, 201.2 µm y 253.9 µm at d_{10}, $d_{50,}$ $d_{90,}$ respectively. EAF slag (previously referenced as EAF2), also known as black steel slag, is derived from primary metallurgy or scrap metal smelting in electric arc furnaces via an oxidation process, where carbon content is adjusted and impurities such as aluminium, manganese, silicates and phosphorus eliminated [145], these slag were obtained from steel production plant and was ground to obtain powder that passed through a 63 µm analytical sieve, similarly to commercial cements, subject to grinding trough jaw, rollers, and balls to obtain particle size values of 1.2 µm, 8.8 µm y 43.1 µm at d_{10}, $d_{50,}$ $d_{90,}$ respectively. Dihydrogen potassium phosphate KH_2PO_4, (Sigma Aldrich Co), with particle size of d_{50} = 39 µm.

The granulometric analysis of the raw materials shows the difference in grain size. It can be observed, a characteristic directly affecting the dissolution capacity of the phosphorite in an acidic environment [148], that leads to favorable reactivity on the part of the slags. The EAF slag can be described as the typical slag obtained from most steel production plants, which is not subject to any grinding treatment and can be classified as a coarse aggregate (gravel size). This means that grinding processes are required to bring the slag to a fine aggregate size (sand size), leading to increased costs. Phosphorite, when commercially obtained, can be considered as a fine aggregate.

4.2.2 Beneficiation of Phosphoric rock

Anionic flotations were carried out in Denver flotation cells of 1 liter capacity. The pH was adjusted by adding H_2SO_4. The primary collector was oleic acid and the secondary collector was fuel oil. Phosphorite was leached using two processes. The first of these used 8% acetic acid solution, with a liquid-to-solid ratio of 5:1; reaction time of 35 minutes; and 350 RPM. The second used 9 Molar H_2SO_4, with a liquid-to-solid ratio of 1:1; reaction time of 120 minutes; and 300 RPM

4.2.3 Mixing process

Chemically bonded ceramics were produced from a concentrate of phosphoric rock treated with 9M H_2SO_4, EAF slag, and KDP, a phosphate compound additional to the mixture, according to the formulations in Table 20. The mixing was carried out in a beaker with the addition of deionized water. After mixing the components for three minutes, the mixture was poured into cubic silicone molds of 1 cm^3, in triplicate. The samples were removed from the molds after 24 hours of preparation for subsequent curing in ambient laboratory conditions (temperature: 23 $^oC \pm 2\ ^oC$, relative humidity: 37 % $\pm$ 1 %).

Table 20. Precursor mixtures ratios

Sample	Liquid/Solid (wt. %)	Phosphate rock/Slag (wt. %)	Phosphate Rock/KDP (wt. %)
PR-1	0.33	2.0	---
PR-2	0.33	3.0	---
PR-3	0.5	2.0	2.0

4.2.4 Chemical, mineralogical and morphological characterization

Instrument (Model Quanta 450 FEG, FEI) at an accelerating voltage of 20 kV, equipped with an energy dispersive X-ray fluorescence spectrometer (EDS) (Model Apollo X, EDAX) was used to

collected images with scanning electron microscope (SEM) on phosphorite, slag and binder samples after 28 days of curing.

Chemical analysis of the phosphorite, was performed by XRF spectrometry in a Thermo ARL Optim'X WDXRF device, in a disc in crucible at 1100 °C of the phosphate rock molten.

The powder sample of phosphorite was analyzed by means FTIR spectroscopy with a Shimadzu IRTracer-100 infra-red device and a scanning range (cm^{-1}) of 400 – 4000 and 24 cycles. The attenuated total reflectance technique (ATR) was used.

For the mineralogical characterization of the raw material and the obtained ceramic, a Bruker D8 Advance Bragg Brentano θ-θ diffractometer was used, with Cu Kα radiation of 40 mA and 40 kV, for an acquisition range of 2θ (10° - 80°) in the X-ray patterns. The software High Score Plus was used to identify the minerals present in the samples, based on the standards of the COD (Crystallography Open Database) of the ICSD (Inorganic Crystal Structure Database).

Thermogravimetric analysis (DTA-TGA) of the phosphorite powders was carried out using a TA Instruments model SDT Q 600 device, at a heating rate of 10 °C/minute, a temperature range between 20 and 1000 °C, and with an air atmosphere.

To enable measurement of the free phosphorus contents in the phosphorite concentrate and phosphorite leached with CH_3COOH and H_2SO_4, one (1) gram of each sample was diluted in 70ml of deionized water and stirred at 300 RMP for 72 hours, before filtering the liquid and completing the dilution in a volumetric flask (100 ml). Following this, the analysis was carried out using a Spectro Blue (Spectro) inductively coupled plasma optical emission spectrometer (ICP-OES), equipped with a Paschen-Runge polychromator. The line at 178.287 was used for the P quantifications.

Isothermal conduction calorimetry (ICC) analysis, was carried out on the mixture of EAF slag, KH_2PO_4 and leached phosphoric rock, in accordance with the formulations in Table 20. For this, a TAM-Air device (8 channels, TA Instruments) was used. The components were kept in glass vials until the baseline was established at (25.0 ± 0.1 ° C). The water was then injected, with constant stirring, and the reaction was initiated. The heat flow and total heat were measured for 8 hours.

Compression tests on the sample were performed in 1 cm^3 cubes, using a universal testing system (MTS System) with a loading speed of 0.2 mm/min and maximum load capacity of 50 kN.

4.3 Results and discussion

4.3.1 Characterization of raw materials

4.3.1.1 Characterization of EAF slag

In the XRF chemical analysis of the EAL slag, presence was observed of Fe_2O_3, CaO, SiO_2 and MnO, forming mineral phases of dicalcium silicates (Ca_2SiO_4), iron oxides such as wüstite (FeO) and magnetite (Fe_3O_4), and dicalcium ferrites of the brownmillerite (Ca_2FeAlO_5) and srebrodoslkite ($Ca_2Fe_2O_5$) types. The last of these are potential compounds for the formation of chemically bonded phosphate ceramics [2] and the characterization of them is consistent with previous studies [126].

4.3.1.2 Characterization of phosphoric rock

Fig. 26 shows the elemental composition of the phosphorite, based on the SEM/EDS semi-quantitative general scan. The main elements identified are Ca, O, P, C, F and Si, while Al, S and Fe are also identified, in lower proportions. The XRF results (Table 21) show a significant presence

of P_2O_5 (28.4 %), a compound that is necessary for the formation of chemically bonded phosphate ceramics. These also show the presence of CaO and fluorite, which indicates that the phosphates appear as fluorapatites. The high values recorded for the CaO/P_2O_5 ratio (1.62) and the dry weight of the fluorite (2.54 wt. %), show that the phosphate particles possibly correspond to francolite and fluorapatite [149].

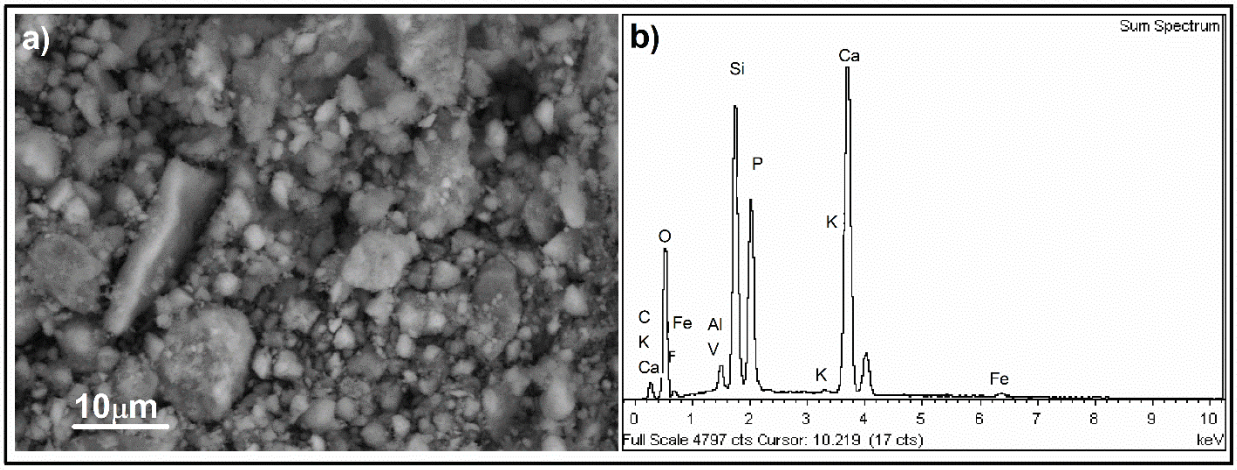

Figure 26. a) SEM image of phosphoric rock.. b) EDS image of phosphoric rock.

Table 21. Chemically composition of phosphate rock. (wt %).

Oxides	MgO	Na_2O	K_2O	BaO	Al_2O_3	SiO_2	P_2O_5	SO_3	CaO	TiO_2	Cr_2O_3	MnO	Fe_2O_3	SrO	F	L.O.I*
wt. %	0.19	0.24	0.17	0.03	1.85	11.0	28.4	0.77	46.07	0.09	0.03	0.04	0.93	0.2	2.54	7.4

*Loss On Ignition 1050°C

In Fig. 27 the bands for the phosphate group can be observed in symmetric and asymmetric stretching vibration modes at $\upsilon_1 = 963$ cm^{-1} and $\upsilon_3 =$ (1092 and 1027) cm^{-1}, and bending vibration modes at $\upsilon_2 = 478$ cm^{-1} and $\upsilon_4 =$ (601 and 566 cm^{-1}). These bands indicate polyhedral structures typical of $(PO_4)^{3-}$ [150]–[152]. Two bands appear at $\upsilon_3 = 1429$ and 1454 cm^{-1}, and $\upsilon_2 = 864$ cm^{-1}. These correspond to the vibrations of the carbonate ions $(CO_3)^{2-}$ [150], [153], specifically B-type carbonate, which is assigned to vibrations for francolite (fluorapatite carbonates), in which the

PO_4^{3-} ion is replaced by the CO_3 ion [151], [154] Calcite is identified with a slight, almost imperceptible band at 713 cm^{-1} [154], likewise is observed two overlapping peaks shows with humps at (544 and 533 cm^{-1}) were associated to presence of kaolinite [155], [156]. Additionally, the characteristic vibrations of quartz are identified at: υ_3 = 1163 cm^{-1}, υ_1 = 798 and 779 cm^{-1}, υ_2 = 695 cm^{-1} and υ_4 = 466 cm^{-1} [157].

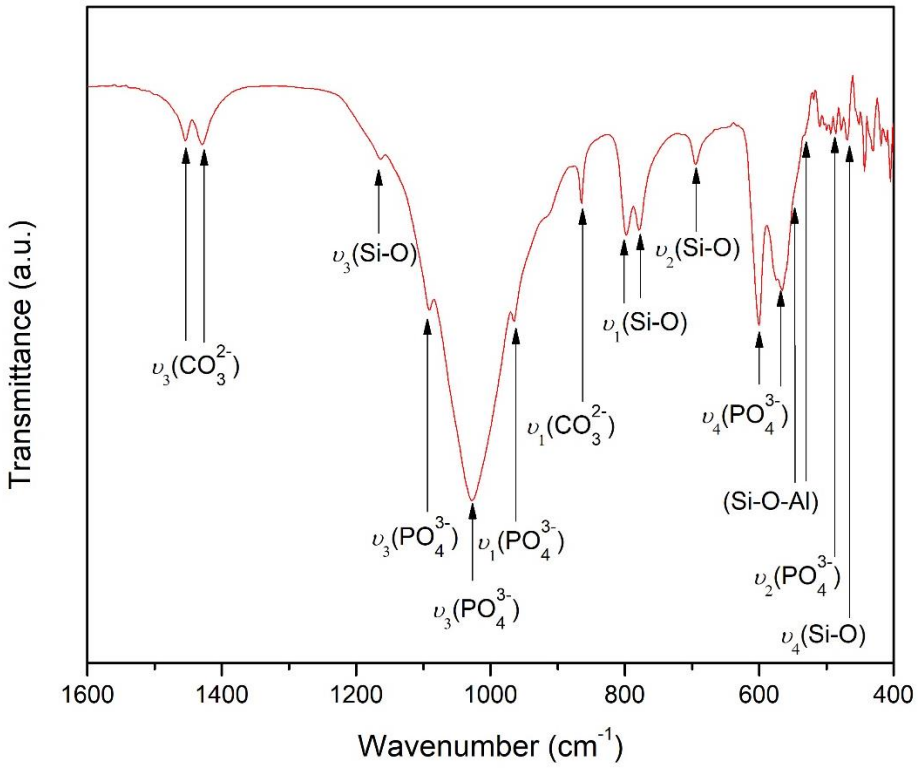

Figure 27. FTIR spectra of phosphate rock.

Fig. 28 shows the diffractogram for phosphorite. The minerals present in the phosphorite, which are observed in their main phases and are referenced according to the ICSC and COD datasheets, are as follows: fluorapatite carbonate ($Ca_5(PO_4,CO_3)_3F$), quartz (SiO_2), calcite ($CaCO_3$), siderite ($FeCO_3$) and kaolinite ($Al_2Si_2O_9$). The minerals found confirm the chemical and elemental composition identified by XRF, SEM/EDS and FTIR. The content of fluorapatite carbonate is

particularly high, and the significant percentages of gangue minerals such as quartz enable the phosphoric rock to be classified as francolite (apatite carbonate) of sedimentary origin.

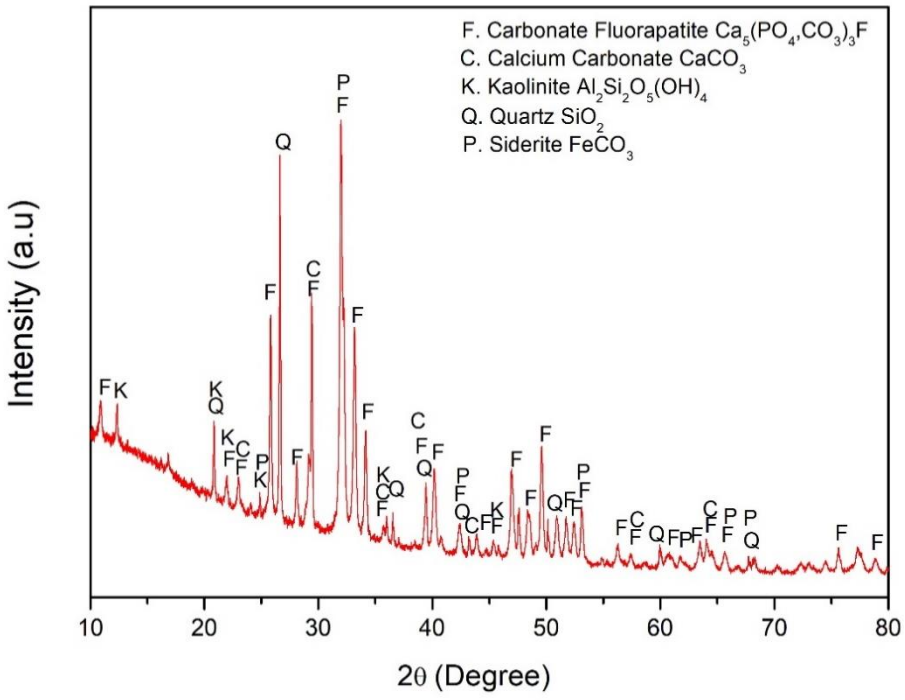

Figure 28. XRD results of the characterization phosphate rock.

The TGA shown in Fig. 29, shows four mass loss zones. The first of these, at 36.4ºC (0.19 %) is related to the loss of moisture. The second zone, at 375.4 ºC (1.53 %) is attributed to the loss of water corresponding to the hydroxyl group of apatite. The third zone, which corresponds to the range between 650 and 900 ºC and a total mass loss of 6.1 %, is associated with the loss of CO_2 in the apatite [151], [154], which confirms the presence of the fluorapatite carbonate identified by FTIR and XRD. The complexity of the thermal behavior of apatite makes it difficult to differentiate the carbonation behavior [158], However, there are two types of CO_2 that are associated with natural substitution in the francolite network. These are: $CO_{2\alpha}$, which is liberated between 500 and 790 °C, and $CO_{2\beta}$, which is liberated between 800 – 1050 °C. These can be associated with the mass losses at 694.2 °C and 812.2 °C respectively[149]. Compounds in a lower proportion, such

as kaolinite, can be associated with the peak between 500 - 600 °C [159]. The total losses corresponded to the ignition losses recorded by XRF (~8.0 %).

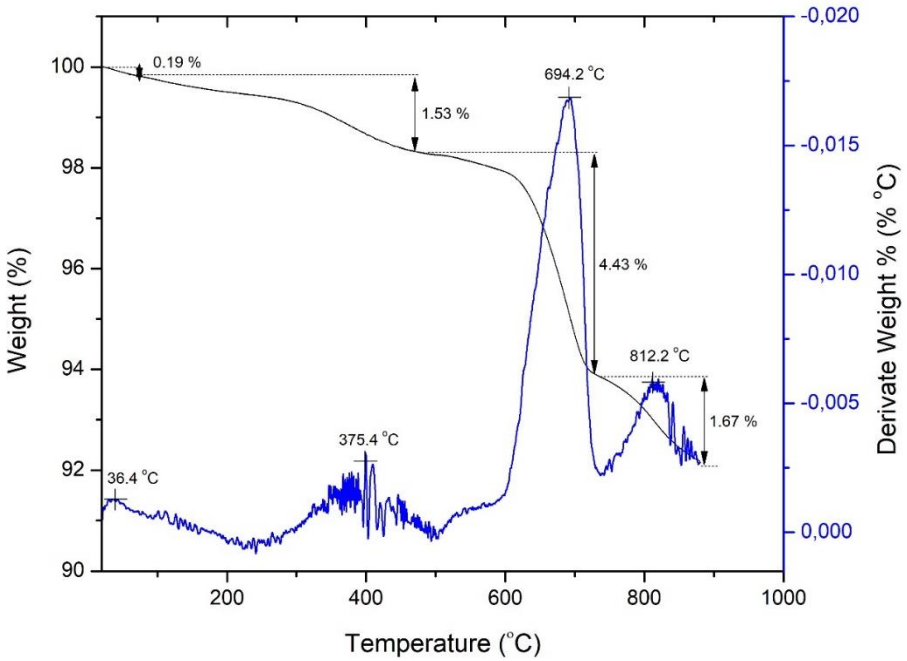

Figure 29. TGA and DTG curves of phosphate rock.

Of the different natural variations observed for apatite, fluorapatite carbonate ($Ca5(PO_4,CO_3)_3F$) is identified as the principal phase in the phosphoric rock. The phosphate mineral is a mixture of francolite and a set of mineral species making up the gangue, which include quartz, calcite and clays. Francolite, as a species that is absorbent of external elements, requires the incorporation of CO_3^{2-} in its structure to replace PO_4^{3-}, generating an increase in the content of F^- fluorite to restore the charge balance[154]. The production of soluble phosphates is made difficult by the high fluorite content, as the similarity in the physical properties of carbonates and phosphates impedes the beneficiation of the mineral [40], The separation of the carbonates and the fluorite significantly affects the cost of conventional beneficiation, which makes it necessary to seek alternative methods of use [160].

4.3.2 Upgrading of phosphoric rock

The fertilizer industry has specified the criteria necessary for phosphoric rock to be used as a precursor to soluble phosphates for agriculture. These are as follows: i) P_2O_5 content above 30 %; ii) CaO/P_2O_5 ratio below 1.6; and iii) MgO content below 1 wt. % [161], The phosphorick rock in this study only complied with the last of these requirements, which reduces its potential for agricultural applications and makes it necessary to consider beneficiation methods. Francolite is insoluble in water and has low solubility in ammonium citrate [25] Therefore, it is not reactive with metallic oxides in acid-base systems for the formation of chemically bonded phosphate ceramics, and the method in Fig. 30 is proposed for its beneficiation through physical and chemical techniques.

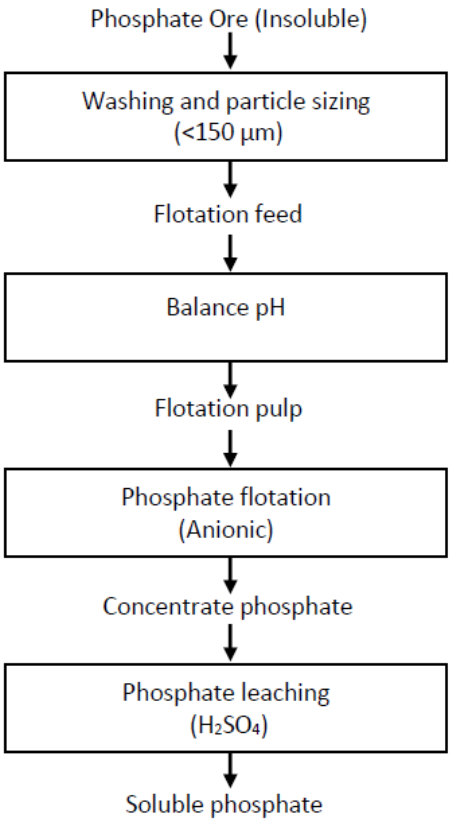

Figure 30. Phosphate rock upgrading process

Source: Adapted from, Crago ‘‘Double Float’’ process. H. Sis and S. Chander (2003) [161].

4.3.2.1 Particle size

Table 22 shows the analysis of particle size in relation to percentage by weight of P_2O_5 using semiquantitative XRF. With regard to the particle size, mesh size # 100 (< 150 microns) was selected, as it is commercially available. While mesh size # 400 (< 28 microns) allows better recovery percentages than # 100, the particle size that passes through does not differ significantly, and its use would incur milling and screening costs.

Table 22. P_2O_5 percentage in phosphate rock according to particle size.

Particle Size (µm)	wt. % P_2O_5
>150	23.45
150 – 75	28.4 – 28.47
75 – 38	27.78 – 24.08
< 38	28.74

4.3.2.2 Flotation

According to the previous characterization, phosphoric rock is classified as a francolite-type sedimentary mineral, whose main phase is fluorapatite carbonite and whose main gangue mineral is silica. Sedimentary deposits whose main gangue is composed of siliceous materials can be successfully beneficiated by flotation [40], [161], [162]. Foam flotation is an appropriate physical method given than the main gangue mineral corresponds to silica, which allows the flotation of phosphates, depressing and eliminating the silica, several authors have identified that the surface of phosphate minerals becomes more hydrophobic in the presence of auxiliary reagents, so a direct flotation process is assumed, with the addition of anionic collectors, such as fatty acids [161] [163] [164] that hydrophobize phosphate minerals allowing the selective adhesion of phosphate and separating solid hydrophilic particles, in this case gangue minerals such as silica. However, it is important to highlight that sedimentary phosphates are more sensitive to similarity in the chemical

properties of the surface of the minerals present, which makes separation by flotation a challenging problem [160].

Various phosphorite flotations were carried out with particle size (< 150 microns), varying the pH between (7.4 – 10.7) with 8.6 being the pH with the best P_2O_5 recovery rate. Additional flotations were carried out to determine the quantity of collector with the best recovery rates, finding that 1462 g/ton concentrated the greatest quantity of P_2O_5. Table 23 shows the parameters for the flotation process. Initially, the pulp was placed in the flotation cell for 20 minutes, before collector and foaming agent were added at 5-minute intervals. The foams collected, corresponding to the floated phosphorite concentrate and tails, were oven-dried at 105ºC for 24 hours. Finally, the results were analyzed by semi-quantitative XRF, finding P_2O_5 concentration values of 30.2 % and a reduction in SiO_2 content of 6.4 %.

Table 23. Parameters considered in phosphate rock flotation.

Item	Characteristic /Values
Flotation Type	Direct- Anionic
Pulp concentration	30%
R.P.M	1200
Collector type	Anionic
Main collector	Oleic acid
Secondary collector	Fuel Oil
Foaming agent	Pine oil
pH Regulator	H_2SO_4
pH Flotation	8.6

To determine the quality of the flotation process the recovery rate (R) was used. This is a metallurgical index which is defined as the ratio between the weight of the mineral of interest in the concentrate and the quantity of this mineral in the feed [163] (equation 5).

$$R = \frac{Weight\ of\ the\ mineral\ of\ interest\ in\ concentrate}{Weight\ of\ the\ mineral\ of\ interest\ in\ feed} \quad (5)$$

To arrive at the following equation (equation 6):

$$R = \frac{C\ x\ tc}{A\ x\ ta} \quad (6)$$

Where: *C* is the weight of the concentrate, *tc* is the tenor of the concentrate, *A* is the weight of the feed, and *ta* is the tenor of the feed.

The recovery rate (Table 24) can be defined as referring to the quality of concentration of P_2O_5, with an ideal recovery index being equal to 1. In the present case, it can be stated that 89 % of the P_2O_5 was recovered in the concentrate, and the remaining 11 % left the circuit via the flow of tails.

Table 24. Direct flotation weights, grades and recovery.

Abv.	Item	Values
A	Weight feed (g)	600
C	Weight Concentrated (g)	466.7
B	Flotation tail (g)	131.0
Ta	Grade feed (%)	28.4
Tc	Grade Concentrated (%)	32.43
Tb	Grade tail (%)	21.65
R	Recovery Index	89

4.3.2.3 Leaching of the phosphoric rick with H_2SO_4

Phosphates that are rich in carbonates can be processed by calcination and leaching with organic acids or mineral acids. The calcination of phosphates frees CO_2, which transforms the apatite carbonates into fluorapatite, which is a less reactive material after calcination [165]. Selective leaching with organic acids such as acetic acid eliminates the carbonates present in the phosphorite, partially solubilizing the phosphates [166]. For the phosphoric rock under study, calcination is inappropriate as it does not make the rock more reactive (soluble). As such, leaching with organic

and mineral acids was used, thereby freeing the phosphates necessary for the obtaining of chemically bonded phosphate ceramics. This method has been validated for the obtaining of partially acidulated and completely acidulated rocks, and phosphoric acid [25], [27]. In order to validate the liberation of phosphates, leaching was performed with acetic acid and sulphuric acid. For the leaching with acetic acid, an 8 % acetic acid solution was used, with a liquid-to-solid ratio of 5:1; and reaction time of 35 minutes at 350 RPM. For the leaching with sulphuric acid, a 9 Molar H_2SO_4 solution was used, with a liquid-to-solid ratio of 1:1; and reaction time of 120 minutes at 300 RPM.

ICP-OES measurements were performed on the phosphorite concentrate in deionized water, and on the phosphorite leached in acetic acid and 9M H_2SO_4, obtaining values of 0.03 mg/L, 37.08 mg/L and 564.95 mg/L respectively. This supports the use of mineral acids to obtain reactive phosphoric rocks.

Leaching of the phosphoric rock with H_2SO_4 is performed considering Equation 7:

$$Ca_{10}(PO_2)_6\,F_2 + 10H_2SO_4 + 20\,H_2O = 6\,H_3PO_4 + 10(CaSO_4.2H_2O) + 2HF \quad [28] \quad (7)$$

4.3.3 Characterization of the Binder paste

4.3.3.1 SEM

In the full area description shown in Fig. 31, EDS shows the presence of O, Si, S, Ca, with a predominant presence of small, lamellae-shaped particles (2-4 μm) associated with $CaSO_4$ or ($CaSO_4 \cdot H_2O$). Additionally, EDS point analysis identifies the presence of O, P and Ca, which may in turn indicate the presence of brushite-type calcium phosphate compounds, as well as silica.

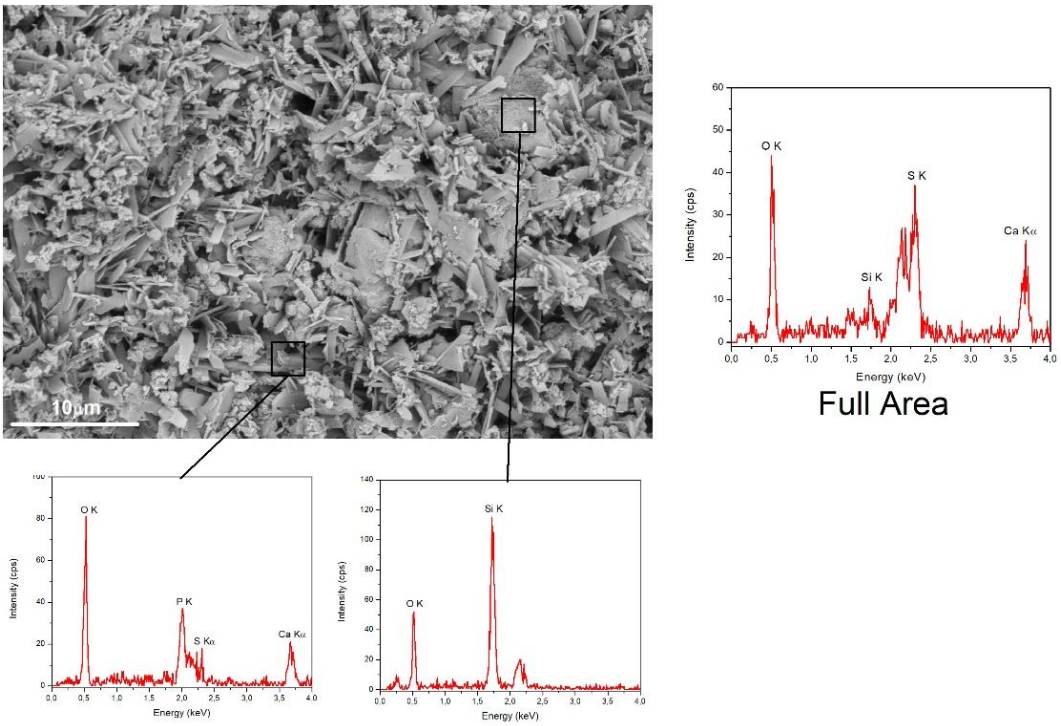

Figure 31. Micrograph and EDS spectra of binder.

4.3.3.2 XRD

32 shows diffractograms corresponding to the phosphoric rock (PR) concentrate, and to the reaction compounds corresponding to the PR-1 and PR-3 mixtures (Table 20). XRD analysis shows a predominant presence of anhydrite ($CaSO_4$), COD 96-900-4097 and gypsum ($CaSO_4 \cdot H_2O$), COD 96-101-1075, a result of the leaching of phosphoric rock with H_2SO_4. Additionally, the main products of the EAF slag and phosphoric rock are shown. The formation of brushite ($CaHPO_4\ H_2O$), COD 96-900-7308, as the main hydration phase was identified, as has previously been found for other phosphate cements [75], [167], Greater presence of this was found in the PR-3 sample, which was probably accentuated by the addition of KDP. Also, intermediate potassium and calcium sulphate hydrate phases of the syngenite ($K_2Ca(SO_4)_2 \cdot H_2O$), COD 96-900-8129, type were found. These were possibly a result of the reaction of KDP and calcium sulphate,

which was shown to occur by the decrease in the intensity of $CaSO_4$ and the appearance of syngenite in PR-3. Finally, unreacted slag particles and SiO_2 residues were found, which indicates the partial dissolution of the slag and the total transformation of the initial phases of the phosphoric rock.

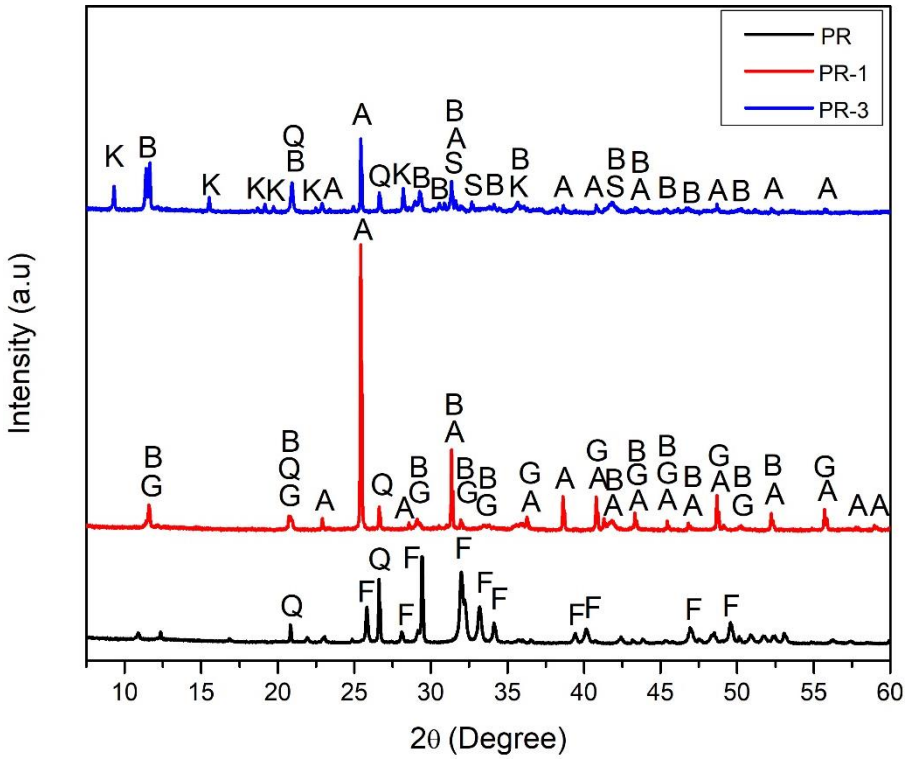

Figure 32. Phosphorite and binder XRD Diffractogram. (A) Anhydrite, (B) Brushite, (Q) Quartz, (S) Slag, (G) Gypsum (K) Singenita, (F) Fluorapatite carbonate.

4.3.3.3 ICC

Fig. 33a shows the heat flow results for the PR-1, PR-2 and PR-3 samples evaluated. There is a conspicuous presence of a single main peak for each sample. However, in sample PR-3 the peak appears to be composed of various peaks superimposed on the main peak, which suggests the possibility of more complex hydration reactions. The maximum heat release points are 40.37 mW, 57.60 mW and 28.40 mW for PR-1, PR-2 and PR-3 respectively. These can be attributed to the

formation of anhydrite, gypsum and brushite for PR-1 and PR-2, and anhydrite, syngenite and brushite for PR-3. The heat flow curves for PR-1 and PR-2 are consistent with previous reports for gypsum and anhydrite [168], [169], which show gypsum as more exothermic than anhydrite, which reacts more slowly and less exothermically [170], This is demonstrated here by the decrease in the heat flow for PR-3 and the increase in the reaction time. Additionally, the XRD results for the PR-3 sample show the formation of syngenite and anhydrite, in contrast to PR-1 and PR-2 where gypsum is predominantly formed. Equally, it is presumed that the dissolution of the slags to form brushite can be attributed to a synchronous hydration reaction of the gypsum and the anhydrite.

The quantity of anhydrite and gypsum is directly proportional to the quantity of leached phosphoric rock present in the mixture (Table 20). This, given the higher hydration rates for samples PR-1 and PR-2, is consistent with ICC records. PR-1 and PR-2, the samples with the greatest quantity of leached phosphoric rock, develop more heat independently of the quantity of water present. This suggests that anhydrite and gypsum are reaction accelerators. The sample with the lowest heat release and hydration rate (PR-3) presents different behavior due to the presence of KDP, which causes the formation of syngenite, thereby slowing the reaction and favoring a greater dilution of the slag. This is consistent with the greater formation of phosphates identified by XRD, which is evidenced by the greater total heat release (301 J) of PR-3 (Fig. 33b), indicating greater dissolution of ions and a probable greater quantity of formed products. The predominant presence of anhydrite, gypsum and small quantities of formed products identified by XRD explain the mechanical resistance characteristics found. It is possible that other peaks are superimposed on the main peaks, making it difficult to identify other reactions of this type of compound.

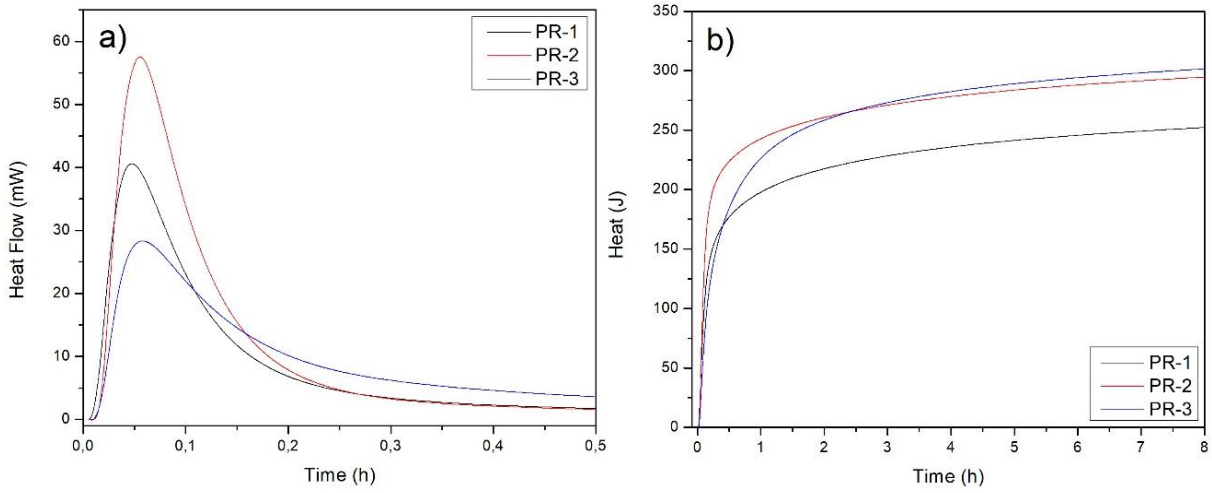

Figure 33. Heat flow and total heat curves of the binder.

4.3.3.4 Potential future improvements of mechanical resistance

The values observed for compression resistance were 1.33 ± 0.01 MPa, 0.67 ± 0.29 MPa and 2.84 ± 0.42 MPa, for PR-1, PR-2 and PR-3 respectively. These are comparable to the compression resistances found for gypsum [171]. This indicates the predominate presence of this compound, which can be explained by a possible inhibition effect on the formation of other reaction products. This makes it necessary to consider cleaning or elimination processes for the gypsum in the future, in order to increase the formation of phosphate ceramics and thereby improve mechanical resistance. The slight difference for mechanical resistance in sample PR-3 results from the greater formation of calcium phosphate compounds found by XRD, and well as from the lower quantity of leached phosphoric rock and the greater presence of KDP.

4.4 Conclusions

Chemical, morphological and mineralogical analyses revealed potential compounds for the synthesis of chemically bonded phosphate ceramics, principally fluorapatite-carbonate and

wüstite, as well as minerals with significant content of oxides such as dicalcium silicate and dicalcium ferrites.

The main phase of the phosphoric rock evaluated in this study corresponds to fluorapatite carbonates which, due to the high replacement percentage of $(PO_4)^{3-}$ in their structure by external elements, generate a sparingly soluble mineral, which inhibits the formation of chemically bonded phosphate ceramics through the acid-base system.

The availability of free phosphate ions in the phosphoric rock, which are necessary for the formation of chemically bonded phosphate ceramics, is dependent on the solubilization of the phosphoric rock through leaching processes with mineral acids such as H_2SO_4.

Leached phosphoric rock and EAF slag, as acid-base system compounds, promote the formation of brushite-type calcium phosphates.

The presence of $CaSO_4$ and ($CaSO_4 \cdot H_2O$) in the mixture modify the reaction rate of the binder, which significantly limits the formation of metallic phosphate compounds in the acid-base reaction system, resulting in fragile and poorly consolidated structures.

5. Formation, properties and microstructure of a new steel slag - based phosphate cement

This chapter corresponds to the article: DOI 10.1061/(ASCE)MT.1943-5533.0003958

Abstract: The process of obtaining chemically bonded phosphate ceramics generally involves the use of metallic oxides, the preparation of which consumes high quantities of energy. The present chapter proposes a method to recycle slags generated by a steel production process that is widely used across the world, namely, the electric arc furnace process. A chemically bonded phosphate ceramic is produced by exploiting the high content of metals present in the slag, realizing the conditions to mitigate the environmental impact of the industrial by-product.

In-situ infrared spectroscopy, isothermal conduction calorimetry and X-ray diffraction patterns revealed that the setting reaction involves the formation of amorphous products in the form of metallic phosphate hydrates and a fraction of calcium silicate hydrates, similar to those found in Portland cement. This phosphate matrix allows the effective immobilization of heavy metals in the slag, such as Cr

and As. According to the results of mechanical tests, which showed compression resistance of 15-25 MPa, as well as those of leaching tests, slag-based phosphate cement can be used without restrictions as a construction material for applications such as mortars or bricks.

5.1 Introduction

The world steel production in 2018 was estimated at around 1.8 billion tons [172], and it has been calculated that for each ton of steel produced, about half a ton of slag is obtained [173]. Based on these statistics, the global annual production of steel slag is likely to be close to one billion tons. The need to mitigate the negative environmental impact of this has prompted efforts to reuse steel slag as secondary raw material. With this aim, slags are frequently recycled in road construction, and, to a lesser extent, in the production of cement and concrete, asphalt, fertilizers and for soil amendment [146], [174]. The extent of slag recycling is far from uniform globally, with virtuous examples (Europe and USA, 87 % and 84.4 %, respectively) [174] and countries with serious problem of storage and disposal [175]. In the latter case, stockpiling frequently causes loss of agricultural land and contamination of soil and groundwater due to leaching of pollutants [176]. The use of other types of slags as supplementary cementitious material (SCM) in Portland cement is well-known, especially granulated blast furnace slag (GGBS) and fly ash (FA). Demand for these has peaked in recent years due to the increase in cement production, to the point that these SCMs are scarce in some countries [177]. However, steel slags, namely, electric arc furnace (EAF) slag, basic oxygen furnace (BOF) slag and ladle furnace (LF) slag, due to their low hydraulic activity, are less attractive for the Portland cement system. In fact, their use as SCMs is limited to thermal, mechanical or chemical activation [146], [174], [178].

BOF is used in fertilizers because of its high phosphorus content [179], [180]. LF has a significant environmental impact in comparison to other steel slags, due to the leaching of hexavalent chromium Cr^{6+} and other toxic metals [181]. EAF slag has been proposed as an aggregate in concrete [146]. The concrete obtained has been shown to exhibit similar or slightly better mechanical properties than traditional concrete [182]. As a raw material for cement clinker, added up to 10.5 wt.%, it was shown to reduce production costs without a negative effect on clinker quality [183]. EAF slags have been considered by some authors as non-hazardous material, and therefore proposed for use in landfilling [119], [146], [184]. However, in practice, they are rarely used for this purpose, due to the large extensions that are required and the high costs associated with this. It is worth noting that the EAF process dominates steel production [185], which has prompted the search for new routes for the re-use of EAF slag, especially in countries where no alternative solution to land disposal/stockpiling is available [145], [173].

Phosphate cements are chemically bonded phosphate ceramics (CBPCs). They represent a completely different chemical environment to Portland cement, because they are based on a reaction in water between acid phosphates and metal oxides or available metal cations (such as Mg, Ca, Al, Fe), to produce insoluble phosphate hydrates [2]. Few studies have reported the partial replacement of steel slag in Mg phosphate cements (MPCs), which are CBPCs produced at industrial scale [42]. The introduction of 10 wt.% - 20 wt.% BOF slag powders has been shown to improve the early and late mechanical strength of the paste, considerably reducing shrinkage [23]. Different amounts of steel slag powder (10 wt.% - 30 wt.%) have been reported to generate a slight decrease in early strength and an increase in late strength and water resistance [22]. In general, MPCs exhibit very high early strength, but very fast reaction rates, which reduce the working time and cause the temperatures to rise to unacceptable values for some applications (>60 °C) [2]. In

order to mitigate the rates, it is deemed necessary to introduce additives and reduce the reactivity of MgO. The latter result is obtained by thermal treatment at high temperature [89], [186]. For the so-called dead-burnt MgO, temperatures in excess of 1600-1700 °C are usually attained, with important consequences in terms of energy requirements and costs in cement manufacturing. Calcium phosphate cement is another important phosphate cement. It has biological properties similar to bone, which have enabled its use in applications in the biomedical sector [57], [187]. Calcium phosphate cements based on the reaction of aqueous phosphoric acid solutions and wollastonite have been used for applications in civil infrastructure [2]. These cements as known commercially as inorganic phosphate cements (IPC) [75], and have demonstrated significant mechanical resistance, although various problems related to heat resistance and ageing have limited their use [47].

To date, there are few reports on the use of steel slag as the only source of metal cations for the production of phosphate cements, therefore knowledge about the formation mechanisms, microstructure, physical-chemical characteristics, among others, is non-existent. In this study, EAF steel slag produced at the Paz de Río steelworks in Colombia is proposed as source of metal cations to form CBPCs with acidic phosphates, facilitating an environmentally friendly alternative to other forms of disposal and adding value to this waste. This process has several potential positive aspects. It represents an opportunity for the use of steel slag as secondary raw material, thereby exploiting the high content of metal cations, which are used in the cement reaction, and the residual hydraulic activity due to the Ca-silicates content. Moreover, the reduction of costs in CBPC formulation is further enhanced by completely eliminating MgO. The mechanical performance, formation kinetics and chemical stability of the obtained cement has been evaluated. The strength

and workability demonstrated by this evaluation indicate that this type of cement can be considered a construction material, as further confirmed by the results of the heavy metals leaching test.

5.2 Materials and Methods

5.2.1 Materials

Pharmaceutical grade potassium dihydrogen phosphate KH_2PO_4 (KDP) (Sigma Aldrich Co), EAF slag from Paz de Río steelworks (Colombia), previously referenced as EAF2, and boric acid H_3BO_3 (Lach-Ner Co), were used as raw materials. KDP was ground to an average particle size of d_{50} = 39 μm. EAF slag was ground to obtain powder that passed through a 63 μm analytical sieve, similarly to commercial cements. The relevant parameters of particle size distribution of EAF slag were: d_{10} = 1.2 μm, d_{50} = 8.8 μm, d_{90} = 43.1 μm.

5.2.2 Cement preparation

The CBPCs were obtained by mixing the EAF slag and KDP in deionized water, adopting the liquid /solid weight ratio and KDP/EAF weight ratio reported in Table 25. On this basis, 2 g of H_2O + 8 g of powders and 1.34 g of H_2O + 8.04 g of powders were mixed for the formulations with liquid/solid ratios of 0.25 and 0.16, respectively. Meanwhile, 1.6 g of KDP + 6.4 g of slag and 1.15 g of KDP + 6.89 g of slag were mixed for the formulations with KDP/EAF weight ratios of 0.25 and 0.16, respectively. When preparing the cements, the liquid and solid components were mixed manually in a glass beaker for 15 seconds and then poured into 1×1×1 cm silicone molds for subsequent curing under ambient laboratory conditions (temperature: 23 ^{o}C $\pm$ 2 ^{o}C, relative humidity: 37 % $\pm$ 1 %). Samples were prepared in triplicate and demolded after one day of curing.

By proposing different formulations, it is sought to evaluate the role played by the reagents in the formation of the cement. The respective quantities of water, metallic oxides present in the slag, and phosphate, affect the behavior of the formulation of phosphate cements based on EAF slag. Moreover, variables such as the hydration time of the cement are controlled by maintaining a constant quantity of retardant ((H_3BO_3) in the different formulations.

Table 25. Formulations of the EAF slag-based phosphate cements adopted in this study.

Sample	Liquid/Solid (wt. / wt.)	(KDP)/Slag (wt. / wt.)	H_3BO_3 (wt. %)
S1	0.25	0.25	0.25
S2	0.25	0.16	0.25
S3	0.16	0.25	0.25
S4	0.16	0.16	0.25

5.2.3 Experimental techniques

5.2.3.1 Cement preparation

The CBPCs were obtained by mixing the EAF slag and KDP in deionized water, adopting the liquid /solid weight ratio and KDP/EAF weight ratio reported in Table 25. On this basis, 2 g of H_2O + 8 g of powders and 1.34 g of H_2O + 8.04 g of powders were mixed for the formulations with liquid/solid ratios of 0.25 and 0.16, respectively. Meanwhile, 1.6 g of KDP + 6.4 g of slag and 1.15 g of KDP + 6.89 g of slag were mixed for the formulations with KDP/EAF weight ratios of 0.25 and 0.16, respectively. When preparing the cements, the liquid and solid components were mixed manually in a glass beaker for 15 seconds and then poured into 1×1×1 cm silicone molds for subsequent curing under ambient laboratory conditions (temperature: 23 ^{o}C $\pm$ 2 ^{o}C, relative humidity: 37 % $\pm$ 1 %). Samples were prepared in triplicate and demolded after one day of curing.

By proposing different formulations, it is sought to evaluate the role played by the reagents in the formation of the cement. The respective quantities of water, metallic oxides present in the slag, and phosphate, affect the behavior of the formulation of phosphate cements based on EAF slag. Moreover, variables such as the hydration time of the cement are controlled by maintaining a constant quantity of retardant ((H_3BO_3) in the different formulations.

5.2.3.2 Additives setting retardants

In order to evaluate different retarders additive in cement, additional formulations of EAF slag-based phosphate cement are made with weight ratios of 0.25 for liquid / solid and KDP / Slag (corresponding to formulation S1), but with different variations in setting retarder additive. Retarder additives are used to slow down the reaction rate of cement and water, affecting the hydration products [188]. EDTA, PSSA and H_3BO_3 were analyzed as possible retarder additives the setting of the slag-based phosphate cements. A magnetic stirrer with a temperature sensor and a digital chronometer were used to evaluate each of the mixtures.

Ethylenediaminetetraacetic acid (EDTA) was used, substance commonly known as a chelating agent, whose function can be described as a compound capable of binding to metal ions to form complex ring-shaped structures, called Chelates [189]. Poly 4- (Styrene sulfonic acid) (PSSA), dispersant on iron phosphates [190], this polymer is sensitive to changes in pH, undergoing changes in surface activity and the number of positively charged groups in the polymer chains, acting as a polyelectrolyte [191]. Boric Acid (H_3BO_3), acts as a retarder additive in magnesium phosphate cements by developing a polymeric coating on the MgO grains, thus affecting the setting reaction [2].

5.2.3.3 In-situ attenuated total reflection Fourier transform infrared spectroscopy (ATR FTIR)

The reaction was monitored *in-situ* with ATR FTIR spectroscopy, at room temperature, using an external module iZ10 of the Nicolet iN10 spectrometer equipped with a DTGS detector. Spectra were collected at a resolution of 4 cm^{-1} in the range of 4000-525 cm^{-1}. The liquid and solid components of the cement formulation S1 were brought into direct contact with the diamond crystal and then mixed while data acquisition began. The spectra were measured continuously using 10 s collection time (8 scans per spectrum) for the first 30 minutes; followed by a rate of two spectra per minute for next 30 minutes; and finally 1 spectrum per minute up to 7 hours. In addition, spectra were collected at 24 h, 3, 7, 14, 21 and 28 days using 64 scans per spectrum.

5.2.3.4 Scanning electron microscope (SEM/EDS)

Cement samples were observed on a fractured surface with a scanning electron microscope (SEM) after 28 days of curing. For the SEM process, a Quanta 450 FEG (FEI) microscope equipped with an energy dispersive X-ray fluorescence detector (EDS) was used, at an accelerating voltage of 20 kV. Samples were mounted on aluminum stubs and coated with a 5 nm gold film.

5.2.3.5 X-ray diffraction (XRD)

X-ray diffraction (XRD) data were collected with a Bruker D8 Advance Bragg Brentano θ-θ diffractometer with Cu K_α radiation at 40 mA and 40 kV. Quantification of the crystalline and amorphous phases was performed with the Rietveld method using the TOPAS 4.2 software (Bruker AXS). The samples were spiked with 10 % ZnO powder calibrated against the standard NIST SRM 676 (α -Al_2O_3), with a certified amorphous content of 0.98% by weight. The main aim of this procedure was to quantify the amorphous phase. Quantitative phase analysis (QPA) by the

Rietveld method is based on the normalization condition, that is, it is assumed that the sum of each weight fraction W_i of each i-th crystalline phase in the sample is 1 ($\sum_i W_i = 1$). When the investigated sample contains an amorphous phase, this condition is not valid. By adding a known quantity of an internal standard, the normalization condition can be re-established and the weight fraction of amorphous phase calculated, given that the amorphous content of the standard is known [192]. This calculation is automated in the TOPAS software adopted for the Rietveld refinement of the XRD spectra, where also the standard deviation on the amorphous content (usually <1 wt. %) is obtained. The accuracy of the method has been verified for several systems [193][194][195] As customary in the recent years, due to the fact that the NIST SRM 676 (α - Al_2O_3) standard for quantitative phase analysis is out-of-stock at the National Institute of Standards and Technology (USA), ZnO, calibrated against NIST SRM 676, was used instead. ZnO 99.9 % (Merck) was annealed for 5 h at 700 °C before use, in order to improve its degree of crystallinity.

5.2.3.6 Isothermal conduction calorimetry (ICC)

Heat signal during the cement reaction was measured by isothermal conduction calorimetry (ICC) using a TAM-Air (TA Instruments) 8 channels calorimeter. EAF steel slag, KH_2PO_4 and H_3BO_3 were dry blended according to the formulations in Table 25 and the powders were placed in glass ampoules. Once the powders were equilibrated at the measuring temperature (25.0 ± 0.1 °C), the water was injected and the slurry was hand mixed for 120 s. Heat flow and total heat were recorded for 8 hours.

5.2.3.7 Mechanical testing

Compressive strength evaluation of the cement samples was performed on 1×1×1 cm cubes using a universal testing machine (MTS System), with loading speed of 0.2 mm/min and a maximum load capacity of 50 kN.

5.2.3.8 Leaching test (ICP-OES)

Leaching test was performed in triplicate according to standard NEN 7345 in cylinders (radius = 1 cm, high = 4 cm). Three samples, corresponding to formulation S1, were immersed in polypropylene containers with 65 cm^3 of water acidified with HNO_3, at pH = 4 (Fig. 34). 8 extractions of the leaching liquid were carried out after 0.25, 1, 2.25, 4, 9, 16, 36, and 64 days. The leached liquid was filtered through 0.45 μm filter paper after extraction for subsequent analysis by ICP-OES. Equation 8 was used to compute the pollutant leachability.

$$Ei = \frac{(Ci - Co)V}{1000A} \qquad (8)$$

Where, Ei = pollutant leachability (mg/m^2), Ci = pollutant concentration (mg/L), Co = pollutant concentration in the blank (mg/L), V = volume of extractant agent (L), A = surface area of the sample (m^2).

Elemental concentrations of liquid samples were determined through optical emission spectroscopy with inductively coupled plasma (ICP-OES) using a Spectro Blue (Spectro) device equipped with Paschen-Runge polychromator. Plasma power was set to 1400 W and coolant, auxiliary and nebulizer flows were kept at 13.0, 0.8 and 0.6 l/min, respectively. Pump speed was 30 rpm. Lines at 267.716, 189.042, 257.611, 259.941, 396.847 and 178.287 were used for the quantifications of Cr, As, Mn, Fe, Ca and P. Blank sample was prepared following the same procedure described above, without the introduction of cement sample.

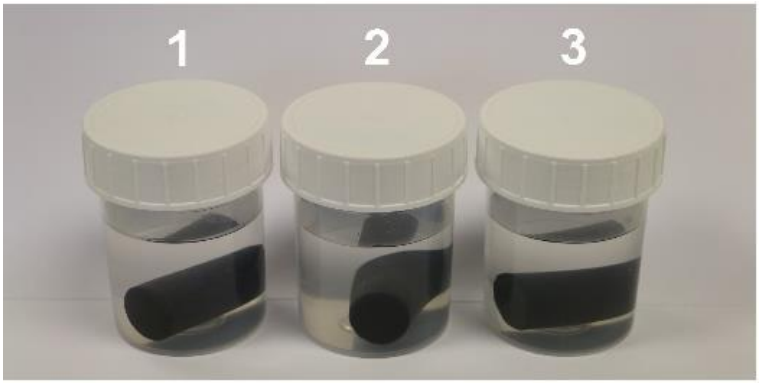

Figure 34. Leaching Test steel slag-based cement phosphate.

5.3 Results

5.3.1 Slag characterization

The typical shape of the slag particles as observed under SEM is illustrated in Fig. 35. The grains exhibited sharp edges, as a consequence of milling. The internal surface evidenced the presence of crystals embedded in an apparently glassy matrix, as a result of the high temperature treatments and fast cooling rates. The results of XRD quantitative phase analysis are reported in Table 26. The slag is mainly composed of dicalcium silicate (mineral larnite, or C_2S in cement nomenclature), iron oxide (wuestite) and calcium aluminoferrite (mineral brownmillerite, or C_4AF in cement nomenclature), with significant quantities of CaO and Fe_3O_4 of 30.91 % by weight and 37.89 % by weight respectively, indicating the availability of metallic cations for the acid-base reaction. Other Ca- and Fe-bearing phases are present in amounts < 10 wt. %. The results are in agreement with the chemical and mineralogical analysis reported in a previous study [126]. It is worth noting that wuestite is an ideal iron mineral for the preparation of CBPCs [2], whereas both C_2S and C_4AF possess good hydraulic properties, and are components of Portland cement clinker.

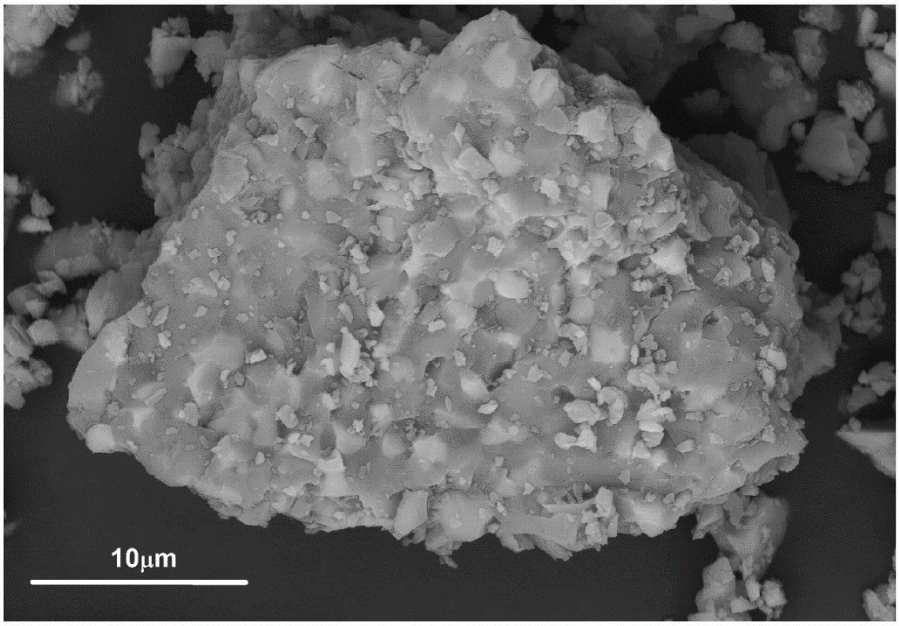

Figure 35. SEM micrograph of a particle of EAF slag.

5.3.2 Cement reaction

5.3.2.1 Analysis of retarder additives

Figure 36 shows the behavior of EAF slag-based phosphate cement corresponding to formulation S1 with variations in the type and percentage of retarder additive. The acid chelating compound EDTA and the dispersant PSSA showed a similar behavior to the reference cement, indicating their low retarding effect, even with a slight change in the acceleration of the reaction for EDTA. The effect of H_3BO_3 to delay the setting time of cement for the 0.25 % wt ratio is noticeable, where the decrease in the phosphate formation reaction is clearly observed for 900 seconds, in addition to a considerable decrease in temperature in relation to the reference cement. For higher proportions of H_3BO_3 of 5 wt. %, the retarding effect is clear, registering the start of formation activity after 1800 seconds.

The adsorption of boric acid on the surface of the slag grains from the boric acid species $B(OH)_3$ and $B(OH)_4^-$ that are adsorbed on the surface of the metal oxide [196] is suggested as a mechanism

to explain the retarding effect of H_3BO_3. The reaction describes the formation of covalent bonds between the metal ion and the borate ion, specifying possible chemisorption processes [197], resulting in a reduction in the dissolution rate of the slags with a consequent extension of the setting time.

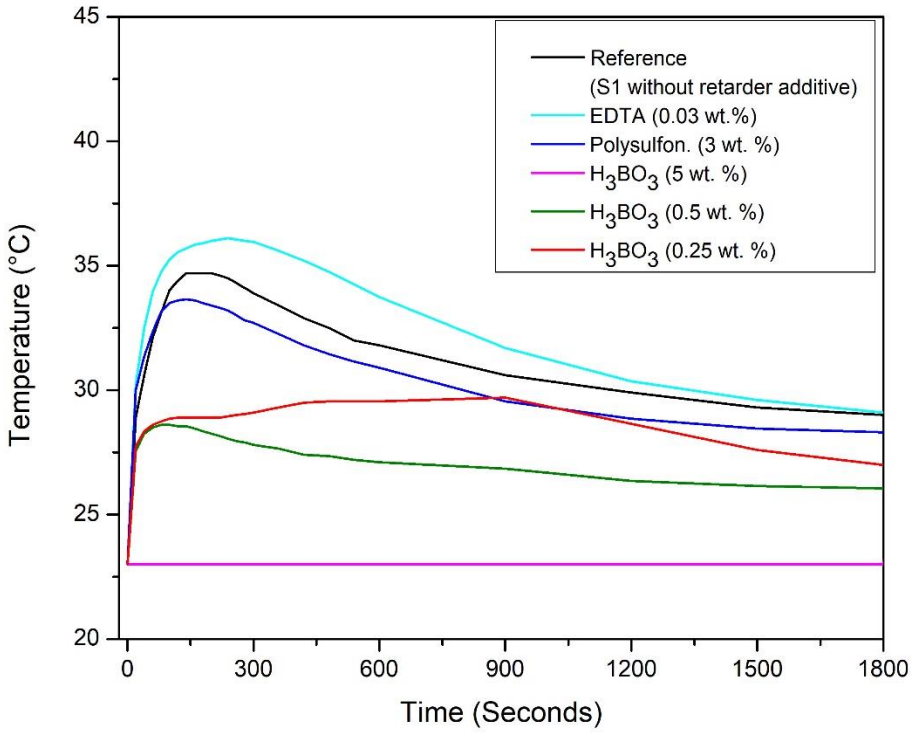

Figure 36. Behavior of the different setting retarder additives.

5.3.2.2 In situ time resolved spectroscopic observation

Fig. 37 illustrates a selection of ATR-FT-IR spectra for the steel slag-based phosphate cement at different times (10 seconds, 3 and 24 hours, 14 and 28 days). The O−H stretching region ν(OH) (3700−2600 cm^{-1}), and H_2O bending vibration region δ(HOH) (1800−1450 cm^{-1}) provide information on the evolution of the hydrogen bonding state of the water molecules. As previously observed in MPCs [7] [11], at lower wavenumbers the distribution of ν(OH) vibrations progressively shifts and the δ(HOH) signal broadens. This reflects the establishment of bonds

between metal ions and water molecules [198] and indicates the conversion of water from free to confined/bound into the reaction products.

The characteristic phosphate bands are located in the range 1300 to 800 cm^{-1}. In CBPCs, the time evolution of the ATR-FT-IR signal in this spectral region results from the concomitant effect of the increase in pH, caused by oxide dissolution, and the bonding of the released metal ions in the condensing phosphates [2], [7], [11]. It has been shown that the reaction products are influenced by the stability of the four protonated forms of phosphoric acid that are stable at increasing pH values [2], [7], [11], [199]. These are H_3PO_4, $H_2PO_4^-$, HPO_4^{2-} and PO_4^{3-} [200], [201]. When dissolution in water of KDP occurs, the pH drops to values close to 4 [201] and, accordingly, after 10 s the infrared spectrum is characterized by vibrations at 1240 cm^{-1}, 1150 cm^{-1}, 1073 cm^{-1}, 940 cm^{-1} and 876 cm^{-1}, which are attributed to the $H_2PO_4^-$ ion in the KDP [202]. A less intense vibration at 1240 cm^{-1} is indicative of aggregation of $H_2PO_4^-$ [202]. The signal of the $H_2PO_4^-$ groups is progressively substituted by vibrations at 1064 cm^{-1}, 987 cm^{-1} and 850 cm^{-1}, assigned to (ν_3) and (ν_1) symmetric stretch vibrations of HPO_4^{2-} [199], the stable phosphate form at higher pH values [201]. This is clearly visible in the spectrum collected after 3 hours. All components of HPO_4^{-2} decrease in intensity with time. The increased intensity at 993 cm^{-1} must be assigned to a phosphate reaction product, as is the case for other CBPCs [7], [11], [199]. Consistently with the aforementioned studies, it corresponds to the asymmetric stretch P-O (ν_3), of the PO_4^{3-} fully deprotonated ion, which is stable at high pH [201]. The position of this maximum shifts in time to 1014 cm^{-1} at 28 days. This may reflect some structural rearrangement of the phosphate environment or an amorphous-amorphous transformation between two orthophosphates hydrates, as has previously been suggested for MPC [11].

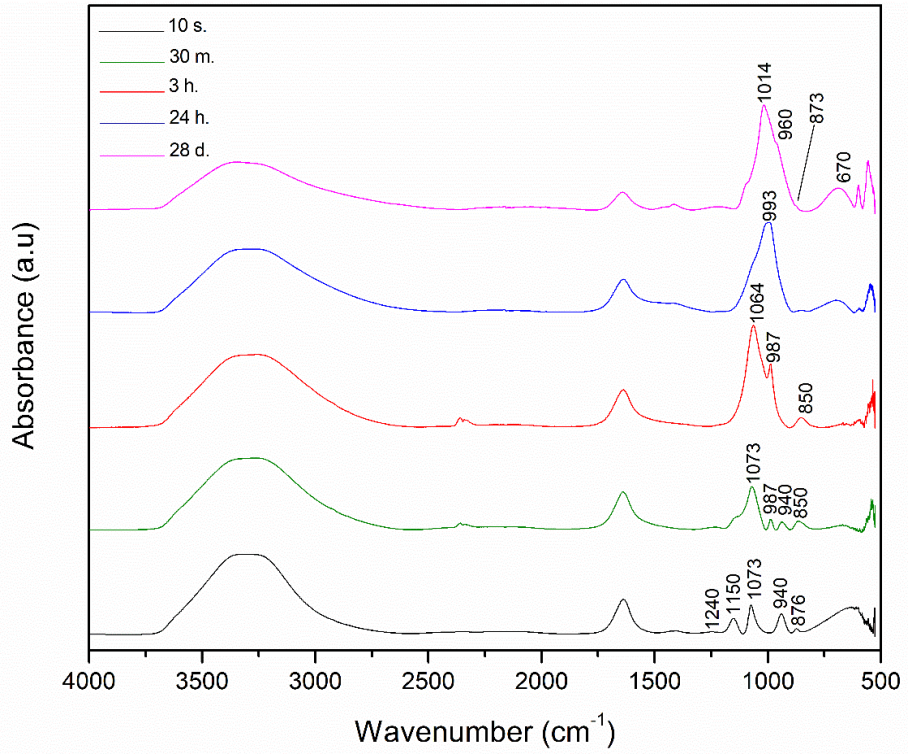

Figure 37. Selected infrared spectra of steel slag-based cement sample S1 recorded after 10 seconds, 30 minutes, 3 hours, 24 hours and 28 days, as indicated.

A vibration at around 960 cm^{-1}, assigned to C-S-H, is clearly visible as a shoulder in the spectrum collected after 28 days, which evidences the hydration reaction of C_2S [203], [204]. The spectrum associated with C-S-H resembles that of mineral tobermorite with a C/S ratio <1.5 [203], [205], so the vibration at 960 cm^{-1} is therefore due to Si-O stretching [94]. An additional contribution to the infrared spectrum of C-S-H comes from Si-O-Si bending vibrations at ~ 670 cm^{-1}. The intensity in the region 1400−1500 cm^{-1}, observed after a long time, is attributed to the asymmetric stretch (ν_3), of CO_2^{3-}, which, together with the vibration at 873 cm^{-1}, indicates the presence of calcium carbonate [203], [206]. It may be argued that this is the result of carbonation of the calcium hydroxide formed during hydration of calcium silicates.

5.3.2.3 Mechanism of the cement formation

From the recorded ICC traces (Fig. 38), four main events can be recognized during the formation of the slag-based phosphate cement. According to the literature [11], [207], [208], these can be attributed as follows: a first endothermic event due to the dissolution of KDP (A), and three exothermic episodes assigned to slag dissolution (B), formation of phosphate products (C) and hydration of silicates to form C-S-H (D).

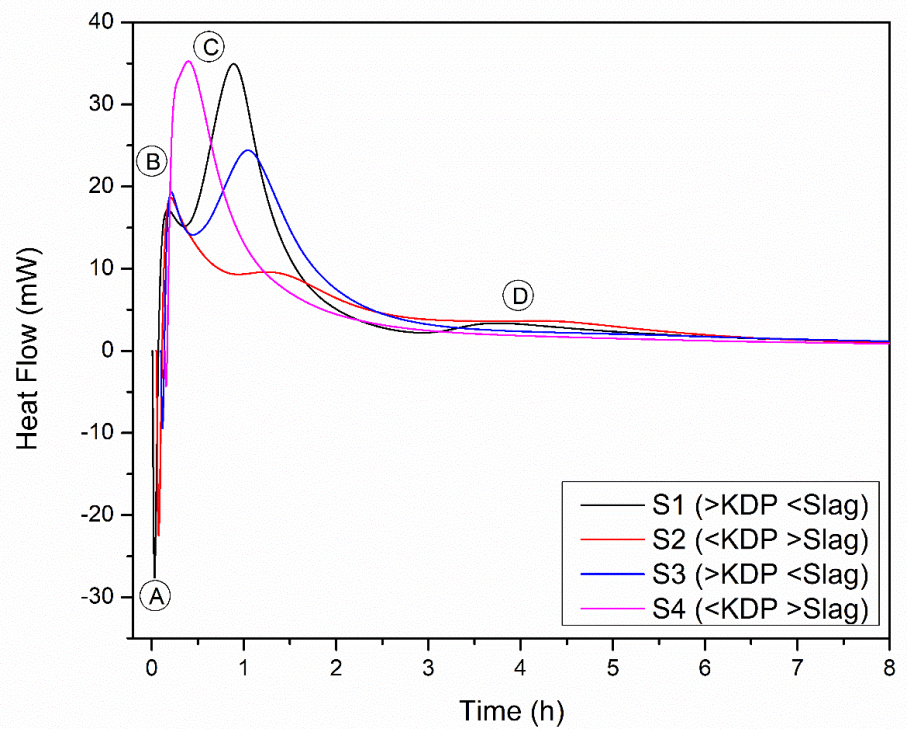

Figure 38. ICC Heat flow curves for cement formulations with high water (S1-S2) and less water (S3-S4). Main events of heat release/absorption are indicated.

The formulations containing more KDP (S1 and S3), (Fig. 38), irrespective of the amount of water employed, develop more heat during step C, which indicates that the amount of phosphate is the limiting factor for these formulations. The total heat released is higher when more water is employed (S1) (Fig. 39), probably due to more effective dissolution of KDP and/or more effective wetting of slag powder.

The increase in slag causes an increase in the heat flow during step B. This increase is higher for the samples with less water (S4), (Fig. 38), because a lower quantity of water increases the concentration of phosphate ions, favoring dissolution of slag. The higher surface area of slag and the lower amount of water in sample S4 accelerated step C, probably because of the higher amount of iron made available in a short time in solution. However, the total heat released is similar to sample S2 (Fig. 39), because they both contain relatively little KDP. This is a further confirmation that the amount of KDP is a limiting factor for the formulation tested.

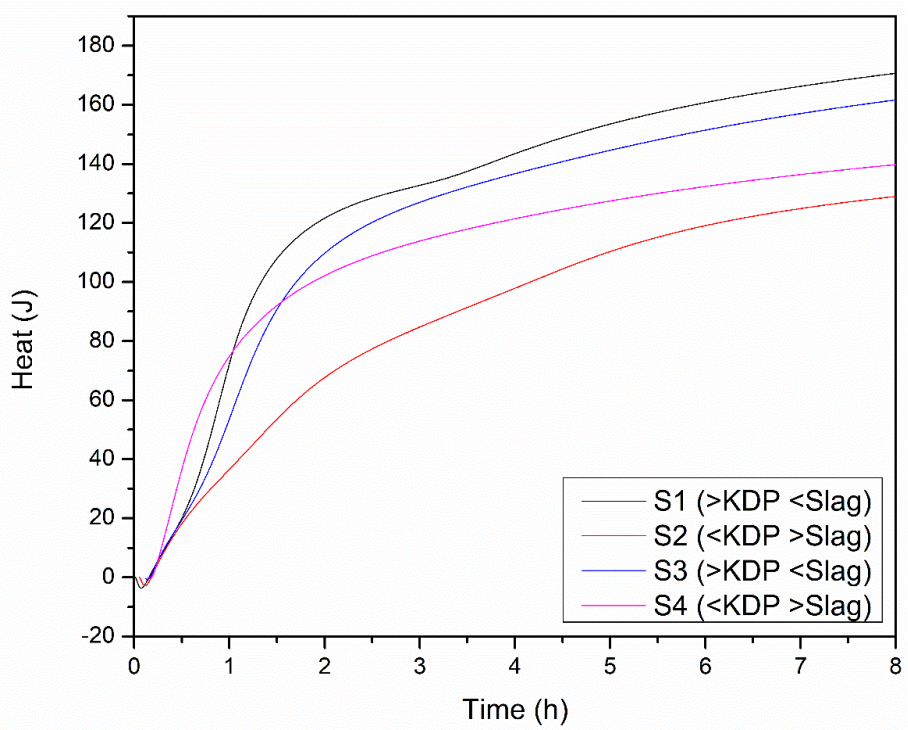

Figure 39. ICC Total heat curves for cement formulations with high water (S1-S2) and less water (S3-S4).

It should be noted that, in the samples containing more water (S1 and S2) (Fig. 38), the small and broad exothermic peak between 3 and 4 h, attributed to hydration of calcium silicates and aluminates (step D) is more visible than in samples S3 and S4. This is apparent in the inflection point in their respective heat curves. Conversely, in the case of the formulations with less water,

such an event is not visible. These facts are explained by the fact that water is first incorporated in the phosphate hydrates, since the corresponding reaction is faster than the hydration of calcium silicates. An appreciable amount of C-S-H may form if enough water is available for the reaction to occur; therefore, this process is more likely in formulations richer in water. Alternatively, since the total amount of heat released is similar in the samples with the same phosphate/slag ratio (Fig. 39), the hydration of silicates is less visible, because it occurs over a wide time interval in a large overlap with the other heating events.

5.3.2.4 Quantitative phase analysis

In the diffractograms of the prepared formulations (fig. 40), diffraction peaks associated with EAF slags corresponding to the mineral phases that did not react completely are detected. Moreover, the presence of the internal standard used for the phase quantification (ZnO) is identified. The X-ray diffraction patterns referenced according to the COD (Crystallography Open Database) datasheets are: zincite (ZnO) COD 96-901-1663, larnite (Ca_2SiO_4) COD 96-901-2795, wuestite (FeO) COD 96-900-9768, magnetite (Fe_3O_4) COD 96-900-7708, gehlenite ($Al_2Ca_2SiO_7$) COD 96-900-6113, srebrodolskite ($Ca_2Fe_2O_5$) COD 96-100-8778, brownmillerite (F Ca_2FeAlO_5) COD 96-900-3349.

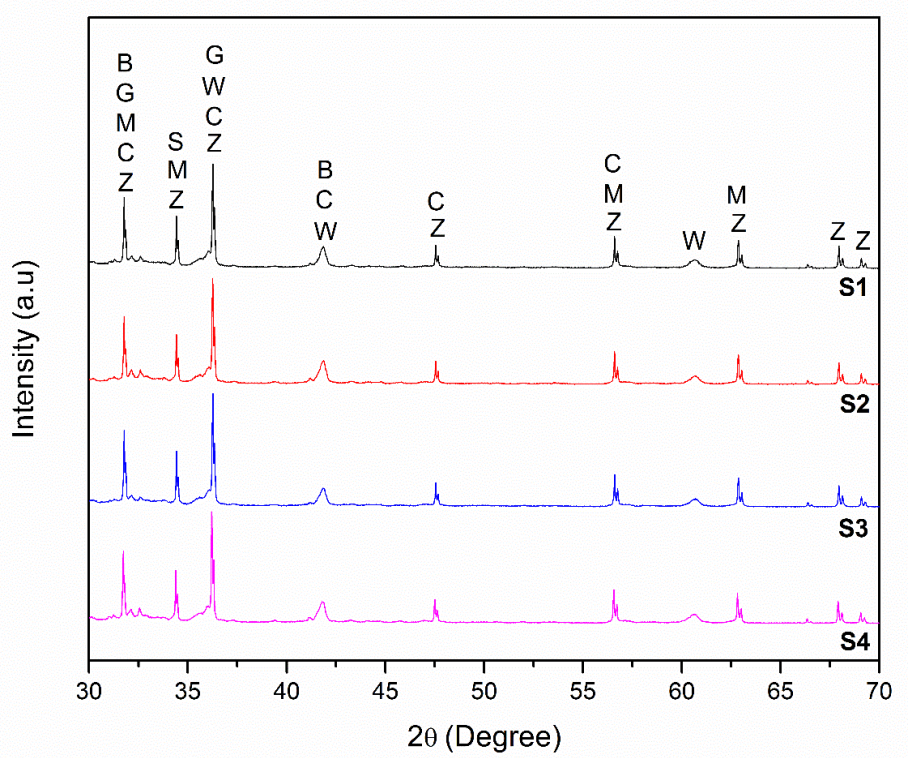

Fig. 40. Analysis XRD, comparison S1, S2, S3, S4 formulations. (Z) Zincite, (C) C_2S, (G) Gehelenite, (B) Brownmillerite, (W) Wüstite, (F) Magnetite, (S) Srebrodolskite.

Table 26 illustrates the results of quantitative phase analysis of the produced cements after 28 days. It can be observed that no new crystalline phases were detected, compared to the slag. It follows that all the cement reaction products are XRD amorphous. This is clearly evidenced by the high amount of amorphous phase. No residual KDP was detected, which indicates the complete consumption of this, which is consistent with the hypothesis that phosphate is the limiting factor for the formulations adopted in this work.

Table 26. Phase composition (in wt. %) of the EAF slag and cement formulations, as indicated, obtained from XRD.

Phases	Formula	EAF Slag	Cement S1	Cement S2	Cement S3	Cement S4
C_2S	Ca_2SiO_4	30.9 ± 0.5	4.6 ± 0.1	6.3 ± 0.1	3.5 ± 0.1	6.4 ± 0.1
Wuestite	FeO	23.0 ± 0.6	9.9 ± 0.1	10.5 ± 0.1	8.3 ± 0.1	9.8 ± 0.1
Magnetite	Fe_3O_4	6.9 ± 0.2	2.5 ± 0.1	2.6 ± 0.1	2.2 ± 0.1	2.7 ± 0.1
Gehlenite	$Al_2Ca_2SiO_7$	2.4 ± 0.3	1.5 ± 0.1	1.3 ± 0.1	1.1 ± 0.1	1.3 ± 0.1
Srebrodolskite	$Ca_2Fe_2O_5$	3.7 ± 0.1	0.7 ± 0.1	0.9 ± 0.1	0.7 ± 0.1	0.9 ± 0.1
Brownmillerite	Ca_2FeAlO_5	12.4 ± 0.3	0.9 ± 0.1	1.1 ± 0.1	1.0 ± 0.1	0.9 ± 0.1
Quartz	SiO_2	n.d.	n.d.	< 0.5	n.d.	n.d.
Amorphous		20.0 ± 1.4	79.9 ± 0.2	76.1 ± 0.2	83.3 ± 0.2	78.1 ± 0.2
C_2S/wuestite		1.34	0.46	0.6	0.42	0.65

The most evident changes are related to the decrease in wuestite, C_2S and C_4AF, suggesting the consumption of these during the formation of the cement. As observed previously, magnetite does not contribute as much as wuestite [2]. From these results, it follows that the amorphous reaction products are rich in Fe^{2+}, Ca^{2+} and SiO_2. Comparing the C_2S/wuestite weight ratio in the slag and the cements, it can be noted that C_2S was dissolved more effectively than the iron oxide. This ratio is almost the same in the samples with same phosphate/slag ratio. Since these differ in their water content, this would suggest that water is not the limiting factor for the product formation, which is in agreement with the ICC results. In fact, a higher amount of slag is dissolved when more KDP is employed (samples S1 and S3), which confirms KDP as a limiting factor. Nonetheless, the proportion of amorphous is always above 78 wt. %; therefore, since the samples exhibit different C_2S/wuestite weight ratios, the composition of the amorphous products must be different. This suggests that the samples should exhibit different microstructures and properties.

5.3.2.5 Microstructural properties

A gallery of SEM micrographs representing the samples after 28 days is shown in Fig. 41. The formulations with less water (samples S3 and S4) exhibited a compact microstructure, with the residual slag particles embedded in the amorphous matrix. Some cracks were likely partially

caused by sample preparation for SEM. At higher water content (samples S1 and S2) the microstructure is more porous, with many small sub-spherical particles, mostly 4-7 μm in size, coated by what appears to be a reaction product resulting from the coalescence of numerous flake-like nanoparticles.

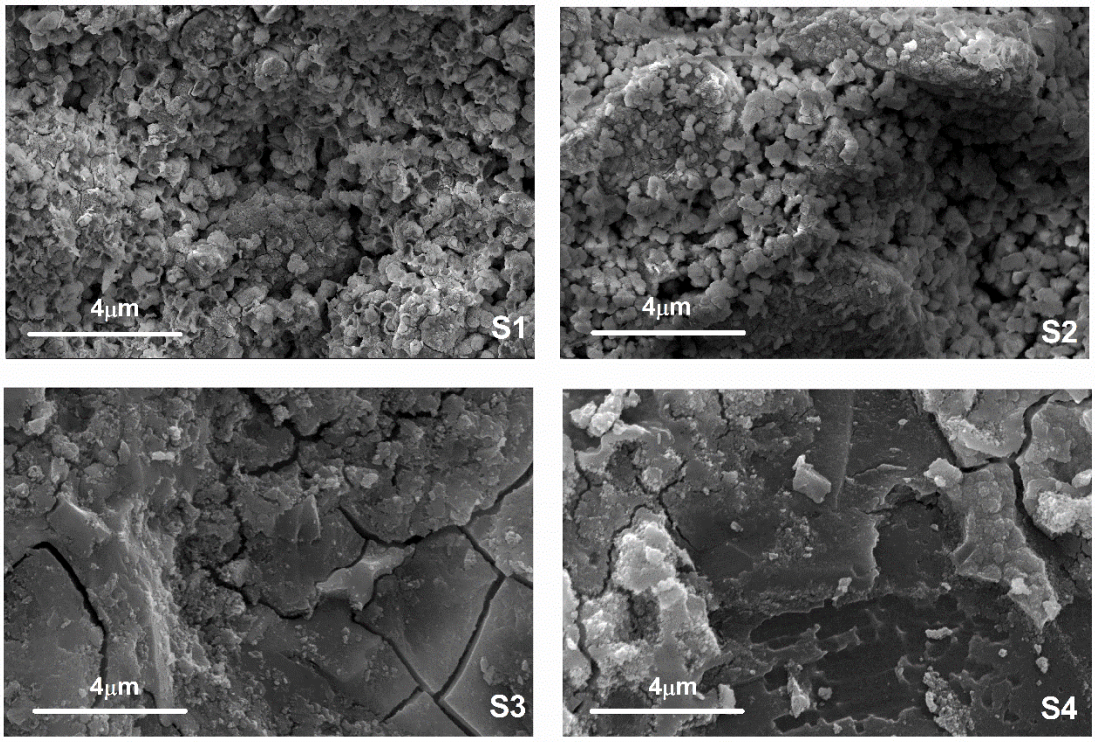

Fig. 41. SEM micrographs of steel slag-based phosphate cement. Formulations S1, S2, S3, S4.

The results of EDS point analysis will be kept qualitative because, in practice, EDS spatial resolution is of the order of 1-10 μm, due to the volume from which the signal originates [209]. Moreover, the results are at best semi-quantitative, due to the analysis of the fractured sample surface, which was chosen in order to characterize the textural features. In samples S1 and S2, P and K, together with Ca, Si, Al and Fe, were detected on the surface of the sub-spherical particles and their external rims (Fig. 42). This strongly suggests that reaction products were observed in both cases, because K and P were introduced with KDP.

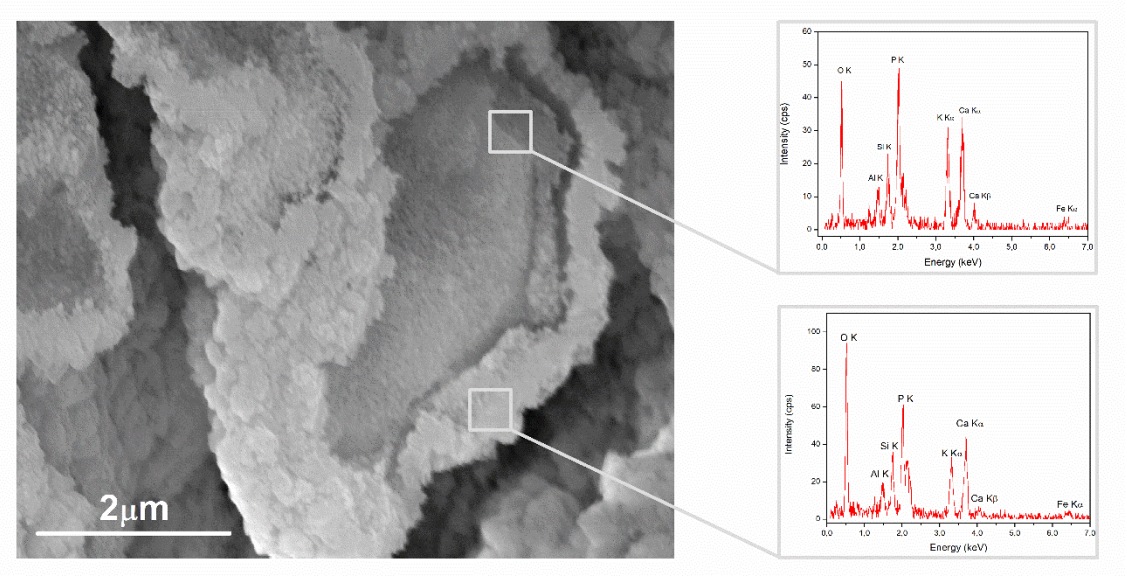

Fig. 42. SEM micrograph of sub-spherical particles corresponding to the S1 cement formulation.

No significant differences were found in the K/P, Ca/P, Ca/Fe and Ca/Si ratios between the grain surfaces and the rims. It is proposed that, in these samples, the grains represent the fine fraction of the slag which was coated with a compact layer of reaction products, and a weak external layer of similar composition. The latter of these assumed the form of flakes because the higher amount of water in the mix allowed crystals to grow freely, due to the high space between grains. The reaction products can be considered metal phosphate hydrates and Ca silicate-aluminate hydrates (C-S-H and C-S-A-H). This is in agreement with the ATR-FT-IR results, considering the similar vibrations of the C-S-H and C-S-A-H [210]. The more compact amorphous matrix, as observed in samples S3 and S4, proved to be mainly composed of Si, P Ca and Fe (Fig. 43), which is consistent with what can be inferred from the amount of dissolved phases as obtained from XRD quantitative phase analysis.

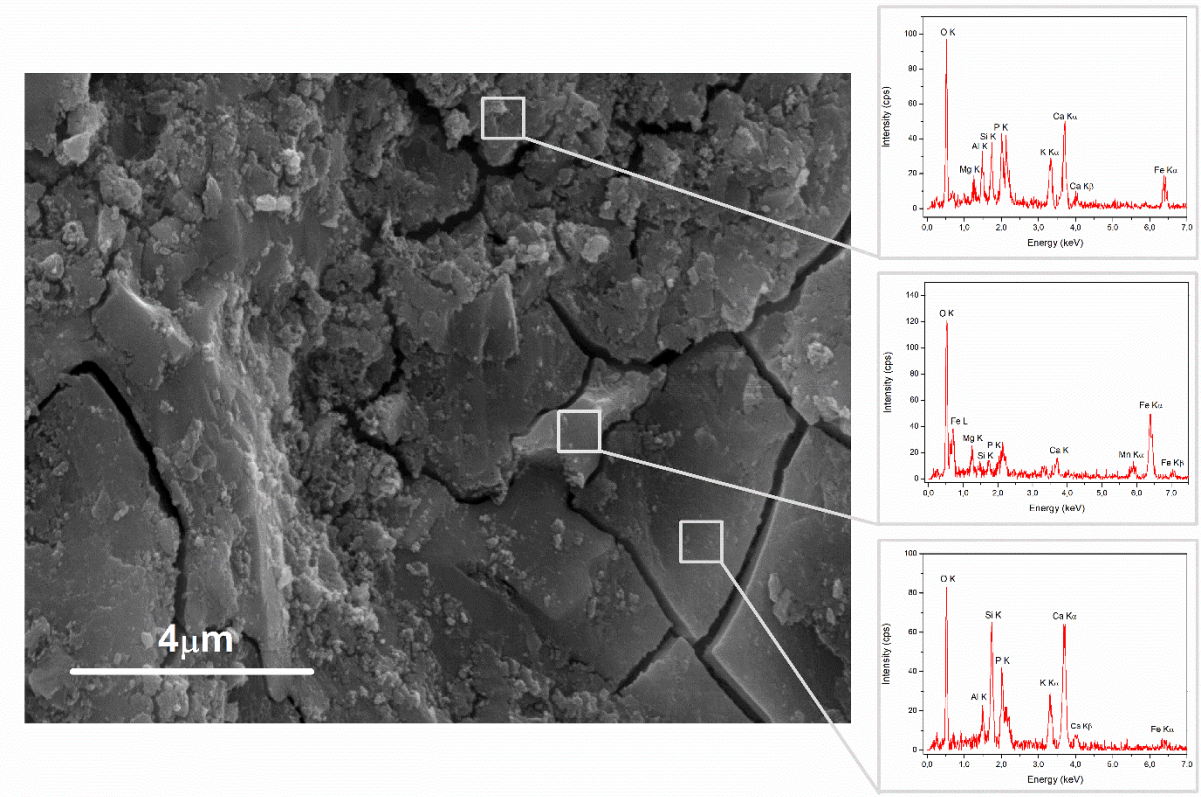

Fig. 43. SEM micrograph of compact microstructure corresponding to S3 cement formulation.

5.3.2.6 Mechanical behavior

Fig. 44 illustrates the results of the mechanical tests, which indicate that formulation S3 exhibits values comparable to cement pastes of medium strength, in the range 15 -25 MPa. Such values can be considered suitable for mortars and construction bricks [211], [212]. It is apparent that formulations with less water (formulations S3 and S4) exhibit higher strength, which could be explained by their more compact microstructure (Fig. 41). In addition, the increase in phosphate content (KDP) appears to be the reason for the increase in mechanical strength, as formulation S3 performs better than S4, whereas S1 performs better than S2. The increase in strength from 7 to 28 days was relatively small for samples S1 and S4. It is therefore confirmed that the amount of phosphate is more essential to the strength than the products of hydration of silicates and

aluminates, since more phosphates are formed when more KDP is present, as indicated by the results of ICC and XRD.

At the same time, given that, for the formulations adopted in this study, the amount of water is not the limiting factor for the reaction, lower water favored strength, by producing a more compact microstructure, which is consistent with the SEM results. It has already been shown that, in CBPCs, excess water is detrimental to performance, since it is segregated in pores/pockets in the sample volume [13], [213].

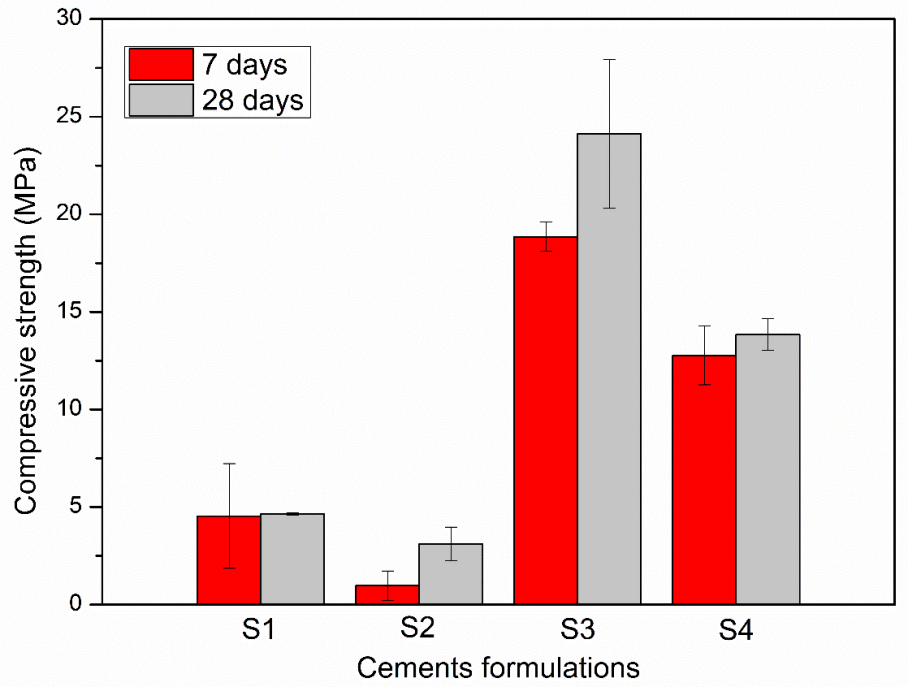

Fig. 44. Compressive strength of different cement formulations.

5.3.2.7 Leaching tests

In a previous study on the chemical composition of the EAF slag, the harmful element released was Cr [126]. This is consistent with another study where a leaching test was performed on a similar slag, where the harmful chemical elements potentially released in relevant amount were As and Cr [120]. The leaching test has been conducted in these elements on the sample with

formulation S1, which is characterized by a weak microstructure, and therefore, is likely to be more leachable.

The measured cumulative concentrations (sum of all 8 values) have been contrasted with the parameters U_1 and U_2 established in the Dutch tank leaching test [214], which describes the concentration limits for hazardous materials. According to the standard, when the U_1 limit is not exceeded, the material can be used as a building material without any restriction. If the results are between the U_1 and U_2 limits, the material can be used, but must be treated after the end of its life cycle. Finally, if the U_2 limit is exceeded, the material cannot be used as building material. The NEN 7345 standard allows the assessment of the leaching potential of monolithic wastes over a long period (64 days) and is frequently adopted for building materials [215], [216]. Similarly, the limits established in the Dutch regulations on soil quality were considered [217]. These stipulate limits in order to prevent soil contamination, apply to building materials that are in contact with rain, surface and groundwater and are among the most important regulations in this field [218]. Fe, Mn, Ca and P were analyzed during the test because, due to their high concentration in cement, they are susceptible to leaching, which affects cement durability [67], [219], [220].

Ei values reported in Table 27 for Cr and As of 1.12 and 0.27 mg/m^2 respectively, indicate that the As and Cr released from the sample are far below the limits established in both the NEN 7345 standard and the Soil Quality Decree. Therefore, it follows that the slag-based phosphate cement matrix favors the immobilization of these elements, so the use of this material does not involve significant risks of soil and water contamination

Table 27. Results of leaching test in slag-based phosphate cement after 8 extractions according to NEN 7345.

Element	U_1 (mg/m^2)	U_2 (mg/m^2)	Soil quality emission limits (mg/m^2)	Max. value during test (mg/L)	***Ei***
Cr	150	950	120	1.12	0.050
As	40	300	260	0.27	0.020
Mn	-	-	-	0.06	0.003
Fe	-	-	-	0.19	0.034
Ca	-	-	-	2.80	0.128
P	-	-	-	512.1	36.500

Fig. 45 illustrates the leaching rates obtained during the test. The highest release was observed after 2 days for all elements but Ca. As observed in other CBPCs, phosphorous is easily leached from the cement in acidic environments [142]. Mobilization of Ca increases with time due to the different rate of dissolution of C-S-H, since, with the decrease in pH, the C-S-H gel becomes unstable and multi-decalcification occurs [221].

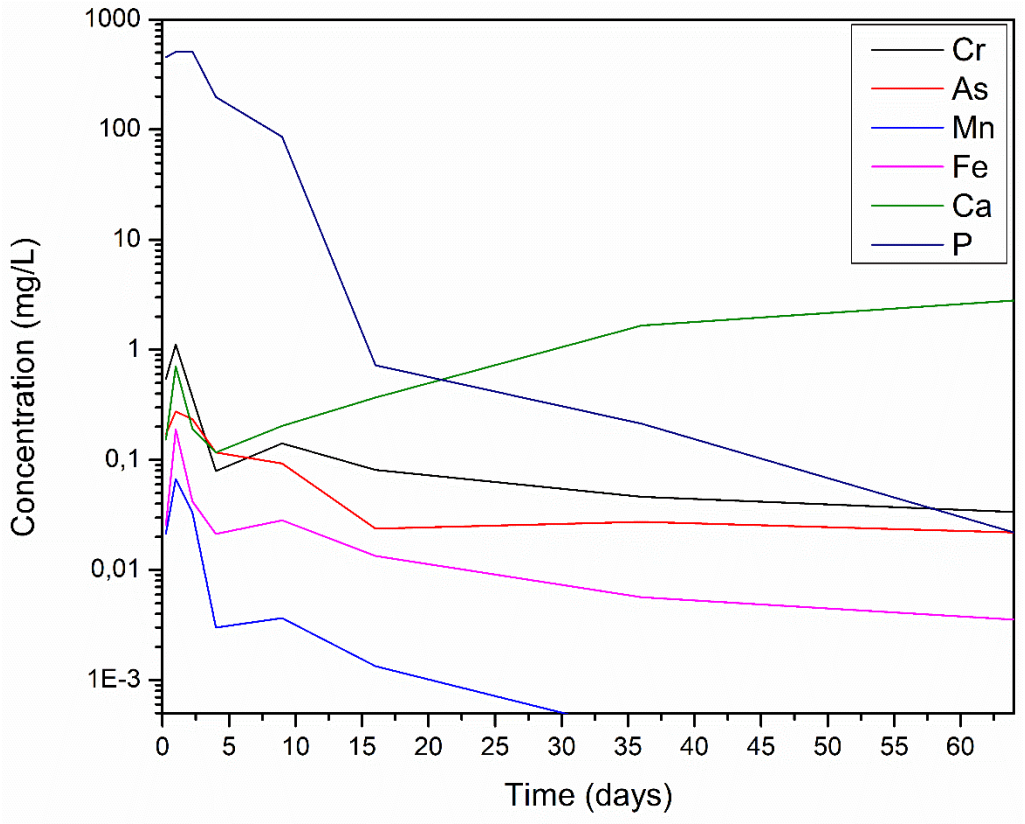

Fig. 45. Graphical illustration of the results of the leaching test according to NEN 7345.

5.4 Discussion

5.4.1 Cement formation

According to the results of quantitative phase analysis (Table 26), the main crystalline phases in the slag are C_2S and wuestite. The behavior of these minerals in acidic environments is relevant to the cement formation process. C_2S reacts immediately in phosphate solutions [2] and has good dissolution at pH > 4 [222]. Wuestite is a well-known precursor to CBPCs [2]. The relevant dissolution equations are (Equations 9-10):

$$FeO + 2H^+ = Fe^+(aq) + H_2O \quad (9)\ [2]$$

$$Ca_2SiO_4 + 4H^+ = 2Ca^{2+} + 2H_2O + SiO_{2(aq)} \quad (10)\ [145]$$

In equilibrium, the dissolution product constant pK_{sp}, dictates the degree of dissolution of FeO and C_2S in acidic environments. The values of 13.29 and 1.66 for FeO and C_2S respectively [2], indicate a higher degree of dissolution for FeO and, possibly, greater availability of Fe^{2+} for the formation of iron phosphates. Thermodynamic arguments indicate that, compared to C_2S, FeO favors the formation of stable and compact ceramics in the pH interval of interest for acid-base systems [89].

Previous studies on CBPCs incorporating slags and industrial wastes containing Al and Fe oxides, agree on the formation of reaction products including both phosphates of the metal oxides and silicate hydrates [23], [143], [223], [224]. Similarly, in the current study, the spectroscopic signature of the reaction products (Fig. 37) points to the coexistence of orthophosphates hydrates and calcium silicate/aluminate hydrates (such as C-S-H). Indeed, the main signal in the region

~1000 cm^{-1} in the infrared spectra has already been considered indicative of amorphous iron phosphate in MPC incorporating iron oxides [143].

Consistently with these results, the SEM micrographs reported in Fig. 41 and the EDS point analysis (Fig. 43) indicate an amorphous structure, which is very compact at low water content (sample S3 and S4), and incorporates the metal oxides dissolved from the slag. Compact microstructure including calcium phosphates and iron phosphates has been documented in a CBPC obtained with steel slag powder [22]. It has been suggested that the presence of alkaline oxides such as CaO, Fe_2O_3, Al_2O_3 allows the formation of complex phosphates containing -O-P-Ca-O-P-O- and -O-P-Fe-O-P-O chains [224]. The EDS analysis suggested the presence of mainly calcium phosphates and iron phosphates, probably accompanied by amorphous silica and other elements (Al, K). This is consistent with several studies in which amorphous phases are identified as new hydration products in MPC matrix cements with additions of slags or other industrial wastes [22], [143], [223]–[225]The formation of calcium silicate hydrates (C-S-H) in slag-based phosphate cements is due to the hydration of the residual C_2S, not dissolved during step B observed with ICC. This has been previously observed by other authors as a product of the hydration of steel slag [226]. The maximum in the ICC trace (step D in Fig. 38) indicates that C-S-H forms later than the main phosphate reaction, which is consistent with the hydration kinetics of C_2S [204]. This is further confirmed by the infrared spectra (Fig. 37). Unlike Portland cement, where C-S-H provides the strength, in the steel slag-based phosphate cement the presence of higher amounts of C-S-H is not beneficial (see samples S1 and S2 in Fig. 44). This can be explained considering that the strength is primarily due to formation of solid phosphate hydrates, which occurs faster than the hydration of C_2S and entails subtraction of water. Any excess water at this stage is detrimental to the mechanical performance, because a more open structure results [13], [227], as confirmed by

the SEM investigation of the samples with high water content (samples S1 and S2 in Fig. 41). The C-S-H formed by the later reaction of C_2S with this fraction of water cannot compensate for this lack of compactness.

5.4.2 Description of the kinetic model in the formation of steel slag-based cement phosphate

Fig. 38 shows the comparative ICC data of the four formulations and proposes the following model to explain the kinetics of steel slag-based phosphate cement formation:

The first step (A) describes the dissolution of dihydrogen potassium phosphate KH_2PO_4 (KDP). In this phase, phosphate anions and protons are released, generating an aqueous acidic environment, a reaction regulated by the amount of water present in the system.

In the next step (B), the slags dissolve in the acidic environment of the phosphate, allowing the release of metal cations, mainly Ca^{+2} and Fe^{+2}. This step is decisive for the consolidation of the high-strength products. The rate of the process is decided by the surface area available and the concentration of protons (pH). KDP is always supersaturated; therefore, the surface area plays a crucial role here. With more slag (more surface area) Ca^{+2} and Fe^{+2} ate more rapidly dissolved (formulations S2-S4), compared to the formulation with less slag (less surface area) (formulations S1-S3), see fig. 38.

When less KDP is used the dissolution (step B) probably ends quickly. KDP becomes a limiting factor; when more KDP is available, step B lasts longer but takes place more slowly (because of diffusion limited process). The layer produced that surrounds the grains of slag slows dissolution, but as long as the KDP is available, the reaction continues and more product is formed. Therefore, a two-step process is proposed: i) surface limited (higher product with high slag content), ii) KDP and diffusion limited (higher product in the long term when there is less slag).

Step (C) of formation (hydrophosphate salts) through the acid-base reaction system, is determined by the availability of ions released in the slag solution and dihydrogen potassium phosphate KH_2PO_4; that is to say, a higher amount of product is formed when higher ionic concentrations of metal cations and phosphate anions converge at a specific pH (Formulations S1-S3). Higher ionic concentrations with a high water content react quickly, allowing a low formation of phosphate cements (formulations S1), whereas higher ionic concentrations with less water react slowly and serve to increase phosphate cement formation (formulations S3). This is an ideal situation that allows higher strength products, see fig. 39. In the case of low ionic concentrations, with higher water, the reaction slows down, limiting the formation of products (formulations S2), whereas with less water it reacts more quickly, decreasing product formation (formulations S4), see fig. 39.

The initial dissolution of the dicalcium silicates and iron oxides provides the metal cations necessary for the formation of phosphate cements, reactions that occur rapidly as the available ions are consumed (Step C). The last step (D), is the hydration of dicalcium silicate particles to form C-S-H. Hydration of dicalcium silicates is observed only in environments with excess water, (formulations S1-S2), see fig. 38. In this step, the still undissolved dicalcium silicates hydrate with the excess water present in the system, causing the formation of C-S-H. It is important to note that the highest content of formed product (amorphous) is related to the highest amount of total heat recorded (formulations S1-S3), directly influencing mechanical strength. However, a clear differentiation is observed between the amorphous products formed from formulation S1 and formulation S3, since their mechanical strengths are very different. A higher mechanical strength is obtained for formulation 3 with a lower total heat, and on the contrary, a lower mechanical strength is obtained for formulation S1 but with a higher total heat. This suggests the formation of different amorphous products: for formulation S1 these would correspond mainly to C-S-H and,

for formulation S3, to phosphate cements, which would be mainly responsible for the mechanical strength of the product.

5.4.3 Chemical stability of slag-based phosphate cement

The chemical stability of As and Cr in phosphate cement matrices provides an alternative route to the recycling of EAF steel slags, since the low concentrations of leachate evidenced after NEN 7345 test indicate that this material does not pose risks of contamination to the soil and hydric sources. The tested sample possesses a less compact microstructure and, therefore, better results are expected for the formulations with less water and better mechanical performance. As and Cr are effectively stabilized in the cement matrix, and, according to the results, the tested slag-based phosphate cement can be classified as inert and suitable as a building material. The main elements contributing to the formation of the matrix are Fe, Ca and P. Fe exhibited reduced mobility, whereas P is initially released in a higher amount, becoming stable towards the end of the test at concentrations similar to the other elements. This has already been observed in other phosphate cements [21], [219]. Ca shows a different behavior, with a considerable release at the end of the test cycle, probably due to the unreacted Ca or dissolution of the C-S-H present in the phosphate cement matrix.

5.5 Conclusions

A new way of recycling EAF slag to obtain phosphate cement is described in this chapter. The proposed process also reduces the environmental impact of the manufacture of phosphate cement, because the high energy-consuming step, consisting of the high temperature annealing of MgO

(the commonly used metal oxide for phosphate cement production), is completely excluded, since MgO is replaced by the EAF slag.

The reaction products were found to consist of amorphous orthophosphates hydrates, most likely of Fe and Ca, derived prevalently from the dissolution of wuestite and C_2S, respectively. Calcium silicate/aluminate hydrates (such as C-S-H) may also form subordinately from hydration of unreacted C_2S. The amount of these depends on the relative amount of water in excess of the fraction needed to form the phosphates, because the latter of the above-mention reactions is faster. The kinetics describe a process similar to that of other phosphate cements. The production of hydrophosphate salts is determined by the amount of ions present for the acid-base reaction, such that limited surface of slag, KDP and limited diffusion, determine the formation of the slag-based phosphate cement.

The main contribution to the mechanical resistance of the cement (15-25 MPa) comes from the formed amorphous products in which the residual slag grains are embedded. This matrix has proven to be efficient in the immobilization of As and Cr contained in the EAF slags, enabling the use of this secondary raw material as a building material for mortars and bricks, without the risk of contamination of water sources and soil.

6. Conclusions and Outlook

The important mechanical strengths from phosphate cements, with similar or even greater values than Portland cements, in addition to a lower environmental impact, has highlighted them in civil construction applications, motivating research in this field. In the present research, different steel slags and phosphoric rock were evaluated as potential formers of iron phosphate cements for applications as building materials.

The following steel slags were evaluated; Electric Arc Furnace slag (EAF), Basic Oxygen Furnace slag (BOF), and FINE slag. FINE slag is classified as final factory waste and consists of a mixture of EAF, BOF and Ladle Furnace slag (LF). The EAF slag was selected for more complete analysis, due to its higher iron oxide contents, the BOF and FINE slag were used directly to obtain cements from orthophosphoric acid. The main mineral phases present in all the analyzed slags were: wüstite, dicalcium silicate, srebrodolskite and brownmillerite, all rich in calcium oxide and iron oxide. In this research work it was demonstrated that the alkaline character, the obtaining of appropriate particle sizes from simple and economical grinding processes, and the content of divalent metal oxides forming different phases, provide the minimum parameters in the formation of CBPC, where steel slag provides the metal cation necessary for acid-base system reactions.

Chemically bonded phosphate ceramics (CBPC) were synthesized, from EAF, BOF and FINE steel slags, the evaluation of the slag-based phosphate cements showed the formation of crystalline calcium phosphate compounds and amorphous iron phosphate compounds mainly. The presence of crystalline and amorphous phases was affected by the precursors.

Using orthophosphoric acid as a precursor, slight and scarce crystalline phases were originated with a very poor chemical stability, showing high solubility in water and acid environments, using

KDP the amorphous phases were favored, their crystallinity is secondary or in some cases insignificant, generating cements of acceptable performance and exceptional chemical stability. The chemical nature of the compounds formed from the reactions of the steel slag with the phosphate compounds has not allowed a total understanding due to their amorphous nature, which makes their characterization difficult. Phosphate cements from aqueous solutions of orthophosphoric acid, precipitated mainly as amorphous phases (80% - 90%) that are attributed to amorphous iron phosphates Fe $(H_2PO_4)_2$ or $FeHPO_4$ and amorphous calcium phosphate (ACP), the crystalline phases found correspond to hydrated calcium dihydrogen phosphate and brushite. The formation of iron phosphate cements is primarily due to the presence of Fe^{2+} metal cations present in wüstite (FeO), magnetite (Fe_3O_4) and dicalcium ferrites, also the Ca^{2+} cations that are predominantly present in dicalcium silicates (Ca_2SiO_4) and dicalcium ferrites dissolved in acidic environments, contributing to the formation of the compounds. Minimum values of the liquid / solid ratios in the mixture and the higher concentration of H_3PO_4 positively affected the compressive strength.

A binder was synthesized from the reaction of EAF slag and leached phosphoric rock with H_2SO_4, presenting low mechanical strengths. The low solubility of phosphoric rock, despite the significant amounts of P_2O_5 present as fluorapatite carbonates, evidenced difficulties for the formation of CBPC, forcing complex leaching processes to release the phosphate anions required for the acid-base reaction. The formation of brushite-type calcium phosphates was evidenced mainly, in addition to a high presence of gypsum and anhydrite as reaction catalysts, which inhibited the formation of metal phosphates, forcing the application of filtering and upgrading processes, factors that induce a significant increase in costs to obtain the cement.

In this doctoral thesis, EAF slag-based phosphate cements were synthesized using potassium dihydrogen phosphate (KDP) as the phosphate component. The high energy consumption necessary for the calcination of alkaline compounds is eliminated, since this process is replaced by an industrial waste such as EAF slag; therefore, a new way of recycling the slag to obtain cement is described, which reduces the environmental impact of phosphate cement manufacturing. In EAF slag-based phosphate cements, the reaction products consisted of hydrated amorphous iron and calcium orthophosphates, without the presence of crystalline phases. The presence of calcium silicate hydrate (C-S-H) was also observed in minor proportion, from the unreacted calcium silicate. In accordance with in-situ observations of EAF slag-based phosphate cements, formation mechanisms similar to other phosphate cements can be inferred. Phenomena such as slag surface area, phosphate saturation level and controlled diffusion determine cement formation. The mechanical compressive strengths attributed to the amorphous matrix allow applications of medium-strength products such as bricks and masonry mortars, (according to standard ASTM 270-07/ASTM C62), also the good chemical stability (according to standard NEN 7345) demonstrated by immobilizing dangerous elements (Cr and As) present in the slag, guarantee their application in building materials, without detriment to environmental conditions.

After the evaluation of raw materials, synthesis and characterization of different phosphate cements based on slags, carried out in the present doctoral research, it is necessary to explore various leaching processes for slags in order to concentrate essential oxides in obtaining CBPC, thus limiting the intervention of other compounds with greater solubility, which substantially modify the cement formation parameters, likewise proposing to obtain matrices with iron phosphate phases that allow the exploration and deepening of functional characteristics such as ferromagnetism among others. It is important to consider the application of methods of leaching

with acetic acid by means of ultrasound, in order to precipitate calcium carbonates and capture CO_2 in the steel slag, thus allowing the visualization of processes that concentrate iron phosphates and at the same time have a favorable impact on the environment.

Recommendations for future research work:

Industrial waste as raw materials in acid-base reaction cementitious systems such as polyalkenoate cements and oxysal binders.

Recovery of calcium oxide and concentration of iron oxides through leaching processes in steel slag.

Ferromagnetic properties of leached steel slag with a high content of iron oxides.

References

[1] A. D. Wilson and J. W. Nicholson, *Acid-base cements Their biomedical and industrial applications*. New York: Cambridge University press, 1993.

[2] A. Wagh, *Chemically Bonded Phosphate Ceramics: Twenty-first Century Materials with Diverse Applications*, 2nd ed., vol. 5. Naperville, IL, United States: Elsevier Ltd, 2016.

[3] W. D. Kingery, "Fundamental Study of Phosphate Bonding in Refractories: II, Cold Setting Properties," *J. Am. Ceram. Soc.*, vol. 33, no. 8, pp. 239–241, 1950, doi: 10.1111/j.1151-2916.1950.tb14171.x.

[4] A. S. Wagh, S. Y. Jeong, and D. Singh, "Iron-Phosphate-based chemically bonded phosphate ceramics for mixed waste stabilization," *Waste Manag. Annu. Meet. Tucson, AZ, March 2-6, 1997*, 1997.

[5] D. Singh, A. S. Wagh, and S. Y. Jeong, "U.S. Pat. No. 6,133,498.Method for producing chemically bonded phosphate ceramics and for stabilizing contaminants encapsulated therein utilizing reducing agents.," 2000.

[6] A. S. Wagh and S.-Y. Jeong, "U.S. Pat. No. 5,846,894 Chemically bonded phosphate ceramics of trivalent oxides of iron and manganese," US 6,498,119 B2, 2002.

[7] P. Mácová and A. Viani, "Investigation of setting reaction in magnesium potassium phosphate ceramics with time resolved infrared spectroscopy," *Mater. Lett.*, vol. 205, pp. 62–66, 2017, doi: 10.1016/j.matlet.2017.06.063.

[8] A. Viani, G. Mali, and P. Mácová, "Investigation of amorphous and crystalline phosphates in magnesium phosphate ceramics with solid-state 1H and 31P NMR spectroscopy," *Ceram. Int.*, vol. 43, no. 8, pp. 6571–6579, 2017, doi: 10.1016/j.ceramint.2017.02.087.

[9] A. Viani, K. Sotiriadis, P. Šašek, and M. S. Appavou, "Evolution of microstructure and

performance in magnesium potassium phosphate ceramics: Role of sintering temperature of MgO powder," *Ceram. Int.*, vol. 42, no. 14, pp. 16310–16316, 2016, doi: 10.1016/j.ceramint.2016.07.182.

[10] Z. Ding, B. Dong, F. Xing, N. Han, and Z. Li, "Cementing mechanism of potassium phosphate based magnesium phosphate cement," *Ceram. Int.*, vol. 38, no. 8, pp. 6281–6288, 2012, doi: 10.1016/j.ceramint.2012.04.083.

[11] A. Viani and P. Mácová, "Polyamorphism and frustrated crystallization in the acid-base reaction of magnesium potassium phosphate cements," *CrystEngComm*, 2018, doi: 10.1039/C8CE00670A.

[12] A. Viani and A. F. Gualtieri, "Preparation of magnesium phosphate cement by recycling the product of thermal transformation of asbestos containing wastes," *Cem. Concr. Res.*, vol. 58, pp. 56–66, 2014, doi: 10.1016/j.cemconres.2013.11.016.

[13] A. Viani, K. Sotiriadis, G. Lanzafame, and L. Mancini, "3D microstructure of magnesium potassium phosphate ceramics from X-ray tomography: new insights into the reaction mechanisms," *J. Mater. Sci.*, vol. 54, no. 5, pp. 3748–3760, 2019, doi: 10.1007/s10853-018-3113-7.

[14] C. Shi, J. Yang, N. Yang, and Y. Chang, "Effect of waterglass on water stability of potassium magnesium phosphate cement paste," *Cem. Concr. Compos.*, vol. 53, pp. 83–87, 2014, doi: 10.1016/j.cemconcomp.2014.03.012.

[15] A. Viani, M. Per??z-Est??banez, S. Pollastri, and A. F. Gualtieri, "In situ synchrotron powder diffraction study of the setting reaction kinetics of magnesium-potassium phosphate cements," *Cem. Concr. Res.*, vol. 79, pp. 344–352, 2016, doi: 10.1016/j.cemconres.2015.10.007.

[16] A. Viani, M. Zbiri, H. N. Bordallo, A. F. Gualtieri, and P. Mácová, “Investigation of the Setting Reaction in Magnesium Phosphate Ceramics with Quasielastic Neutron Scattering,” *J. Phys. Chem. C*, vol. 121, no. 21, pp. 11355–11367, 2017, doi: 10.1021/acs.jpcc.7b01396.

[17] C. Shi, “Steel Slag—Its Production, Processing, Characteristics, and Cementitious Properties,” *J. Mater. Civ. Eng.*, vol. 16, no. 3, pp. 230–236, Jun. 2004, doi: 10.1061/(ASCE)0899-1561(2004)16:3(230).

[18] I. Z. Yildirim and M. Prezzi, “Steel Slag: Chemistry, Mineralogy, and Morphology,” in *IFCEE 2015*, 2015, pp. 2816–2825, doi: 10.1061/9780784479087.263.

[19] J. Waligora, D. Bulteel, P. Degrugilliers, D. Damidot, J. L. Potdevin, and M. Measson, “Chemical and mineralogical characterizations of LD converter steel slags: A multi-analytical techniques approach,” *Mater. Charact.*, vol. 61, no. 1, pp. 39–48, 2010, doi: 10.1016/j.matchar.2009.10.004.

[20] H. Guo *et al.*, “Iron recovery and active residue production from basic oxygen furnace (BOF) slag for supplementary cementitious materials,” *Resour. Conserv. Recycl.*, vol. 129, no. October 2017, pp. 209–218, 2018, doi: 10.1016/j.resconrec.2017.10.027.

[21] D. Sun, K. Wu, W. Kang, H. Shi, and S. Li, “Characterisation of water stability of magnesium phosphate cement blended with steel slag and fly ash,” *Adv. Cem. Res.*, vol. 32, no. 6, pp. 251–261, 2020, doi: 10.1680/jadcr.18.00067.

[22] Y. Jiang, M. R. Ahmad, and B. Chen, “Properties of magnesium phosphate cement containing steel slag powder,” *Constr. Build. Mater.*, vol. 195, pp. 140–147, 2019, doi: 10.1016/j.conbuildmat.2018.11.085.

[23] J. Yang, J. Lu, Q. Wu, M. F. Xia, and X. Li, “Influence of steel slag powders on the properties of MKPC paste,” *Constr. Build. Mater.*, vol. 159, pp. 137–146, 2018, doi:

10.1016/j.conbuildmat.2017.10.081.

[24] J. Choi, W. Um, and S. Choung, “Development of iron phosphate ceramic waste form to immobilize radioactive waste solution,” *J. Nucl. Mater.*, vol. 452, no. 1–3, pp. 16–23, 2014, doi: 10.1016/j.jnucmat.2014.04.033.

[25] FAO, *Use of phosphoric rocks for sustainable agriculture*, vol. 13. Rome, 2007.

[26] T. Theys, “Newcomer in Phosphoric Acid Process Routes : The DA-HF Process,” vol. 5, pp. 63–69, 2016.

[27] T. F. Al-Fariss, H. O. Ozbelge, F. A. A. Aleem, and S. M. Abdulrazik, “Evaluation of Saudi Phosphate Rocks for Wet Process Phosphoric Acid Production,” *J. King Saud Univ. - Eng. Sci.*, vol. 4, no. 1, pp. 33–44, 1992, doi: 10.1016/S1018-3639(18)30554-3.

[28] M. Aminul Haque, B. Chen, Y. Liu, S. Farasat Ali Shah, and M. R. Ahmad, “Improvement of physico-mechanical and microstructural properties of magnesium phosphate cement composites comprising with Phosphogypsum,” *J. Clean. Prod.*, vol. 261, p. 121268, 2020, doi: 10.1016/j.jclepro.2020.121268.

[29] C. Cárdenas-Escudero, V. Morales-Flórez, R. Pérez-López, A. Santos, and L. Esquivias, “Procedure to use phosphogypsum industrial waste for mineral CO 2 sequestration,” *J. Hazard. Mater.*, vol. 196, pp. 431–435, 2011, doi: 10.1016/j.jhazmat.2011.09.039.

[30] E. Gartner, “Industrially interesting approaches to ‘low-CO2’ cements,” *Cem. Concr. Res.*, vol. 34, no. 9, pp. 1489–1498, 2004, doi: 10.1016/j.cemconres.2004.01.021.

[31] M. Schneider, M. Romer, M. Tschudin, and H. Bolio, “Sustainable cement production—present and future,” *Cem. Concr. Res.*, vol. 41, no. 7, pp. 642–650, Jul. 2011, doi: 10.1016/j.cemconres.2011.03.019.

[32] J. S. Damtoft, J. Lukasik, D. Herfort, D. Sorrentino, and E. M. Gartner, “Sustainable

development and climate change initiatives," *Cem. Concr. Res.*, vol. 38, no. 2, pp. 115–127, 2008, doi: 10.1016/j.cemconres.2007.09.008.

[33] G. Habert, C. Billard, P. Rossi, C. Chen, and N. Roussel, "Cement production technology improvement compared to factor 4 objectives," *Cem. Concr. Res.*, vol. 40, no. 5, pp. 820–826, 2010, doi: 10.1016/j.cemconres.2009.09.031.

[34] N. Yang, C. Shi, J. Yang, and Y. Chang, "Research Progresses in Magnesium Phosphate Cement – Based Materials," *J. Mater. Civ. Eng.*, vol. 26, no. 10, pp. 1–8, 2014, doi: 10.1061/(ASCE)MT.1943-5533.0000971.

[35] S. Jeong and A. S. Wagh, "Chemically bonded phosphate ceramics: cementing the gap between ceramics and cements.," 2004.

[36] J. Formosa *et al.*, "Magnesium Phosphate Cements formulated with a low-grade MgO by-product: Physico-mechanical and durability aspects," *Constr. Build. Mater.*, vol. 91, pp. 150–157, Aug. 2015, doi: 10.1016/j.conbuildmat.2015.05.071.

[37] M. S. Imbabi, C. Carrigan, and S. McKenna, "Trends and developments in green cement and concrete technology," *Int. J. Sustain. Built Environ.*, vol. 1, no. 2, pp. 194–216, 2012, doi: 10.1016/j.ijsbe.2013.05.001.

[38] S. M. Calle-Castañeda, M. A. Márquez-Godoy, and J. P. Hernández-Ortiz, "Phosphorus recovery from high concentrations of low-grade phosphate rocks using the biogenic acid produced by the acidophilic bacteria Acidithiobacillus thiooxidans," *Miner. Eng.*, vol. 115, no. October 2017, pp. 97–105, 2018, doi: 10.1016/j.mineng.2017.10.014.

[39] Z. I. Zafar and M. Ashraf, "Selective leaching kinetics of calcareous phosphate rock in lactic acid," *Chem. Eng. J.*, vol. 131, no. 1–3, pp. 41–48, 2007, doi: 10.1016/j.cej.2006.12.002.

[40] P. Ptáček, "Mining and Beneficiation of Phosphate Ore," in *Apatites and their Synthetic*

Analogues - Synthesis, Structure, Properties and Applications, InTech, 2016, pp. 383–414.

[41] D. M. Roy, "New strong cement materials: chemically bonded ceramics.," *Science*, vol. 235, no. 4789, pp. 651–8, 1987, doi: 10.1126/science.235.4789.651.

[42] A. S. Wagh, "Recent Progress in Chemically Bonded Phosphate Ceramics," *ISRN Ceram.*, vol. 2013, pp. 1–20, 2013, doi: 10.1155/2013/983731.

[43] A. Wilson and J. Nicholson, "Acid–base cements: Their biomedical and industrial applications.," *Polym. Int.*, vol. 35, no. 2, pp. 215–215, Oct. 1994, doi: 10.1002/pi.1994.210350213.

[44] A. S. Wagh, "Chemically Bonded Phosphate Ceramic Matrix Composites," in *Chemically Bonded Phosphate Ceramics*, 1st ed., vol. 24, U. Argonne National Laboratory 9700 S. Cass Avenue Argonne, IL 60439 and 2004, Eds. Argonne National Laboratory 9700 S. Cass Avenue Argonne, IL 60439, USA 2004: Elsevier, 2004, pp. 157–176.

[45] J. P. Attfield, "Phosphates," *Encyclopedia of Materials: Science and Technology*, vol. 3. Elsevier Ltd, pp. 6896–6901, 2001.

[46] F. Glasser, "4 - Application of inorganic cements to the conditioning and immobilisation of radioactive wastes," *Woodhead Publ. Ser. Energy*, pp. 67–135, 2011, doi: http://dx.doi.org/10.1533/9780857090959.1.67.

[47] M. Alshaaer, H. Cuypers, G. Mosselmans, H. Rahier, and J. Wastiels, "Evaluation of a low temperature hardening Inorganic Phosphate Cement for high-temperature applications," *Cem. Concr. Res.*, vol. 41, no. 1, pp. 38–45, Jan. 2011, doi: 10.1016/j.cemconres.2010.09.003.

[48] H. A. Colorado, Z. Wang, and J. M. Yang, "Inorganic phosphate cement fabricated with wollastonite, barium titanate, and phosphoric acid," *Cem. Concr. Compos.*, vol. 62, pp. 13–

21, 2015, doi: 10.1016/j.cemconcomp.2015.04.014.

[49] P. Parhi, V. Manivannan, S. Kohli, and P. McCurdy, “Room temperature metathetic synthesis and characterization of α-hopeite, Zn3(PO4)2·4H2O,” *Mater. Res. Bull.*, vol. 43, no. 7, pp. 1836–1841, Jul. 2008, doi: 10.1016/j.materresbull.2007.07.005.

[50] N. Liu and B. Chen, “Experimental research on magnesium phosphate cements containing alumina,” *Constr. Build. Mater.*, vol. 121, pp. 354–360, 2016, doi: 10.1016/j.conbuildmat.2016.06.010.

[51] A. S. Wagh and S. Y. Jeong, “Chemically Bonded Phosphate Ceramics: III, Reduction Mechanism and Its Application to Iron Phosphate Ceramics,” *J. Am. Ceram. Soc.*, vol. 86, no. 11, pp. 1850–1855, Nov. 2003, doi: 10.1111/j.1151-2916.2003.tb03571.x.

[52] E. Soudée and J. Péra, “Mechanism of setting reaction in magnesia-phosphate cements,” *Cem. Concr. Res.*, vol. 30, no. 2, pp. 315–321, Feb. 2000, doi: 10.1016/S0008-8846(99)00254-9.

[53] J. Formosa, M. A. Aranda, J. M. Chimenos, J. R. Rosell, A. I. Fernández, and O. Ginés, “Cementos químicos formulados con subproductos de óxido de magnesio,” *Bol. la Soc. Esp. Ceram. y Vidr.*, vol. 47, no. 5, pp. 293–297, 2008.

[54] L. J. Gardner, S. A. Bernal, S. A. Walling, C. L. Corkhill, J. L. Provis, and N. C. Hyatt, “Characterisation of magnesium potassium phosphate cements blended with fly ash and ground granulated blast furnace slag,” *Cem. Concr. Res.*, vol. 103, pp. 78–87, 2015, doi: 10.1016/j.cemconres.2017.07.011.

[55] P. Kinnunen *et al.*, “Recycling mine tailings in chemically bonded ceramics – A review,” *J. Clean. Prod.*, vol. 174, pp. 634–649, Feb. 2018, doi: 10.1016/j.jclepro.2017.10.280.

[56] S. V. Dorozhkin and M. Epple, “Biological and medical significance of calcium

phosphates," *Angew. Chemie - Int. Ed.*, vol. 41, no. 17, pp. 3130–3146, 2002, doi: 10.1002/1521-3773(20020902)41:17<3130::AID-ANIE3130>3.0.CO;2-1.

[57] J. S. Al-Sanabani, A. A. Madfa, and F. A. Al-Sanabani, "Application of calcium phosphate materials in dentistry," *Int. J. Biomater.*, vol. 2013, 2013, doi: 10.1155/2013/876132.

[58] M.-S. A. Alberto Viani, Konstantinos Sotiriadis, Ivana Kumpová, Lucia Mancini, "Microstructural characterization of dental zinc phosphate cements using combined small angle neutron scattering and microfocus X-ray computed tomography," *Dent. Mater.*, vol. 33, no. 4, pp. 402–417, 2017, doi: http://dx.doi.org/10.1016/j.dental.2017.01.008.

[59] M. P. Ginebra, C. Canal, M. Espanol, D. Pastorino, and E. B. Montufar, "Calcium phosphate cements as drug delivery materials," *Adv. Drug Deliv. Rev.*, vol. 64, no. 12, pp. 1090–1110, 2012, doi: 10.1016/j.addr.2012.01.008.

[60] A. Wang, Z. Yuan, J. Zhang, L. Liu, J. Li, and Z. Liu, "Effect of raw material ratios on the compressive strength of magnesium potassium phosphate chemically bonded ceramics," *Mater. Sci. Eng. C*, vol. 33, no. 8, pp. 5058–5063, Dec. 2013, doi: 10.1016/j.msec.2013.08.031.

[61] A. Wang, J. Zhang, J. Li, A. Ma, and L. Liu, "Effect of liquid-to-solid ratios on the properties of magnesium phosphate chemically bonded ceramics," *Mater. Sci. Eng. C*, vol. 33, no. 5, pp. 2508–2512, Jul. 2013, doi: 10.1016/j.msec.2013.02.014.

[62] F. Tamimi, Z. Sheikh, and J. Barralet, "Dicalcium phosphate cements: Brushite and monetite," *Acta Biomater.*, vol. 8, no. 2, pp. 474–487, 2012, doi: 10.1016/j.actbio.2011.08.005.

[63] H. A. Colorado, J. Pleitt, C. Hiel, J. M. Yang, H. T. Hahn, and C. H. Castano, "Wollastonite based-Chemically Bonded Phosphate Ceramics with lead oxide contents under gamma

irradiation," *J. Nucl. Mater.*, vol. 425, no. 1–3, pp. 197–204, Jun. 2012, doi: 10.1016/j.jnucmat.2011.08.043.

[64] Y.-S. Wang, J.-G. Dai, Z. Ding, and W.-T. Xu, "Phosphate-based geopolymer: Formation mechanism and thermal stability," *Mater. Lett.*, vol. 190, no. January, pp. 209–212, 2017, doi: 10.1016/j.matlet.2017.01.022.

[65] A. S. Wagh, S. Grover, and S. Y. Jeong, "Chemically Bonded Phosphate Ceramics: II, Warm-Temperature Process for Alumina Ceramics," *J. Am. Ceram. Soc.*, vol. 86, no. 11, pp. 1845–1849, Nov. 2003, doi: 10.1111/j.1151-2916.2003.tb03570.x.

[66] A. S. Wagh and D. Singh, "U.S. Pat. No. 5,645,518 Method for stabilizing low-level mixed wastes at room temperature," 1997.

[67] Y. Li, T. Shi, and J. Li, "Effects of fly ash and quartz sand on water-resistance and salt-resistance of magnesium phosphate cement," *Constr. Build. Mater.*, vol. 105, pp. 384–390, 2016, doi: 10.1016/j.conbuildmat.2015.12.154.

[68] R. del Valle-Zermeño, J. E. Aubert, A. Laborel-Préneron, J. Formosa, and J. M. Chimenos, "Preliminary study of the mechanical and hygrothermal properties of hemp-magnesium phosphate cements," *Constr. Build. Mater.*, vol. 105, pp. 62–68, Feb. 2016, doi: 10.1016/j.conbuildmat.2015.12.081.

[69] H. He, X. Zhou, Z. Luo, G. Shi, and M. Zhang, "Preparation of iron based chemically bonded phosphate ceramics using copper slag and its utilization on immobilization of Pb2," *Cailiao Daobao/Materials Rev.*, vol. v 30, n 9, p. p 117-121, 2016, doi: 10.11896/j.issn.1005-023X.2016.18.025.

[70] M. Morales, J. Formosa, E. Xuriguera, M. Niub??, M. Segarra, and J. M. Chimenos, "Elastic modulus of a chemically bonded phosphate ceramic formulated with low-grade magnesium

oxide determined by Nanoindentation," *Ceram. Int.*, vol. 41, no. 9, pp. 12137–12146, 2015, doi: 10.1016/j.ceramint.2015.06.031.

[71] J. Formosa, J. M. Chimenos, A. M. Lacasta, and M. Niubó, "Interaction between low-grade magnesium oxide and boric acid in chemically bonded phosphate ceramics formulation," *Ceram. Int.*, vol. 38, no. 3, pp. 2483–2493, Apr. 2012, doi: 10.1016/j.ceramint.2011.11.017.

[72] Z. Lu, D. Hou, H. Ma, T. Fan, and Z. Li, "Effects of graphene oxide on the properties and microstructures of the magnesium potassium phosphate cement paste," *Constr. Build. Mater.*, vol. 119, pp. 107–112, 2016, doi: 10.1016/j.conbuildmat.2016.05.060.

[73] L. Hou, J. H. Li, L. X. Tong, and Q. Zhang, "Effect of Calcined Coal Gangue on the Mechanical Property and Microstructure of Magnesium Phosphate Cement," *Appl. Mech. Mater.*, vol. 174–177, pp. 943–946, 2012, doi: 10.4028/www.scientific.net/AMM.174-177.943.

[74] P. K. Donahue and M. D. Aro, "Durable phosphate-bonded natural fiber composite products," *Constr. Build. Mater.*, vol. 24, no. 2, pp. 215–219, Feb. 2010, doi: 10.1016/j.conbuildmat.2007.05.015.

[75] M. Alshaaer, H. Cuypers, H. Rahier, and J. Wastiels, "Production of monetite-based Inorganic Phosphate Cement (M-IPC) using hydrothermal post curing (HTPC)," *Cem. Concr. Res.*, vol. 41, no. 1, pp. 30–37, Jan. 2011, doi: 10.1016/j.cemconres.2010.09.002.

[76] H. Cuypers, J. Wastiels, P. Van Itterbeeck, E. De Bolster, J. Orlowsky, and M. Raupach, "Durability of glass fibre reinforced composites experimental methods and results," *Compos. Part A Appl. Sci. Manuf.*, vol. 37, no. 2, pp. 207–215, Feb. 2006, doi: 10.1016/j.compositesa.2005.03.027.

[77] H. A. Colorado, C. Hiel, and H. T. Hahn, "Chemically bonded phosphate ceramics

composites reinforced with graphite nanoplatelets," *Compos. Part A Appl. Sci. Manuf.*, vol. 42, no. 4, pp. 376–384, Apr. 2011, doi: 10.1016/j.compositesa.2010.12.007.

[78] F. Qiao, C. K. Chau, and Z. Li, "Property evaluation of magnesium phosphate cement mortar as patch repair material," *Constr. Build. Mater.*, vol. 24, no. 5, pp. 695–700, 2010, doi: 10.1016/j.conbuildmat.2009.10.039.

[79] C. De Roover *et al.*, "Modelling of an IPC-concrete modular pedestrian bridge," *Comput. Struct.*, vol. 80, no. 27–30, pp. 2133–2144, Nov. 2002, doi: 10.1016/S0045-7949(02)00258-4.

[80] A. S. Wagh, D. Singh, and S.-Y. Jeong, "U.S. Pat. No. 5,830,815 Method of waste stabilization via chemically bonded phosphate ceramics," 1998.

[81] H. A. Colorado and D. Singh, "High-sodium waste streams stabilized with inorganic acid–base phosphate ceramics fabricated at room temperature," *Ceram. Int.*, vol. 40, no. 7, pp. 10621–10631, Aug. 2014, doi: 10.1016/j.ceramint.2014.03.045.

[82] H. A. Colorado and D. Singh, "High-sodium waste streams stabilized with inorganic acid-base phosphate ceramics fabricated at room temperature," *Ceram. Int.*, vol. 40, no. 7 PART B, pp. 10621–10631, 2014, doi: 10.1016/j.ceramint.2014.03.045.

[83] G. Sierra, L. A. Palacio, and C. Saldarriaga, "Síntesis y caracterización de un nuevo material tipo fosfato de cobre," *Rev. Fac. Ing. Univ. Antioquia. N. oevista Fac. Ing.*, vol. 27, pp. 104–109, 2002.

[84] M. Nabiyouni, T. Brückner, H. Zhou, U. Gbureck, and S. B. Bhaduri, "Magnesium-based bioceramics in orthopedic applications," *Acta Biomater.*, vol. 66, pp. 23–43, 2018, doi: 10.1016/j.actbio.2017.11.033.

[85] A. S. Wagh, "An overview of chemical processes to manufacture red mud construction

products," *Travaux*, vol. 36, no. 40, pp. 235–242, 2011.

[86] H. A. Colorado, Z. Wang, and J.-M. Yang, "Inorganic phosphate cement fabricated with wollastonite, barium titanate, and phosphoric acid," *Cem. Concr. Compos.*, vol. 62, pp. 13–21, Sep. 2015, doi: 10.1016/j.cemconcomp.2015.04.014.

[87] J. . Agudelo, S. J.H, and J. . Parra, "Caracterización química y mineralógica de escorias de acería," *Rev. Fac. Ing. Univ. Antioquia. N. o*, vol. 21, pp. 77–82, 2000.

[88] B. H. Toby, "R factors in Rietveld analysis: How good is good enough?," *Powder Diffr.*, vol. 21, no. 01, pp. 67–70, 2006, doi: 10.1154/1.2179804.

[89] A. S. Wagh and S. Y. Jeong, "Chemically Bonded Phosphate Ceramics: I, A Dissolution Model of Formation," *J. Am. Ceram. Soc.*, vol. 86, no. 11, pp. 1838–1844, Nov. 2003, doi: 10.1111/j.1151-2916.2003.tb03569.x.

[90] T. Bai, Z. G. Song, Y. G. Wu, X. Di Hu, and H. Bai, "Influence of steel slag on the mechanical properties and curing time of metakaolin geopolymer," *Ceram. Int.*, no. April, pp. 0–1, 2018, doi: 10.1016/j.ceramint.2018.05.243.

[91] J. Setién, D. Hernández, and J. J. González, "Characterization of ladle furnace basic slag for use as a construction material," *Constr. Build. Mater.*, vol. 23, no. 5, pp. 1788–1794, 2009, doi: 10.1016/j.conbuildmat.2008.10.003.

[92] A. Sáez-De-Guinoa Vilaplana *et al.*, "Utilization of Ladle Furnace slag from a steelwork for laboratory scale production of Portland cement," *Constr. Build. Mater.*, vol. 94, pp. 837–843, 2015, doi: 10.1016/j.conbuildmat.2015.07.075.

[93] J. Madias, "The control of phosphorus in the mining and steelmaking process," *Acero Latinoam.*, pp. 32–41, 2013.

[94] S. Wang, X. Peng, L. Tang, L. Zeng, and C. Lan, "Influence of inorganic admixtures on the

11 Å-tobermorite formation prepared from steel slags: XRD and FTIR analysis," *Constr. Build. Mater.*, vol. 60, pp. 42–47, 2014, doi: 10.1016/j.conbuildmat.2014.03.002.

[95] J. Li, Q. Yu, J. Wei, and T. Zhang, "Structural characteristics and hydration kinetics of modified steel slag," *Cem. Concr. Res.*, vol. 41, no. 3, pp. 324–329, 2011, doi: 10.1016/j.cemconres.2010.11.018.

[96] P. Delvasto, B. Ibanez Aldao, and D. Sandoval Ravotti, "Characterization of Electric Arc Furnace Steel Dust Generated in Venezuela and Preliminary Assessment of Its Leachability With Diluted Organic Acids," *Dyna-Colombia*, vol. 78, no. 169, pp. 221–229, 2011.

[97] N. V Chukanov, *Infrared spectra of mineral species*. Dordrecht: Springer Netherlands, 2014.

[98] A. K. Duarte and P. R. G. Brandao, "Ceramic encapsulation of refractory and mineral residues based on potassium and magnesium phosphate," *Miner. Eng.*, vol. 21, no. 4, pp. 302–309, 2008, doi: 10.1016/j.mineng.2007.10.010.

[99] R. L. Frost, "An infrared and Raman spectroscopic study of natural zinc phosphates," *Spectrochim. Acta - Part A Mol. Biomol. Spectrosc.*, vol. 60, no. 7, pp. 1439–1445, 2004, doi: 10.1016/j.saa.2003.08.009.

[100] M. P. Hofmann, A. M. Young, U. Gbureck, S. N. Nazhat, and J. E. Barralet, "FTIR-monitoring of a fast setting brushite bone cement: effect of intermediate phases," *J. Mater. Chem.*, vol. 16, no. 31, p. 3199, 2006, doi: 10.1039/b603554j.

[101] A. Mladenovič, B. Mirtič, A. Meden, and V. Zalar Serjun, "Calcium aluminate rich secondary stainless steel slag as a supplementary cementitious material," *Constr. Build. Mater.*, vol. 116, pp. 216–225, 2016, doi: 10.1016/j.conbuildmat.2016.04.141.

[102] S. Gunasekaran, G. Anbalagan, and S. Pandi, "Raman and infrared spectra of carbonates of

calcite structure," *J. Raman Spectrosc.*, vol. 37, no. 9, pp. 892–899, 2006, doi: 10.1002/jrs.1518.

[103] K. Sriram, P. Uma Maheswari, K. M. Meera Sheriffa Begum, G. Arthanareeswaran, M. Gover Antoniraj, and K. Ruckmani, "Curcumin drug delivery by vanillin-chitosan coated with calcium ferrite hybrid nanoparticles as carrier," *Eur. J. Pharm. Sci.*, vol. 116, no. February, pp. 48–60, 2018, doi: 10.1016/j.ejps.2018.01.023.

[104] S. A. Speakman, "Precision and Accuracy - Agreement Indices in HSP (An Introduction to Rietveld Refinement using PANalytical X'Pert HighScore Plus v2.2d)," *Massachusets Inst. Technol.*, p. 17, 2010.

[105] L. de A. Gobbo, "Aplicação da difração de raios-X e método de Rietveld no estudo de Cimento Portland," Universidade de São Paulo, São Paulo, 2009.

[106] N. Menad, N. Kanari, and M. Save, "Recovery of high grade iron compounds from LD slag by enhanced magnetic separation techniques," *Int. J. Miner. Process.*, vol. 126, pp. 1–9, 2014, doi: 10.1016/j.minpro.2013.11.001.

[107] S. Chand, B. Paul, and M. Kumar, "A comparative study of physicochemical and mineralogical properties of ld slag from some selected steel plants in India," *J. Environ. Sci. Technol.*, vol. 9, no. 1, pp. 75–87, 2016, doi: 10.3923/jest.2016.75.87.

[108] D. Mombelli *et al.*, "Analisys of electric arc furnace slag," *Steel Res. Int.*, vol. 83, no. 11, pp. 1012–1019, 2012, doi: 10.1002/srin.201100259.

[109] J. M. Tinjum and H. Xu, "Quantification of Mineralogical and Amorphous Species in," no. March 2016, 2012.

[110] H. A. Colorado, H. Clem, T. Hahn, and J.-M. Yang, "Wollastonite-Based Chemically Bonded Phosphate Ceramic Composites," in *Trends in Helicobacter pylori Infection*, vol. i,

no. tourism, InTech, 2014, p. 13.

[111] M. Le Rouzic, T. Chaussadent, L. Stefan, and M. Saillio, “On the influence of Mg/P ratio on the properties and durability of magnesium potassium phosphate cement pastes,” *Cem. Concr. Res.*, vol. 96, pp. 27–41, 2017, doi: 10.1016/j.cemconres.2017.02.033.

[112] M. Biesemans *et al.*, “Thermal hardening and structure of a phosphorus containing cementitious model material,” *J. Therm. Anal. Calorim.*, vol. 88, no. 3, pp. 723–729, 2007, doi: 10.1007/s10973-006-8225-7.

[113] L. Jia, F. Zhao, J. Guo, and K. Yao, “Magnesium Phosphate Cement Mixed with Ferroaluminate Cement,” 2019, doi: 10.3390/ma12162561.

[114] L. Chong, J. Yang, and C. Shi, “Effect of curing regime on water resistance of magnesium – potassium phosphate cement,” *Constr. Build. Mater.*, vol. 151, pp. 43–51, 2017, doi: 10.1016/j.conbuildmat.2017.06.056.

[115] D. Deng, “The mechanism for soluble phosphates to improve the water resistance of magnesium oxychloride cement,” *Cem. Concr. Res.*, vol. 33, no. 9, pp. 1311–1317, 2003, doi: 10.1016/S0008-8846(03)00043-7.

[116] Q. Wang, P. Yan, J. Yang, and B. Zhang, “Influence of steel slag on mechanical properties and durability of concrete,” *Constr. Build. Mater.*, vol. 47, pp. 1414–1420, 2013, doi: 10.1016/j.conbuildmat.2013.06.044.

[117] N. Palankar, A. U. Ravi Shankar, and B. M. Mithun, “Durability studies on eco-friendly concrete mixes incorporating steel slag as coarse aggregates,” *J. Clean. Prod.*, vol. 129, pp. 437–448, 2016, doi: 10.1016/j.jclepro.2016.04.033.

[118] H. Qasrawi, “The use of steel slag aggregate to enhance the mechanical properties of recycled aggregate concrete and retain the environment,” *Constr. Build. Mater.*, vol. 54, pp.

298–304, 2014, doi: 10.1016/j.conbuildmat.2013.12.063.

[119] D. Proctor *et al.*, “Physical and Chemical Characteristics of Blast Furnace, Basic Oxygen Funace and Electric Arc Furnace Steel Industry Slags,” *Environ. Sci. Technol.*, vol. 34, no. 8, pp. 1576–1582, 2000, doi: https://doi.org/10.1021/es9906002.

[120] H. Shen and E. Forssberg, “An overview of recovery of metals from slags,” *Waste Manag.*, vol. 23, no. 10, pp. 933–949, 2003, doi: 10.1016/S0956-053X(02)00164-2.

[121] T. Sugama, M. Allan, and J. M. Hill, “Calcium Phosphate Cements Prepared by Acid-Base Reaction,” *J. Am. Ceram. Soc.*, vol. 75, no. 8, pp. 2076–2087, Aug. 1992, doi: 10.1111/j.1151-2916.1992.tb04468.x.

[122] H. Lahalle *et al.*, “Investigation of magnesium phosphate cement hydration in diluted suspension and its retardation by boric acid,” *Cem. Concr. Res.*, vol. 87, pp. 77–86, 2016, doi: 10.1016/j.cemconres.2016.04.010.

[123] S. Manso, M. A. Calvo, A. Aguado, and N. De Belie, “Sustainable cements in construction: magnesium phosphate cements to stimulate colonization by photosynthetic organisms of building materials,” *J. Sustain. Cem. Mater.*, vol. 6, no. 2, pp. 139–148, 2017, doi: 10.1080/21650373.2016.1201018.

[124] C. A. Cárdenas-Balaguera and M. A. Gómez-Botero, “Engineering applications of chemically-bonded phosphate ceramics,” *Ing. e Investig.*, vol. 39, no. 3, pp. 10–19, 2019, doi: 10.15446/ing.investig.v39n3.81424.

[125] D. Montgomery, *Diseño y análisis de experimentos*, Segunda Ed. Mexico D.F., 2004.

[126] C. A. Cárdenas and M. A. Gómez, “Characterization of steel slag for the production of chemically bonded phosphate ceramics (CBPC),” *Constr. Build. Mater.*, vol. 241, p. 118138, Apr. 2020, doi: 10.1016/j.conbuildmat.2020.118138.

[127] D. A. Hall, R. Stevens, and B. El Jazairi, “Effect of water content on the structure and mechanical properties of magnesia-phosphate cement mortar,” *J. Am. Ceram. Soc.*, vol. 81, no. 6, pp. 1550–1556, 1998, doi: 10.1111/j.1151-2916.1998.tb02515.x.

[128] Q. Yang and X. Wu, “Factors influencing properties of phosphate cement-based binder for rapid repair of concrete,” *Cem. Concr. Res.*, vol. 29, no. 3, pp. 389–396, 1999, doi: 10.1016/S0008-8846(98)00230-0.

[129] I. A. Karampas and C. G. Kontoyannis, “Characterization of calcium phosphates mixtures,” *Vib. Spectrosc.*, vol. 64, pp. 126–133, 2013, doi: 10.1016/j.vibspec.2012.11.003.

[130] B. Boonchom, “Parallelogram-like microparticles of calcium dihydrogen phosphate monohydrate (Ca(H2PO4)2·H2O) obtained by a rapid precipitation route in aqueous and acetone media,” *J. Alloys Compd.*, vol. 482, no. 1–2, pp. 199–202, Aug. 2009, doi: 10.1016/j.jallcom.2009.03.157.

[131] C. Combes and C. Rey, “Amorphous calcium phosphates: Synthesis, properties and uses in biomaterials,” *Acta Biomater.*, vol. 6, no. 9, pp. 3362–3378, Sep. 2010, doi: 10.1016/j.actbio.2010.02.017.

[132] Y. Kojima, K. Sakama, T. Toyama, T. Yasue, and Y. Arai, “Dehydration of water molecule in amorphous calcium phosphate,” *Phosphorus Res. Bull.*, vol. 4, pp. 47–52, 1994, doi: 10.3363/prb1992.4.0_47.

[133] G. Socrates, *Characteristic Group Frequencies*, 3rd Revise., vol. 3, no. 1. London U.K., 2011.

[134] P. M. Hallam, M. Gómez-Mingot, D. K. Kampouris, and C. E. Banks, “Facile synthetic fabrication of iron oxide particles and novel hydrogen superoxide supercapacitors,” *RSC Adv.*, vol. 2, no. 16, pp. 6672–6679, 2012, doi: 10.1039/c2ra01139e.

[135] N. Li, G. W. Huang, X. J. Shen, H. M. Xiao, and S. Y. Fu, “Controllable fabrication and magnetic-field assisted alignment of Fe3O4-coated Ag nanowires via a facile co-precipitation method,” *J. Mater. Chem. C*, vol. 1, no. 32, pp. 4879–4884, 2013, doi: 10.1039/c3tc30270a.

[136] H. Lee *et al.*, “Liquid phase plasma synthesis of iron oxide/carbon composite as dielectric material for capacitor,” *J. Nanomater.*, vol. 2014, no. June, 2014, doi: 10.1155/2014/132032.

[137] B. Demri and D. Muster, “XPS study of some calcium compounds,” *J. Mater. Process. Tech.*, vol. 55, no. 3–4, pp. 311–314, 1995, doi: 10.1016/0924-0136(95)02023-3.

[138] C. C. Chusuei, “Calcium phosphate phase identification using XPS and time-of-flight cluster SIMS,” *Anal. Chem.*, vol. 71, no. 1, pp. 149–153, 1999, doi: 10.1021/ac9806963.

[139] K. J. A. Raj, R. Shanmugam, R. Mahalakshmi, and B. Viswanathan, “XPS and IR spectral studies on the structure of phosphate and sulphate modified titania - A combined DFT and experimental study,” *Indian J. Chem. - Sect. A Inorganic, Phys. Theor. Anal. Chem.*, vol. 49, no. 1, pp. 9–17, 2010.

[140] P. M. A. Sherwood, “Introduction to Studies of Phosphorus-Oxygen Compounds by XPS,” *Surf. Sci. Spectra*, vol. 9, no. 1, pp. 62–66, 2004, doi: 10.1116/11.20030101.

[141] T. Finch and J. H. Sharp, “Chemical reactions between magnesia and aluminium orthophosphate to form magnesia-phosphate cements,” *J. Mater. Sci.*, vol. 24, no. 12, pp. 4379–4386, Dec. 1989, doi: 10.1007/BF00544516.

[142] L. Chong, C. Shi, J. Yang, and H. Jia, “Effect of limestone powder on the water stability of magnesium phosphate cement-based materials,” *Constr. Build. Mater.*, vol. 148, pp. 590–598, 2017, doi: 10.1016/j.conbuildmat.2017.04.207.

[143] Y. Liu, B. Chen, Z. Qin, D. Pen, and M. Aminul Haque, “Experimental research on properties and microstructures of magnesium-iron phosphate cement,” *Constr. Build. Mater.*, vol. 257, p. 119570, Oct. 2020, doi: 10.1016/j.conbuildmat.2020.119570.

[144] A. M. Rashad, “Phosphogypsum as a construction material,” *J. Clean. Prod.*, vol. 166, pp. 732–743, 2017, doi: 10.1016/j.jclepro.2017.08.049.

[145] N. M. Piatak, M. B. Parsons, and R. R. Seal, *Characteristics and environmental aspects of slag: A review*, vol. 57. Elsevier Ltd, 2015.

[146] Y. Jiang, T. C. Ling, C. Shi, and S. Y. Pan, “Characteristics of steel slags and their use in cement and concrete—A review,” *Resour. Conserv. Recycl.*, vol. 136, no. April, pp. 187–197, 2018, doi: 10.1016/j.resconrec.2018.04.023.

[147] Sanchez A. Hector Mauricio, “Estado del arte sobre las Escorias Negras de Horno de Arco Electrico y sus aplicaciones en pavimentos,” 2016.

[148] F. Sevim, H. Saraç, M. M. Kocakerim, and A. Yartaşı, “Dissolution Kinetics of Phosphate Ore in H 2 SO 4 Solutions,” *Ind. Eng. Chem. Res.*, vol. 42, no. 10, pp. 2052–2057, May 2003, doi: 10.1021/ie020168o.

[149] A. Mgaidi, F. Ben Brahim, D. Oulahna, A. Nzihou, and M. El Maaoui, “Chemical and Structural Changes of Raw Phosphate during Heat Treatment,” *High Temp. Mater. Process.*, vol. 23, no. 3, pp. 185–194, 2004, doi: 10.1515/HTMP.2004.23.3.185.

[150] R. Ebrahimi-Kahrizsangi, B. Nasiri-Tabrizi, and A. Chami, “Characterization of single-crystal fluorapatite nanoparticles synthesized via mechanochemical method,” *Particuology*, vol. 9, no. 5, pp. 537–544, 2011, doi: 10.1016/j.partic.2011.07.001.

[151] H. Bachouâ, M. Othmani, Y. Coppel, N. Fatteh, M. Debbabi, and B. Badraoui, “Structural and thermal investigations of a Tunisian natural phosphate rock,” *J. Mater. Environ. Sci.*,

vol. 5, no. 4, pp. 1152–1159, 2014.

[152] A. Paz, D. Guadarrama, M. López, J. E. González, N. Brizuela, and J. Aragón, "A comparative study of hydroxyapatite nanoparticles synthesized by different routes," *Quim. Nova*, vol. 35, no. 9, pp. 1724–1727, 2012, doi: 10.1590/S0100-40422012000900004.

[153] S. Veerasingam and R. Venkatachalapathy, "Estimation of carbonate concentration and characterization of marine sediments by Fourier Transform Infrared Spectroscopy," *Infrared Phys. Technol.*, vol. 66, pp. 136–140, 2014, doi: 10.1016/j.infrared.2014.06.005.

[154] I. Birken, M. Bertucci, J. Chappelin, and E. Jorda, "Quantification of Impurities, Including Carbonates Speciation for Phosphates Beneficiation by Flotation," *Procedia Eng.*, vol. 138, no. 0, pp. 72–84, 2016, doi: 10.1016/j.proeng.2016.02.059.

[155] P. V. Campos, A. R. L. Albuquerque, R. S. Angélica, and S. P. A. Paz, "FTIR spectral signatures of amazon inorganic phosphates: Igneous, weathering, and biogenetic origin," *Spectrochim. Acta - Part A Mol. Biomol. Spectrosc.*, vol. 251, p. 119476, 2021, doi: 10.1016/j.saa.2021.119476.

[156] B. J. Saikia and G. Parthasarathy, "Fourier Transform Infrared Spectroscopic Characterization of Kaolinite from Assam and Meghalaya, Northeastern India," *J. Mod. Phys.*, vol. 01, no. 04, pp. 206–210, 2010, doi: 10.4236/jmp.2010.14031.

[157] B. J. Saikia, G. Parthasarathy, and N. C. Sarmah, "Fourier transform infrared spectroscopic estimation of crystallinity in SiO2 based rocks," *Bull. Mater. Sci.*, vol. 31, no. 5, pp. 775–779, Oct. 2008, doi: 10.1007/s12034-008-0123-0.

[158] H. Galai and F. Sliman, "Mineral characterization of the Oum El Khacheb phosphorites (Gafsa-Metlaoui basin; S Tunisia)," *Arab. J. Chem.*, vol. 12, no. 7, pp. 1607–1614, 2019, doi: 10.1016/j.arabjc.2014.10.007.

[159] H. Majdoubi *et al.*, “Thermal, mechanical and microstructural properties of acidic geopolymer based on moroccan kaolinitic clay,” *J. Build. Eng.*, vol. 35, no. December 2020, p. 102078, 2021, doi: 10.1016/j.jobe.2020.102078.

[160] A.-Z. M. Abouzeid, “Physical and thermal treatment of phosphate ores — An overview,” *Int. J. Miner. Process.*, vol. 85, no. 4, pp. 59–84, Jan. 2008, doi: 10.1016/j.minpro.2007.09.001.

[161] H. Sis and S. Chander, “Reagents used in the flotation of phosphate ores: A critical review,” *Miner. Eng.*, vol. 16, no. 7, pp. 577–585, 2003, doi: 10.1016/S0892-6875(03)00131-6.

[162] Kawatra Komar and J. . Carlson, *Beneficiation of Phosphate Ore*, First Edit. Englewood, Colorado, USA: Society for Mining, Metallurgy & Exploration (SME), 2014.

[163] M. O. Bustamante-rúa, A. J. Daza-aragón, P. Bustamante-baena, and J. D. Osorio-, “Recovery evaluation of P 2 O 5 through three models of froth flotation of phosphoric rock • Evaluación de la recuperación de P 2 O 5 a través de tres modelos de flotación espumante de roca fosfórica,” no. February, pp. 1–7, 2019.

[164] A. C. Silva, E. Maria, S. Silva, and T. C. Silva, “Apatite Froth Flotation Using Pequi ’ s Yellow Pulp Oil as Collector,” no. 343, pp. 1–7, 2015.

[165] W. Sadeddin and S. I. Abu-Eishah, “Minimization of free calcium carbonate in hard and medium-hard phosphate rocks using dilute acetic acid solution,” *Int. J. Miner. Process.*, vol. 30, no. 1–2, pp. 113–125, 1990, doi: 10.1016/0301-7516(90)90069-B.

[166] M. Gharabaghi, M. Irannajad, and M. Noaparast, “A review of the beneficiation of calcareous phosphate ores using organic acid leaching,” *Hydrometallurgy*, vol. 103, no. 1–4, pp. 96–107, 2010, doi: 10.1016/j.hydromet.2010.03.002.

[167] J. Blom, H. Rahier, and J. Wastiels, “Effect of curing conditions on the dimensional and

thermal stability of calcium phosphate cement for elevated temperature applications," *Cem. Concr. Res.*, vol. 66, pp. 102–109, 2014, doi: 10.1016/j.cemconres.2014.07.019.

[168] V. Tydlitát, A. Trník, L. Scheinherrová, R. Podoba, and R. Černý, "Application of isothermal calorimetry and thermal analysis for the investigation of calcined gypsum-lime-metakaolin-water system," *J. Therm. Anal. Calorim.*, vol. 122, no. 1, pp. 115–122, 2015, doi: 10.1007/s10973-015-4727-5.

[169] B. A. Clark and P. W. Brown, "Formation of ettringite from monosubstituted calcium sulfoaluminate hydrate and gypsum," *J. Am. Ceram. Soc.*, vol. 82, no. 10, pp. 2900–2905, 1999, doi: 10.1111/j.1151-2916.1999.tb02174.x.

[170] R. X. Magallanes-Rivera and J. I. Escalante-García, "Anhydrite/hemihydrate-blast furnace slag cementitious composites: Strength development and reactivity," *Constr. Build. Mater.*, vol. 65, pp. 20–28, 2014, doi: 10.1016/j.conbuildmat.2014.04.056.

[171] N. Flores, M. Barbero, and R. Bustamante, "Filler de grafito reciclado de EDM en pastas de yeso = EDM recycled graphite filler in gypsum pastes," *An. Edif.*, vol. 3, no. 2, p. 27, 2017, doi: 10.20868/ade.2017.3569.

[172] World Steel Association, "Steel Statistical Yearbook 2019 Concise version," *World Steel Assoc.*, pp. 1–6, 2019.

[173] N. C. C. Lobato, E. A. Villegas, and M. B. Mansur, "Management of solid wastes from steelmaking and galvanizing processes: A brief review," *Resour. Conserv. Recycl.*, vol. 102, pp. 49–57, 2015, doi: 10.1016/j.resconrec.2015.05.025.

[174] J. Guo, Y. Bao, and M. Wang, "Steel slag in China: Treatment, recycling, and management," *Waste Manag.*, vol. 78, pp. 318–330, 2018, doi: 10.1016/j.wasman.2018.04.045.

[175] H. Yi, G. Xu, H. Cheng, J. Wang, Y. Wan, and H. Chen, “An Overview of Utilization of Steel Slag,” *Procedia Environ. Sci.*, vol. 16, pp. 791–801, 2012, doi: 10.1016/j.proenv.2012.10.108.

[176] J. Liu, B. Yu, and Q. Wang, “Application of steel slag in cement treated aggregate base course,” *J. Clean. Prod.*, vol. 269, p. 121733, 2020, doi: 10.1016/j.jclepro.2020.121733.

[177] Q. Wang, P. Yan, and J. Feng, “A discussion on improving hydration activity of steel slag by altering its mineral compositions,” *J. Hazard. Mater.*, vol. 186, no. 2–3, pp. 1070–1075, 2011, doi: 10.1016/j.jhazmat.2010.11.109.

[178] M. S. Amin, S. M. A. El-Gamal, S. A. Abo-El-Enein, F. I. El-Hosiny, and M. Ramadan, “Physico-chemical characteristics of blended cement pastes containing electric arc furnace slag with and without silica fume,” *HBRC J.*, vol. 11, no. 3, pp. 321–327, 2015, doi: 10.1016/j.hbrcj.2014.07.002.

[179] T. A. Branca *et al.*, “Investigation of (BOF) Converter slag use for agriculture in europe,” *Metall. Res. Technol.*, vol. 111, no. 3, pp. 155–167, 2014, doi: 10.1051/metal/2014022.

[180] T. A. Branca and V. Colla, “Possible Uses of Steelmaking Slag in Agriculture : An Overview,” *Mater. Recycl. - Trends Perspect.*, pp. 336–356, 2012.

[181] V. Z. Serjun, A. Mladenovič, B. Mirtič, A. Meden, J. Ščančar, and R. Milačič, “Recycling of ladle slag in cement composites: Environmental impacts,” *Waste Manag.*, vol. 43, pp. 376–385, 2015, doi: 10.1016/j.wasman.2015.05.006.

[182] J. T. San-José, I. Vegas, I. Arribas, and I. Marcos, “The performance of steel-making slag concretes in the hardened state,” *Mater. Des.*, vol. 60, pp. 612–619, 2014, doi: 10.1016/j.matdes.2014.04.030.

[183] P. E. Tsakiridis, G. D. Papadimitriou, S. Tsivilis, and C. Koroneos, “Utilization of steel slag

for Portland cement clinker production," *J. Hazard. Mater.*, vol. 152, no. 2, pp. 805–811, 2008, doi: 10.1016/j.jhazmat.2007.07.093.

[184] A. Rastovčan-Mioč, T. Sofilić, and B. Mioč, "Application of Electric Arc Furnace Slag," *Proc. Matrib 2009*, no. January, pp. 436–444, 2009.

[185] R. I. Iacobescu, D. Koumpouri, Y. Pontikes, R. Saban, and G. N. Angelopoulos, "Valorisation of electric arc furnace steel slag as raw material for low energy belite cements," *J. Hazard. Mater.*, vol. 196, pp. 287–294, 2011, doi: 10.1016/j.jhazmat.2011.09.024.

[186] W. Eubank, "Calcination Studies of Magnesium Oxides," *J. Am. Ceram. Soc.*, vol. 34, no. 8, pp. 225–229, 1951, doi: 10.1111/j.1151-2916.1951.tb11644.x.

[187] L. Chow, "Calcium phosphate cements: chemistry, properties, and applications," *MRS Proc.*, vol. 599, pp. 27–37, 1999.

[188] K. Oien, "SINTEF Report Survey." pp. 1–12, 2005.

[189] S. J. S. Flora and V. Pachauri, "Chelation in metal intoxication," *Int. J. Environ. Res. Public Health*, vol. 7, no. 7, pp. 2745–2788, 2010, doi: 10.3390/ijerph7072745.

[190] C.-C. Li, X.-W. Peng, J.-T. Lee, and F.-M. Wang, "Using Poly(4-Styrene Sulfonic Acid) to Improve the Dispersion Homogeneity of Aqueous-Processed LiFePO[sub 4] Cathodes," *J. Electrochem. Soc.*, vol. 157, no. 4, p. A517, 2010, doi: 10.1149/1.3308595.

[191] G. Kocak, C. Tuncer, and V. Bütün, "PH-Responsive polymers," *Polym. Chem.*, vol. 8, no. 1, pp. 144–176, 2017, doi: 10.1039/c6py01872f.

[192] A. F. Gualtieri, V. Riva, A. Bresciani, S. Maretti, M. Tamburini, and A. Viani, "Accuracy in quantitative phase analysis of mixtures with large amorphous contents. the case of stoneware ceramics and bricks," *J. Appl. Crystallogr.*, vol. 47, no. 3, pp. 835–846, 2014,

doi: 10.1107/S160057671400627X.

[193] A. G. De la Torre and M. A. G. Aranda, “Accuracy in Rietveld quantitative phase analysis of Portland cements,” *J. Appl. Crystallogr.*, vol. 36, no. 5, pp. 1169–1176, 2003, doi: 10.1107/S002188980301375X.

[194] A. G. De La Torre, S. Bruque, and M. A. G. Aranda, “Applied Crystallography Rietveld quantitative amorphous content analysis,” *J. Appl. Cryst*, vol. 34, pp. 196–202, 2001.

[195] J. Ibáñez, O. Font, N. Moreno, J. J. Elvira, S. Alvarez, and X. Querol, “Quantitative Rietveld analysis of the crystalline and amorphous phases in coal fly ashes,” *Fuel*, vol. 105, pp. 314–317, 2013, doi: 10.1016/j.fuel.2012.06.090.

[196] D. A. Hall, R. Stevens, and B. El-Jazairi, “The effect of retarders on the microstructure and mechanical properties of magnesia-phosphate cement mortar,” *Cem. Concr. Res.*, vol. 31, no. 3, pp. 455–465, 2001, doi: 10.1016/S0008-8846(00)00501-9.

[197] M. A. Blesa, A. J. G. Maroto, and A. E. Regazzoni, “Boric acid adsorption on magnetite and zirconium dioxide,” *J. Colloid Interface Sci.*, vol. 99, no. 1, pp. 32–40, 1984, doi: 10.1016/0021-9797(84)90082-1.

[198] H. D. Lutz and H. Haeuseler, “Infrared and Raman spectroscopy in inorganic solids research,” *J. Mol. Struct.*, vol. 511–512, pp. 69–75, Nov. 1999, doi: 10.1016/S0022-2860(98)00630-9.

[199] K. Sotiriadis, P. Mácová, A. S. Mazur, P. M. Tolstoy, and A. Viani, “A solid state NMR and in-situ infrared spectroscopy study on the setting reaction of magnesium sodium phosphate cement,” *J. Non. Cryst. Solids*, vol. 498, no. May, pp. 49–59, 2018, doi: 10.1016/j.jnoncrysol.2018.06.006.

[200] A. K. Lynn and W. Bonfield, “A novel method for the simultaneous, titrant-free control of

pH and calcium phosphate mass yield," *Acc. Chem. Res.*, vol. 38, no. 3, pp. 202–207, 2005, doi: 10.1021/ar040234d.

[201] J. Baril, J.-J. Max, and C. Chapados, "Titrage infrarouge de l'acide phosphorique," *Can. J. Chem.*, vol. 78, no. 4, pp. 490–507, Apr. 2000, doi: 10.1139/v00-038.

[202] C. Sun, D. Xu, and D. Xue, "In situ FTIR-ATR observation of structural dynamics of H2PO 4 in precrystallisation solution," *Mater. Res. Innov.*, vol. 18, no. 5, pp. 370–375, 2014, doi: 10.1179/1433075X13Y.0000000155.

[203] P. Yu, R. J. Kirkpatrick, B. Poe, P. F. McMillan, and X. Cong, "Structure of Calcium Silicate Hydrate (C-S-H): Near-, Mid-, and Far-Infrared Spectroscopy," *J. Am. Ceram. Soc.*, vol. 82, no. 3, pp. 742–748, Dec. 2004, doi: 10.1111/j.1151-2916.1999.tb01826.x.

[204] W. Kurdowski, *Cement and Concrete Chemistry*. New York London: Spriger, 2014.

[205] H. F. W. Taylor, "Proposed Structure for Calcium Silicate Hydrate Gel," *J. Am. Ceram. Soc.*, vol. 69, no. 6, pp. 464–467, 1986, doi: 10.1111/j.1151-2916.1986.tb07446.x.

[206] L. Ševula, J. Madej, J. Kozánková, and J. Madejová, "Hydration products at the blastfurnace slag aggregate - cement paste interface," *Cem. Concr. Res.*, vol. 24, no. 3, pp. 413–423, 1994, doi: 10.1016/0008-8846(94)90128-7.

[207] Z. Qin, S. Zhou, C. Ma, G. Long, Y. Xie, and B. Chen, "Roles of metakaolin in magnesium phosphate cement: Effect of the replacement ratio of magnesia by metakaolin with different particle sizes," *Constr. Build. Mater.*, vol. 227, p. 116675, 2019, doi: 10.1016/j.conbuildmat.2019.116675.

[208] B. Xu, B. Lothenbach, and F. Winnefeld, "Influence of wollastonite on hydration and properties of magnesium potassium phosphate cements," *Cem. Concr. Res.*, vol. 131, no. December 2019, p. 106012, 2020, doi: 10.1016/j.cemconres.2020.106012.

[209] A. V. Girão, G. Caputo, and M. C. Ferro, “Application of Scanning Electron Microscopy–Energy Dispersive X-Ray Spectroscopy (SEM-EDS),” *Compr. Anal. Chem.*, vol. 75, pp. 153–168, 2017, doi: 10.1016/bs.coac.2016.10.002.

[210] F. Puertas, M. Palacios, H. Manzano, J. S. Dolado, A. Rico, and J. Rodríguez, “A model for the C-A-S-H gel formed in alkali-activated slag cements,” *J. Eur. Ceram. Soc.*, vol. 31, no. 12, pp. 2043–2056, 2011, doi: 10.1016/j.jeurceramsoc.2011.04.036.

[211] ASTM, “ASTM C 270-07 Standard Specification for Mortar for Unit Masonry,” *United States Am. Soc. Test. Mater.*, pp. 2–13, 2007, doi: 10.1520/C0270-19AE01.2.

[212] ASTM C62, “Standard Specification for Building Brick,” *Am. Soc. Test. Mater.*, no. November 2001, pp. 2–7, 2017, doi: 10.1520/C0062-17.2.

[213] H. Ma, B. Xu, J. Liu, H. Pei, and Z. Li, “Effects of water content, magnesia-to-phosphate molar ratio and age on pore structure, strength and permeability of magnesium potassium phosphate cement paste,” *Mater. Des.*, vol. 64, pp. 497–502, 2014, doi: 10.1016/j.matdes.2014.07.073.

[214] NEN 7345, “Leaching characteristics of solid earthy and stony building and waste materials. Leaching tests. Dermination of the leaching of inorganic components from building and monolithic waste materials with the diffusion tests.,” Delft, Netherlands, 1995.

[215] M. A. I. Juel, A. Mizan, and T. Ahmed, “Sustainable use of tannery sludge in brick manufacturing in Bangladesh,” *Waste Manag.*, vol. 60, no. October, pp. 259–269, 2017, doi: 10.1016/j.wasman.2016.12.041.

[216] C. Leiva *et al.*, “Use of FGD gypsum in fire resistant panels,” *Waste Manag.*, vol. 30, no. 6, pp. 1123–1129, 2010, doi: 10.1016/j.wasman.2010.01.028.

[217] Soil Quality Decree, *469 Decree of 22 November 2007 containing rules with respect to the*

quality of soil (Soil Quality Decree), vol. 7, no. 3. Netherland, 2007, pp. 213–221.

[218] R. T. Eikelboom, E. Ruwiel, and J. J. J. M. Goumans, "The building materials decree: an example of a dutch regulation based on the potential impact of materials on the environment," *Waste Manag. Ser.*, vol. 1, no. C, pp. 963–974, 2000, doi: 10.1016/S0713-2743(00)80104-X.

[219] G. Zhang, G. Li, and T. He, "Effects of sulphoaluminate cement on the strength and water stability of magnesium potassium phosphate cement," *Constr. Build. Mater.*, vol. 132, pp. 335–342, 2017, doi: 10.1016/j.conbuildmat.2016.12.011.

[220] L. Chong, J. Yang, and C. Shi, "Effect of curing regime on water resistance of magnesium–potassium phosphate cement," *Constr. Build. Mater.*, vol. 151, pp. 43–51, 2017, doi: 10.1016/j.conbuildmat.2017.06.056.

[221] S. H. Yin, Y. F. Yang, T. S. Zhang, G. F. Guo, and F. Yu, "Effect of carbonic acid water on the degradation of Portland cement paste: Corrosion process and kinetics," *Constr. Build. Mater.*, vol. 91, pp. 39–46, 2015, doi: 10.1016/j.conbuildmat.2015.05.046.

[222] F. Engström, D. Adolfsson, C. Samuelsson, Å. Sandström, and B. Björkman, "A study of the solubility of pure slag minerals," *Miner. Eng.*, vol. 41, pp. 46–52, 2013, doi: 10.1016/j.mineng.2012.10.004.

[223] Q. Wang, C. Yu, J. Yang, L. Chong, X. Xu, and Q. Wu, "Influence of nickel slag powders on properties of magnesium potassium phosphate cement paste," *Constr. Build. Mater.*, vol. 205, pp. 668–678, 2019, doi: 10.1016/j.conbuildmat.2019.02.014.

[224] Y. Liu, Z. Qin, and B. Chen, "Experimental research on magnesium phosphate cements modified by red mud," *Constr. Build. Mater.*, vol. 231, p. 117131, 2020, doi: 10.1016/j.conbuildmat.2019.117131.

[225] Y. Liu and B. Chen, “Research on the preparation and properties of a novel grouting material based on magnesium phosphate cement,” *Constr. Build. Mater.*, vol. 214, pp. 516–526, 2019, doi: 10.1016/j.conbuildmat.2019.04.158.

[226] Q. Wang and P. Yan, “Hydration properties of basic oxygen furnace steel slag,” *Constr. Build. Mater.*, vol. 24, no. 7, pp. 1134–1140, 2010, doi: 10.1016/j.conbuildmat.2009.12.028.

[227] A. Viani *et al.*, “Microstructural evolution and texture analysis of magnesium phosphate cement,” *J. Am. Ceram. Soc.*, vol. 103, no. 2, pp. 1414–1424, 2020, doi: 10.1111/jace.16782.